1992

Enhancement of ion transmission and reduction of background and interferences in inductively coupled plasma mass spectrometry

Ke Hu
Iowa State University

INFORMATION TO USERS

This manuscript has been reproduced from the microfilm master. UMI films the text directly from the original or copy submitted. Thus, some thesis and dissertation copies are in typewriter face, while others may be from any type of computer printer.

The quality of this reproduction is dependent upon the quality of the copy submitted. Broken or indistinct print, colored or poor quality illustrations and photographs, print bleedthrough, substandard margins, and improper alignment can adversely affect reproduction.

In the unlikely event that the author did not send UMI a complete manuscript and there are missing pages, these will be noted. Also, if unauthorized copyright material had to be removed, a note will indicate the deletion.

Oversize materials (e.g., maps, drawings, charts) are reproduced by sectioning the original, beginning at the upper left-hand corner and continuing from left to right in equal sections with small overlaps. Each original is also photographed in one exposure and is included in reduced form at the back of the book.

Photographs included in the original manuscript have been reproduced xerographically in this copy. Higher quality 6" x 9" black and white photographic prints are available for any photographs or illustrations appearing in this copy for an additional charge. Contact UMI directly to order.

U·M·I

University Microfilms International
A Bell & Howell Information Company
300 North Zeeb Road, Ann Arbor, MI 48106-1346 USA
313/761-4700 800/521-0600

Order Number 9302022

Enhancement of ion transmission and reduction of background and interferences in inductively coupled plasma mass spectrometry

Hu, Ke, Ph.D.

Iowa State University, 1992

U·M·I
300 N. Zeeb Rd.
Ann Arbor, MI 48106

Enhancement of ion transmission and reduction of background and interferences in inductively coupled plasma mass spectrometry

by

Ke Hu

A Dissertation Submitted to the
Graduate Faculty in Partial Fulfillment of the
Requirements for the Degree of
DOCTOR OF PHILOSOPHY

Department: Chemistry
Major: Analytical Chemistry

Approved:

Signature was redacted for privacy.

In Charge of Major Work

Signature was redacted for privacy.

For the Major Department

Signature was redacted for privacy.

For the Graduate College

Iowa State University
Ames, Iowa
1992

TABLE OF CONTENTS

GENERAL INTRODUCTION

After its first decade of development and application (1), inductively coupled plasma-mass spectrometry (ICP-MS) continues to gain popularity because of its low detection limits (1 - 50 ng L^{-1}), easy determination of isotopic ratios, and simple mass spectra from analyte elements. Now this technique has gained rapid and wide acceptance in the analytical community. There are over 600 instruments worldwide, which are being used in a range of fields for the analysis of geological, environment, biological, metallurgical, food, medical, and industrial samples (2-42). However, the analytical performance of ICP-MS is still limited by problems like spectral overlap from polyatomic ions (e.g., ArO^+ and $ArCl^+$), noise in the background, matrix effects, and clogging of the sampling orifice by deposited solids (2).

The ICP is an intense source of both ions and photons and emits some strong lines in the vacuum ultraviolet (43). These photons are usually screened from the detector by blocking the line-of-sight through the device with an optical baffle incorporated into the ion lens (44-46). Alternatively, the multiplier or mass analyzer can be offset far from the axis, with appropriate optics to deflect the ions (47-50). Despite these measures to screen the detector from the plasma, most quadrupole-based ICP-MS instruments still have a substantial continuum background (i.e., background at a m/z value devoid of ions) of 5 to 20 counts s^{-1}. Further attenuation of the background is obviously desirable.

The diameter of the sampling orifice (usually $\sim$1 mm) affects signal characteristics strongly in ICP-MS. For example, Vaughan and Horlick reported that the count rate of

monatomic analyte ions (M^+) increased by a factor of ten and the ratio of oxide ions to analyte ions (MO^+/M^+) changed greatly when the diameter of the sampler was altered from 0.51 to 0.94 mm (51). Increasing the size of the sampling orifice would also improve the tolerance of the sampler to clogging from solids deposited from the sample (52).

The most abundant species in the plasma are Ar, H, and O. These species may combine with each other or with elements from the analyte matrix. The major elements present in the solvents or acids used during sample preparation (e.g., N and Cl) also participate in these reactions. Many polyatomic ion peaks can therefore occur but these are significant only up to about 82 m/z. A number of papers (1,2, 53-58) have documented the basic background spectral features and polyatomic species observed in ICP-MS. The extent of polyatomic ion formation depends on many factors including extraction geometry, operating parameters for plasma and nebulizer system and, most importantly, on the nature of the acid and sample matrix (59). In addition, the extent of polyatomic ion formation can also depend on the specific instrument design (59,60,61).

The ion current through the skimmer is typically 1 mA. This current is balanced by an equal electron current in the plasma and in the supersonic jet. In these regions the beam acts as if it were electrically neutral (62). However, as the beam leaves the skimmer, the electric field established by the lens collects ions and repels electrons, the beam no longer acts as if it were neutral, and the ions begin to repel each other. This effect is called space charge and should become substantial in ICP-MS at a total beam current of the order of 1 μA (63, 64), roughly three orders of magnitude below the actual beam current cited above. Generally, the ions can be detected at the ratio of $1/10^6$, e.g., if 10^6 ions pass through the

skimmer, only 1 ion reaches the detector. This considerable ion loss results mostly from space charge. Other problems caused by the space charge effect are matrix interferences and mass discrimination. In the presence of a matrix elements, heavy analyte ions are suppressed less severely than light ones. Heavy matrix ions suppress analyte signals more extensively than light matrix ions (64-68). Accelerating the ions to higher energies could improve ion transmission and attenuate the mass discrimination by overcoming the space charge problem. This method has been adopted in high resolution ICP-MS devices that use magnetic sector mass analyzers (49,70), but matrix effects and mass discrimination with these instruments have not been reported. Using an extra metal cone at a high negative voltage as the first ion lens might increase ion sensitivity, especially for low mass ions, thereby reducing the mass discrimination problem (71,72).

Matrix effects are also influenced by ion lens geometry (73,74) and lens potentials (66,73). Caruso and co-workers have described an interesting and potentially valuable scheme in which the ion lens voltages are adjusted to maximize the analyte signal with the sample matrix present (75,76). This procedure can reduce the extent of the matrix effect significantly. Ross and Hieftje (77) removed the second stage ion lens electrodes and photon stop. The sensitivity and detection limits with this arrangement were approximately the same as those measured with their conventional ion lens (77-79), but matrix induced interference effects were almost eliminated (77).

Mass-resolved ions leaving the analyzer are generally detected by a Channeltron electron multiplier in the pulse counting mode. Although good analytical performance can certainly be obtained with Channeltron electron multiplier, they do have several undesirable

characteristics as detectors for ICP-MS. A Channeltron has a limited lifetime of approximately 1.5 years under normal analytical use. The response of a Channeltron is linear up to count rates of approximately $1x10^6$ counts s^{-1}; above this value, calibration curves tend to droop.

Several other detectors have been tried with ICP-MS. These include discrete dynode electron multipliers (80) and the coniphot detector in the Nermag instrument. The Daly detector (81-83) was used with ICP-MS by Huang, Jiang, and Houk (84). The Daly detector offers some potential advantages in the problem areas found for the Channeltron detector. Huang et al (84) reported that the Daly detector gave modest improvements in linear range and precision. Furthermore, the gain of the Daly detector should not deteriorate with time. However, the pressure in the detector chamber on ICP-MS instruments is usually about 10^{-5}-10^{-6} torr. At these pressures, a very high potential could not be utilized because of electrical discharge. Even at the potential that yielded the best signal to noise ratio (5 kV), the background was 500 counts s^{-1}. Sensitivities and detection limits were similar to those obtained with the Channeltron electron multiplier with their ICP-MS facility (84). This high background probably comes from the electrical discharge of residual gas in the detection chamber. Reducing the pressure in the detector chamber would reduce the discharge, and thus reduce the background. Furthermore, if photons from the plasma can be totally blocked, the continuum background detected either by a Channeltron detector or by a Daly detector would be reduced.

Mass spectrometry is a very sensitive method for analytical applications. Ion deposition (85-98) and ion implantation (99-103) with conventional ion sources are also well-

established techniques. Both techniques employ an ion source and mass analyzer, but in the former technique mass-selected ions are detected for calculating the amount of the elements in the original sample. In the latter method, mass-selected ions are accumulated on a target for material synthesis or modification.

Direct ion beam deposition is a thin film formation method which exploits a mass-separated, low energy ion beam of the film constituents. Intensive work has already been reported for a variety of materials including metal and semiconductors materials (85-98). If the ions are accelerated to high ion energies, they penetrate more deeply into the solid target material, and ion implantation occurs. The principles and applications of ion implantation have been investigated and reported in detail elsewhere (99-103).

Use of ICP-MS as an ion deposition device could extend the scope of ion deposition to new studies and applications because of its multielement capabilities. One critical problem for using an ICP as an ion source for ion deposition or ion implantation is the ion beam intensity available. In order to deposit the thin film on the substrate within a reasonable time, the ion beam intensity should be increased as much as possible. On the other hand, the methods developed to intensify the ion beam may also be useful for analytical purposes i.e., to increase sensitivity for analyte ions in ICP-MS.

This dissertation describes instrumental methods for enhancement of ion transmission and reduction of background and interference effects in ICP-MS. The improvements in the ICP-MS instrument involve enlarging the orifices in the sampling interface, floating parts of the interface, and using offset ion optics, a four-stage vacuum system, and a Daly detector. Ion beam deposition or ion implantation using ICP-MS as an ion source is also described in

this dissertation. This dissertation is presented such that each paper stands independent of the others as a complete scientific manuscript including figures, tables, and literature cited. Additional literature citations from the general introduction and the summary are given after the summary.

The first paper describes instrumentation, ion trajectories, and detector performance of the new home made ICP-MS with a enlarged sampling orifice and offset ion lens. A new four-stage vacuum system is constructed. A tube is used as the ion exit lens between the third and fourth vacuum chambers. The pressure in the detector chamber is lower than in a usual ICP-MS vacuum system, so the Daly detector can be successfully used. The large sampling orifice (1.31 mm diameter) increases ion signals and minimizes solid condensation on the orifice. Some ion lens electrodes are offset from the central axis, which greatly reduces continuum background to close to the dark current level for a Channeltron detector and to only a few counts s^{-1} for the Daly detector. Entrance and exit RF-only quadrupole rods are used in this home made instrument for improving ion transmission and ion beam intensity.

Polyatomic ion interferences and matrix effects with this ICP-MS instrument are described in the second paper. Polyatomic ion peaks such as ArO^+, ArN^+, $ArCl^+$, and Ar_2^+ are greatly suppressed compared to those seen on any other ICP-MS device. Moreover, when the first cylindrical ion lens electrode is grounded, matrix interference effects can be greatly reduced without sacrificing too much sensitivity for analyte ions. Alternatively, matrix effects can also be mitigated by re-adjusting the voltage applied to the first lens with the matrix present.

The third paper describes an electrically floating interface. Several different arrangements are investigated. Ion transmission is improved by a factor of at least 4 to 6. The upper end of linearity of the calibration curve (i.e., a plot of ion signal vs. concentration of the element of interested in the sample) is extended. Mass discrimination is greatly reduced.

The final paper describes a new application of ICP-MS: ion beam deposition or ion implantation. The advantages of ICP-MS for thin film growth are described. Two critical shortcomings of ICP-MS for ion deposition are the low intensity of the ion beam and the relatively high residual pressure in the deposition chamber. Experimental methods to improve the performance of ICP-MS in these areas are described. Eventually, a new method of modifying materials or growing thin films by ion deposition or ion implantation using ICP-MS as an ion source is developed. Primary data shown in this section indicate that ICP-MS has a bright future for material modification.

PAPER I.

INDUCTIVELY COUPLED PLASMA MASS SPECTROMETRY WITH AN ENLARGED SAMPLING ORIFICE AND OFFSET ION LENS

I. ION TRAJECTORIES AND DETECTOR PERFORMANCE

INTRODUCTION

ICP-MS has become an important technique for elemental and isotopic analysis because of its high selectivity and excellent detection limits (1 - 50 pptr). Despite these features, the analytical performance of ICP-MS is still limited by problems like spectral overlap from polyatomic ions (e.g., ArO^+ and $ArCl^+$), noise in the background, matrix effects and clogging of the sampling orifice by deposited solids (1). This paper and its companion (2) address instrumental studies designed to improve the performance of ICP-MS in these areas.

The ICP is an intense source of both ions and photons and emits some strong lines in the vacuum ultraviolet (3). These photons are usually screened from the detector by blocking the line-of-sight through the device with an optical baffle incorporated into the ion lens (4-6). Alternatively, the multiplier or mass analyzer can be offset far from the axis, with appropriate optics to deflect the ions (7-10). Despite these measures to screen the detector from the plasma, most quadrupole-based ICP-MS instruments still have a substantial continuum background (i.e., background at a m/z value devoid of ions) of 5 to 20 counts s^{-1}. The cause(s) of this remaining background are not known precisely. Perhaps a few ions pass straight down the axis of the quadrupole and are not filtered regardless of the m/z setting. Alternatively, photons that are created when ions with unstable paths strike the rods may reach the detector. Further attenuation of the background is obviously desirable regardless of its cause.

The diameter of the sampling orifice (usually $\sim$ 1 mm) affects signal characteristics

strongly in ICP-MS. For example, Vaughan and Horlick reported that the count rate of monatomic analyte ions (M^+) increased by a factor of ten and the ratio of oxide ions to analyte ions (MO^+/M^+) changed greatly when the diameter of the sampler was altered from 0.51 to 0.94 mm (11). Increasing the size of the sampling orifice would also be expected to improve the tolerance of the sampler to clogging from solids deposited from the sample (12).

In this paper, the performance of a new ion lens is described. The ions from the skimmer are deflected and then brought back to the central axis. The lens electrodes themselves block photons effectively from the detector. A large sampling orifice (1.31 mm diam.) improves ion signals and resists plugging. These experiments are performed on an ICP-MS device with four differentially pumped chambers, as opposed to the usual three, to handle the additional gas load from the larger sampling aperture. With the four-stage chamber, the pressure in the detector chamber is low enough for proper use of the Daly detector (13,14). The relative merits of this detection method are compared with those obtained with a Channeltron electron multiplier. The companion paper (2) describes spectral overlap and matrix interferences with the new ICP-MS instrument, both of which are substantially less severe than those seen with most other ICP-MS devices.

EXPERIMENTAL

Vacuum System

The sampling interface and MS part of the apparatus are depicted in Figure 1. Instrumental components and operating conditions are identified in Table I. The basic features of the ultrasonic nebulizer (16,17), ICP, and sampling interface (18,19) have been described previously. The expansion chamber was pumped by a rotary pump (TRIVAC Model D30A, Leybold Vacuum Products, Inc.; pumping speed, 10 L s^{-1}). The ion lens chamber was pumped by a diffusion pump equipped with a liquid nitrogen cooled baffle (Model VHS-6, Varian Associates; net pumping speed, 1600 L s^{-1}). The quadrupole and detector chambers were pumped by turbo molecular pumps (Model TMP 360V, Leybold Vacuum Products Inc.; pumping speed, 400 L s^{-1}). Unlike most ICP-MS devices, there was no isolation valve behind the skimmer. Instead, slide valves to the rotary pump and the diffusion pump were closed and the turbomolecular pumps were turned off to vent the chamber for maintenance. A small Viton disk was pressed gently onto the outside of the sampler to seal off the system for evacuation after service.

Ion Sampling Interface

A scale drawing of the ICP-MS sampling interface is shown in Figure 1. The sampling cone (A, Figure 1) was made from nickel. The orifice diameter was enlarged to 1.31 mm from the usual 1.0 mm. The diameter of the skimmer orifice was also 1.31 mm. The angles and other dimensions of the sampler and skimmer were described elsewhere (18).

The distance between the sampler orifice and skimmer orifice was varied by changing the thickness of the copper spacer between the skimmer base and the vacuum chamber until the best signals were obtained for Co^+ and Ho^+. The skimmer position was re-optimized when each different sampling orifice size was drilled. Eventually, the sampler-skimmer spacing was set to 11 mm with the 1.31 mm sampling orifice and skimmer orifice. At this position, the skimmer tip was 2/3 of the way from the sampling orifice to the onset of the Mach disk, which also yielded optimum sensitivity for Douglas and French (19). The copper flange which mounted the skimmer to the vacuum chamber (Figure 1) was water cooled.

Ion Lens

The new ion lens is shown in Figure 2. Ions passing the skimmer orifice (A, Figure 2) entered the first stainless steel cylinder (1, Figure 2). Numerous holes were drilled in the side wall of the cylinder, so that neutral atoms could be evacuated. The second electrode of the lens (2, Figure 2) was a copper cone with a circular orifice of 2.5 mm diameter. After the copper cone, ions passed a series of circular apertures (6.35 mm diameter) in stainless steel plates (3-6, Figure 2) which were 1.65 mm thick. Lens 3 was made thicker by putting three plates together. The spacing between each lens was 2.5 mm. Thinner spacers between lenses were tried but yielded poorer ion signals. Ions passing lens 6 were bent back further to center to pass the differential pumping orifice (7, Figure 2) which was a tube 2.50 mm diam. x 6.4 mm long. The ICP, sampler, skimmer, and quadrupole were kept on the same center line.

Separate voltages (V_1, V_2, V_3, V_4, V_5, V_6, V_7) were applied to the ion lens electrodes.

For maximum transmission of $^{153}Eu^{+}$ (a typical ion in the middle of the mass range for atomic ions), the optimum voltages were: V_1, +3 V; V_2, -250 V; V_3 + 1 V; V_4, + 18 V; V_5, -250 V; V_6, + 18 V; V_7, -180 V; and V_8, -20 V. It is interesting that applying voltages of opposite polarity to adjacent lenses tended to yield maximum ion transmission. This lens may operate somewhat like the periodic ion lens used to focus high density ion beams (20).

RF-only Quadrupole and Exit Lens

As shown in Figure 1, short RF-only quadrupoles were mounted both before and after the mass analyzer. Both RF-only quadrupoles had the same rod diameter (1.60 cm) as the mass analyzer quadrupole and were separated from the analyzer by a gap of 1.25 mm. A single RF power supply was used to drive the three quadrupoles. The two sets of RF-only quadrupole rods were connected in parallel to each other. High voltage capacitors (50 pF, 7.5 kV max.) were connected between the RF-only rods and the mass analyzer rods to shield the DC component from the RF-only quadrupoles. The mean DC bias of the two RF-only quadrupoles was applied through resistances (1 MΩ) and was the same and could be adjusted differently from that of mass analyzer.

Ions leaving the exit RF-only quadrupole then passed through a long, thin stainless steel tube (2.5 cm x 6 mm inside diam.) called the exit lens. This lens is shown as L in Figure 1. The exit lens was sealed with an electrically insulating gasket and was maintained at -50 V. The exit lens also served as the differential pumping orifice between the quadrupole and detector chambers. Because of this conductance restriction and the separate pump used, the pressure in the detector chamber was quite low (1.5×10^{-7} torr) during

operation. This additional pumping stage helped compensate for the high gas load through the large sampler and skimmer.

Channeltron Electron Multiplier

The basic features of the Channeltron electron multiplier have been described elsewhere (21). The detector arrangement (M, Figure 1) is shown in Figure 1. The multiplier and ion deflector (N, Figure 1) were offset above and below the center line of the sampler, skimmer, and quadrupoles. The Channeltron was shielded in a grounded, stainless steel case. A stainless steel plate with a circular aperture (1.25 cm diam.) was placed in front of the stainless steel case and was used to attract ions into the Channeltron. This plate was 5.0 cm from the center line through the quadrupole and was operated with an applied potential of -250 V. The deflecting plate (see Figure 1) was aligned with the mouth of the Channeltron, was placed 2.5 cm below the ion exit lens, and was operated at +240 V.

Daly Detector

The basic features of the Daly detector and the procedures for preparing the aluminum target and scintillator for ICP-MS have been described (13,14). The detector assembly is shown in Figure 3. The target (M, Figure 3) was 2.5 cm above the center line through the quadrupole and the scintillator was 5.7 cm below it. The PMT assembly (N, Figure 3) also has been described (5). The RF leads to the mass filter did not pass through the detector chamber so that RF radiation from the quadrupole power supply did not interfere with the detector.

Data Acquisition

Detection limits were measured as described in reference 14. The detection limit is generally considered the solution concentration necessary to yield a net peak height equivalent to 3 times the standard deviation of the background. However, the background with the Channeltron detector was so low that the standard deviation for most elements was below 1 count s^{-1} and was difficult to measure directly. Therefore, the detection limit was estimated to be the solution concentration necessary to yield a net peak height equivalent to 3 times the estimated standard deviation, $B^{1/2}$, where B was the background count rate. Calibration curves were determined in the multichannel scanning mode (ref. 1 p. 44) using the signal peak height. The dwell time was 50 μs $address^{-1}$ for 4096 addresses over a mass window of 20 m/z units wide. Fifty such sweeps were averaged. The mass analyzer was operated at unit mass resolution in the mass range measured.

Ion kinetic energies were measured by applying a positive stopping voltage as the mean DC bias to the quadrupole mass filter (22-24). The stopping voltage necessary to attenuate the ion signal to 5% of the original signal level was measured and is referred to as "maximum ion energy" subsequently.

Ion Trajectories

The trajectories through the ion lens were modeled with SIMION (a computer program for ion trajectory simulation) (25) on an IBM personal computer. No corrections for space-charge effects (18,26,27) were used. Trajectories were calculated for initial ion kinetic energies of 4 to 11 eV to account for the dependence of kinetic energy on m/z ratio

(23). The ion kinetic energy of 7 eV was used for the rest of ion trajectory calculations. The sloped surfaces of the skimmer and conical ion lens were approximated by small interconnected squares echeloned at 45°.

Solutions and Standards

Standard solutions of Co, Cu, and Mo were 0.5 mg L^{-1} (ppm), Zn was 1.0 ppm, and Y, Rh, Cs, Ce, Ho, Tl, Pb, and U were 0.2 ppm and were prepared by diluting aliquots of commercial stock solutions (1000 ppm, Fisher Scientific) with distilled deionized water (18 MΩ, Barnstead).

RESULTS AND DISCUSSION

Diameter of Sampling Orifice

These experiments were performed by drilling out the circular aperture in a single nickel cone progressively. After each drilling, the separation between sampler and skimmer was adjusted empirically to maximize ion signal by substituting various spacers of different thickness behind the skimmer (Figure 2). This procedure was necessary because the background pressure increased and the supersonic jet shrank when the sampling orifice was enlarged (18,19,28), and thus the optimum separation between sampler and skimmer changed as well.

The effect of sampling orifice diameter on ion signals for $^{59}Co^{+}$ and $^{209}Bi^{+}$ is shown in Figure 4. The signals increased by a factor of 8 when the sampling orifice was enlarged from 0.79 to 1.31 mm diam. Each point in Figure 4 was measured at the sampler-skimmer separation that yielded maximum ion signal for each orifice diameter, as described in the previous paragraph. Vaughan and Horlick observed a similar increase in ion signal when they increased the diameter of the sampling orifice from 0.51 mm to 0.94 mm on their Sciex instrument (11). The background pressure in the expansion chamber increased by a factor of 2.4 for the range of sampler diameters studied in the present work.

For three of the orifice diameters chosen, the pressure in the expansion chamber was also monitored as a function of time during continuous nebulization of a concentrated solution of yttrium (1000 ppm). This experiment was intended to evaluate the effect of sampling orifice size on tolerance to clogging. These results are shown in Figure 5. Each

pressure measurement was normalized to the pressure obtained at time zero, i.e., before the yttrium solution was introduced. With the 1.31 mm diam. sampler, the pressure did not decrease noticeably over 100 minutes. In contrast, the pressure decreases seen in Figure 5 for the smaller samplers indicated that they plugged readily. Note that these studies were conducted with a continuous flow ultrasonic nebulizer, which transported material to the plasma at a rate at least 10 times greater than that obtained with a conventional pneumatic nebulizer (16,17,29). Thus, the 0.1% Y solution used here was probably the equivalent of a 1% solution from a conventional nebulizer in terms of the rate of transport of material, which governed the deposition and clogging problems. At any rate, the 1.31 mm diam. sampler used here proved quite resistant to clogging from deposited solids. This sampler was used for all the studies reported subsequently in this paper and its companion (2).

Position of First Ion Lens

Calculations by Olivares and Houk (18), Gillson et al. (26) and Tanner (27) indicate that efficient collection of ions leaving the skimmer is hampered by space charge effects, which disperse the ion beam due to the very high current ($\sim$ 1 mA) therein. We attempted to mitigate these effects and improve the collection efficiency by thrusting the first ion lens (1, Figure 2) as far as possible into the skimmer. A similar arrangement is employed in the high resolution ICP-MS device marketed by VG Elemental (30). As shown in Figure 6, a substantial increase in ion signal (by a factor of two to five) was seen when the separation between the skimmer tip and the entrance to the first lens was reduced to 2.4 cm. At this position, the mouth of the first lens was only $\sim$ 5 mm from the nearest surface of the

skimmer wall. Closer separations were tried, but the voltage output of the power supply for the first lens then became unstable, possibly due to an electrical discharge between the ion lens and the skimmer wall or to a high current flow to the lens. Drilling holes through the wall of the first ion lens, as shown in Figure 2, also helped prevent this discharge problem. The 2.4 cm separation was used for all subsequent work.

Ion Trajectories and Kinetic Energies

SIMION was used to model ion trajectories through the lens. First, the effect of ion kinetic energy on trajectory is shown in Figure 7. Ions that started on center with kinetic energies of 4 eV to 11 eV were focussed at a common point inside lens 5 and were then deflected through the differential pumping orifice. After the differential pumping orifice, the ion paths diverged, so the efficiency with which ions of different energy were injected into the mass filter varied somewhat.

This range of energies of 4 eV to 11 eV corresponded closely to that observed for ions of different m/z with this instrument (Figure 8). The increase in ion energy with m/z was caused by the acceleration of all ions to the same velocity in the supersonic jet, as described by Fulford and Douglas (23). The measured kinetic energy for Li^+ was slightly above the line through the energies of the heavier ions, again in agreement with the results of Fulford and Douglas (23) and Tanner (27). The latter author has attributed the slightly high value of kinetic energy for light ions such as Li^+ to space charge effects behind the skimmer.

The trajectories in Figure 9 illustrated the fate of ions that left the skimmer either at

an angle or displaced radially relative to the central axis. SIMION indicated that such ions were focussed in front of the conical lens, but these simulations ignored space charge effects, which were probably quite substantial here (26,27). Even if off-axis ions entered the conical lens efficiently, they then struck one of the downstream lens electrodes and were not transmitted to the mass analyzer. Similar behavior was seen for off-axis ions of different kinetic energy than the 7 eV ions selected for Figure 9.

The spatial selectivity of this lens for on-axis ions contrasted strongly with the behavior of the lens in Perkin Elmer SCIEX ICP-MS instruments. Because of the shadow stop and photon stop, this latter lens transmitted only ions that left the skimmer off-axis (31). Detailed simulations have not been reported for other lens assemblies, but it was likely that all lenses with a central stop to block photons showed the same general behavior as the Perkin Elmer SCIEX lens, at least to some extent.

It is also important to note another interesting difference between these ion optical simulations and those of Vaughan and Horlick (31). The voltages used in the SIMION calculations in the present work were close to (i.e., within a few volts) of the ones that yielded maximum ion transmission experimentally. In previous simulations with the Perkin Elmer SCIEX lens, the voltages required by SIMION for ion transmission differed substantially from those actually used on the instrument (31), although the general conclusions drawn as to the overall behavior of characteristics of this lens were probably still reasonable.

Effect of Ion Lens Voltages on Mass Discrimination

The variation of ion energy with m/z (Figure 8) is one cause of mass discrimination in ICP-MS. This problem complicates selection of a single set of lens voltages for multielement analysis. Similar effects were seen with the offset lens studied in the present work, as shown in Figures 10 - 12. For simplicity, these figures were referred to as "focussing curves." For each figure, only one lens voltage was varied at a time. The other lenses were kept at the voltages that yield maximum transmission for Rh^+.

Inspection of these focussing curves showed that their overall shapes and the order of voltages corresponding to maximum transmission for different elements varied for the three electrodes of the ion lens. For example, for the third electrode (V_3, Figure 10), the order of voltages that yielded maximum transmission was $U^+ < Rh^+ < Li^+$. For the fourth electrode (V_4, Figure 11), the order was $Rh^+ \leq Li^+ \leq U^+$, whereas for the sixth electrode (V_6, Figure 12) the order was $Rh^+ \leq U^+ \leq Li^+$. For the sixth electrode (Figure 12), mass discrimination was minimal at a voltage of +35 V, i.e., the signals for Li^+, Rh^+ and U^+ were all near their maxima at the same applied voltage. In contrast, some compromise in transmission was necessary when selecting the voltages applied to the third and fourth electrodes. The focussing curve for Li^+ was substantially broader than those for Rh^+ and U^+ for electrodes 3 and 6, whereas U^+ had the broadest focussing curve for electrode 4. Focussing curves for the negative electrodes (V_2, V_5 and V_7 in Figure 2) were broad and featureless and were therefore not reported here.

Background and Signal with Channeltron Electron Multiplier

The detector arrangement shown in Figure 1 was used for these studies. Measurements of dark current (i.e., with the sampler closed) and background are listed in Table II. These values were so low that long counting times (10 min) were required to obtain useful counting statistics. The dark current was ~0.3 counts s^{-1}. Next, ions were sampled from the ICP with the mass analyzer set at a DC offset voltage of -1 V. In this condition, ions were injected into the mass analyzer, but the m/z window was set to a high value in a part of the spectrum devoid of ions. The background increased only slightly to ~ 0.4 counts s^{-1}. Finally, a high positive offset voltage (+50 V) was applied to the quadrupole rods so that ions could not enter the mass filter. The background did not change perceptibly, which indicated that the background was not caused by ions in or leaking out of the mass analyzer. Also, the background did not change noticeably as aerosol gas flow rate, plasma power, or ion lens voltages were changed. Our general experience with other lenses has been that adjusting the voltages to maximize ion transmission also induced an increase in background, but this problem was not seen with the offset lens described in the present paper.

These background values were much lower than those obtained on other quadrupole-based ICP-MS devices (1,4) and rivalled those obtained with ICP-MS instruments based on double focussing mass spectrometers (8,9). The background with this ICP-MS device with on-center, cylindrical ion lenses has been typically 1000 counts s^{-1}. With a photon stop, the background improved somewhat to ~150 counts s^{-1}. The offset ion lens and displaced detector arrangement described here provided much lower backgrounds than we have

obtained on any of our "home-made" device with any of a variety of photon stops or detector geometries (5,18,32,33).

The mass spectrum of Ho^+, a monoisotopic rare earth element, is shown in Figure 13. For this figure, the ion lens voltages were adjusted to maximize transmission specifically for Ho^+. The sensitivity (i.e., the count rate per unit concentration) was $\sim 10^4$ counts s^{-1} per ppb Ho, which would be equivalent to $\sim 10^7$ counts s^{-1} per ppm, if the linear dynamic range extended to such high count rates. The sensitivity observed for Ho^+ compared well with that obtained for most other quadrupole-based ICP-MS devices (1), although two mitigating factors must be kept in mind: 1) a highly-efficient ultrasonic nebulizer was used in the present work, and 2) the kinetic energy of Ho^+ ($\sim$7 eV) was right in the best range for transmission through this lens, as indicated by the trajectory plots in Figure 7. The peak shapes were also much better than seen previously with this instrument, perhaps because of the RF-only rods on the entrance. Background counts were not shown in Figure 13 because few (if any) were seen in the time required ($\sim$ 1 min) to measure this spectrum.

The sensitivities and detection limits obtained with the Channeltron detector are listed in Table III. These data were obtained with two separate schemes for adjusting the voltages applied to the lenses. The values labelled "single element conditions" were measured with the lens voltages adjusted separately to maximize signal for each group of elements of similar m/z. For example, $^{59}Co^+$, $^{63}Cu^+$, and $^{64}Zn^+$ were measured with the same lens settings, which differed from those used for $^{98}Mo^+$ and $^{103}Rh^+$, or for $^{208}Pb^+$ and $^{238}U^+$. Alternatively, the values listed under "multielement conditions" were measured with the lens voltages adjusted for best transmission of $^{133}Cs^+$ only. Comparison of the sensitivities in Table III

shows that the "multielement conditions" involved little sacrifice in sensitivity compared to that obtained under "single element conditions" for the lighter elements such as Co and Cu. However, signals for heavier elements such as U were reduced by a factor of about two under "multielement conditions."

In either case, detection limits were in the range 0.3 - 5 ng L^{-1} (pptr) for the elements shown. These elements represented favorable cases in that all but Zn were quite efficiently ionized in the ICP (1). These values were comparable to those obtained with most quadrupole-based instruments, which normally used the standard, less-efficient pneumatic nebulizers (1). Apparently, the somewhat-lower sensitivity (accounting for differences in nebulization) seen with the present instrument was compensated by the lower background. It is interesting that both quadrupole ICP-MS instruments with substantially better detection limits and sensitivity (i.e., the Yokogawa PMS 2000 and the TS Sola) also use offset ion lenses (10,34,35), but of different geometries than the one described in this paper.

In a supplementary experiment, the turbo pump on the detector chamber (Figure 1) was shut off during sampling of ions from the ICP. The pressure in the detector chamber therefore rose gradually from 1.5×10^{-7} torr to 3×10^{-5} torr. The background and ion signal observed were not affected by this increase in pressure in the detector chamber. Thus, the fourth pumping stage was not strictly necessary when the Channeltron was used. Three differentially-pumped stages would have sufficed, despite the high gas load through the enlarged sampler and skimmer.

Comparison with Daly Detector

The Daly detector is shown in Figure 3. The variation of background with target voltage for this detector is shown in Figure 14. Background changed little until the target voltage was more negative than ~ - 18 kV, after which the background rose sharply. This behavior indicated that the pressure in the target chamber (1.5×10^{-7} torr) was still a little high for the Daly detector, although a much more negative target voltage was possible than the -5 kV used in our early experience with this detector at a pressure of ~ 10^{-6} torr (14). The target voltage was kept at -18 kV for subsequent studies.

As shown in Table II, the dark current was ~3 counts s^{-1}, and the background was ~4 counts s^{-1} with the Daly detector. These values were a bit higher than those seen with the Channeltron, and the background exceeded the dark current by about the same factor (1.3) as seen with the Channeltron.

Sensitivities and detection limits obtained with the Daly detector under "multielement conditions" are given in Table IV. In general, sensitivity was similar (i.e., within a factor of two) for the two detectors. Detection limits were 0.6 - 20 pptr. These values with the Daly detector were a bit poorer than those obtained with the Channeltron but were still quite respectable.

Finally, linearity, stability and precision were evaluated with both detectors. As shown in Figure 15, the linear part of the calibration curve obtained with the Daly detector extended to somewhat higher count rate (~2×10^6 counts s^{-1}) than that obtained with the Channeltron, as seen previously (14). A solution of 200 ppb Rh was analyzed repetitively to evaluate precision and stability. The relative standard deviation of 5 successive

measurements of $^{103}Rh^+$ signal was 0.9% with the Daly detector and 3.0% with the Channeltron. The latter figure was representative of the short-term precision obtained in many experiments with the Channeltron detector on the instrument described here. Signal drift was measured over a longer period (2 hours). The signal observed from either detector drifted down over this period, as is common in ICP-MS. With the Daly detector, the average signal for $^{103}Rh^+$ at 200 ppb drifted down by 3% in two hours. With the Channeltron, the signal drifted down by 10% in the same time period.

These measurements substantiate the following observations concerning stability and precision. First, the Daly detector yielded somewhat better stability and precision than the Channeltron, as seen previously (14). Second, the difference in drift characteristics seen with the two detectors indicated that some of the drift in ICP-MS may have been attributed to the Channeltrons that were commonly used. Perhaps there was a change in gain of a Channeltron over a time span of a few hours during ICP-MS operation. Finally, the offset ion lens was not particularly vulnerable to drift. The drift value reported here for the Channeltron (-10% over two hours) was only ~2X worse than the drift typically seen on modern commercial ICP-MS devices that use the same detectors. These latter instruments have the advantage of being engineered and tested exhaustively to minimize drift, whereas no special effort to minimize drift was expended in the present work. The 3% drift value obtained with the Daly detector is quite competitive with the drift performance of present ICP-MS devices.

CONCLUSION

This paper describes experimental modifications to ICP-MS that provide improved tolerance to orifice plugging and lower continuum background and less background noise than that obtained with other quadrupole-based instruments. The ion lens used to reduce the background sacrifices analyte count rates somewhat. This lens differs markedly from most other lenses used in ICP-MS in that it transmits only those ions that leave the skimmer on center. Modest improvements in precision and linear dynamic range are possible with the Daly detector, if an additional stage of differential pumping is provided. Spectral interferences and matrix effects can also be reduced dramatically with this apparatus, as described in the accompanying paper (2).

LITERATURE CITED

1. Jarvis, K. E.; Gray, A. L.; Houk, R. S. Handbook of Inductively Coupled Plasma Mass Spectrometry; Blackie: Glasgow, 1991.
2. Hu, K.; Houk, R. S. J. Amer. Soc. Mass Spectrom. 1992, Submitted.
3. LaFreniere, B. R.; Houk, R. S.; Fassel, V. A. Anal. Chem. 1987, 59, 2276-2282.
4. Kawaguchi, H.; Tanaka, T.; Mizuike, A. Spectrochim. Acta Part B 1988, 43B, 955-962.
5. Houk, R. S.; Fassel, V. A.; Flesch, G. D.; Svec, H. J.; Gray, A. L. Taylor, C. E. Anal. Chem. 1980, 52, 2283-2289.
6. Gray, A. L.; Date, A. R. Analyst 1983, 108, 1033-1050.
7. Ross, B. S.; Hieftje, G. M. Spectrochim. Acta Part B 1991, 46B, 955-962.
8. Bradshaw, N.; Hall, E. F. H.; Sanderson, N. E. J. Anal. Atomic Spectrom. 1989, 4, 801-803.
9. Morita, M.; Ito, H.; Uehiro, T.; Otsuka, K. Anal. Sci. (Japan) 1989, 5, 609-610.
10. Sakata, K. 18th FACSS Conf., Anaheim, CA October 1991, Paper No. 528.
11. Vaughan, M. A.; Horlick, G. Spectrochim. Acta Part B 1990, 45B, 1289-1299.
12. Douglas, D. J.; Kerr, L. A. J. Anal. Atomic Spectrom. 1988, 3 749-752.
13. Daly, N. R. Rev. Sci. Instrum. 1960, 37, 1385-1390.
14. Huang, L. Q.; Jiang, S.-J.; Houk, R. S. Anal. Chem. 1987, 59, 2316-2320.
15. Scott, R. H.; Fassel, V. A.; Kniseley, R. N.; Nixon, D. E. Anal. Chem. 1974, 46, 75-80.

16. Olson, K. W.; Haas, W. J., Jr.; Fassel, V. A. Anal. Chem. 1977, 49, 632-637.

17. Bear, B. R.; Fassel, V. A. Spectrochim. Acta, Part B 1986, 41B, 1089-1113.

18. Olivares, J. A.; Houk, R. S. Anal. Chem. 1985, 57, 2674-2679.

19. Douglas, D. J.; French, J. B. J. Anal. Atom. Spectrom. 1988, 3, 743-747.

20. Tien, P. K. J. App. Phy. 1954, 25, 1281-1288.

21. Kurz, E. A. American Lab. March 1979, 11(3), 67-82.

22. Olivares, J. A.; Houk, R. S. Appl. Spectrosc. 1985, 39, 1070-1077.

23. Fulford, J. E.; Douglas, D. J. Appl. Spectrosc. 1986, 40, 971-974.

24. Chambers, D. M.; Hieftje, G. M. Spectrochim. Acta Part B 1991, 46B, 761-784.

25. Dahl, D. A.; Delmore, J. E. PC/PS2 SIMION Version 4.0, Idaho Nuclear Engineering Laboratory, E. G. & G Idaho, Inc. Idaho Falls, ID. 1990.

26. Gillson, G. R.; Douglas, D. J.; Fulford, J. E.; Halligan, K. W.; Tanner, S. D. Anal. Chem. 1988, 60 1472-1474.

27. Tanner, S. D. Spectrochim. Acta Part B 1992, 47B, accepted.

28. Gray, A. L. J. Anal. Atomic Spectrom. 1989, 4, 371-373.

29. Tarr, M. A.; Zhu, G.; Browner, R. F. Appl. Spectrosc. 1991, 45, 1424-1432.

30. Bradshaw, N.; Sanderson, N. E. High Resolution Plasma Mass Spectrometer, International Patent Appl. No. PCT/GB89/00622, 1989.

31. Vaughan, M. A.; Horlick, G.; Spectrochim. Acta 1990, 45B, 1301-1312.

32. Crain, J. S.; Smith, F. G.; Houk, R. S. Spectrochim. Acta 1990, 45B, 249-259.

33. Rowan, J. T.; Houk, R. S. Appl. Spectrosc. 1989, 43, 976-980.

34. Turner, P. J. Fourth Surrey Conf. on Plasma Source Mass Spectrometry, Guildford, UK, July 1991.

35. Turner, P. J. In Applications of Plasma Source Mass Spectrometry, 1991, Holland, G.; Eaton, A. N. Eds.; Thomas Graham House: Science Park, Cambridge.

Table I. Instrumental Facilities

Component	Operation conditions, materials of dimensions
Ultrasonic Nebulization	Solution uptake rate 3.0 mL min^{-1}
continuous flow	Heater temperature 140 °C
Model U-5000	
CETAC Technologies, Inc.	Condenser temperature 0 °C
Neslab Instrument, Inc.	
ICP generator	Plasma forward power: 1.30 kW
Type HFP-2500D	Plasma reflected power: < 5 W
Plasma-Therm Inc.	Frequency: 27.12 MHz
(now RF Plasma Products)	
Plasma torch	Argon flow rates (L min^{-1})
All quartz construction	Plasma: 17
Ames Laboratory design (15)	Auxiliary: 0
Outer tube extended 25 mm	Aerosol: 1.3
beyond aerosol injector	
Load coil	Three turns
	Grounded to shielding box at
	downstream end with copper strap

Table I. continued

Ion extraction interface	Sampling position 13 mm from load coil,
Ames Laboratory construction	on center
	Sampler-skimmer separation: 11 mm
Vacuum system (see Figure 1)	Operation Pressure (torr)
4 stages, differentially pumped	Expansion chamber 2.35
welded stainless steel construction	Second stage $5x10^{-4}$
Ames Laboratory	Quadrupole chamber $5x10^{-6}$
	Detector chamber $1.5x10^{-7}$
Pressure measurement	
First stage	Convectron thermocouple gauge
	Series 275 digital model
	Granville-Phillips
Second stage	Ionization gauges
Third and Fourth stages	Model 843, Varian
	Model 307, Granville-Phillips
Mass analyzer	Mean rod bias -1 V dc
Model 270-9 with 012-15 rf head	
Extranuclear Laboratory	
(now Extrel)	

Table I. continued

Rf only quadrupole	Entrance rods: 50.8 mm long
Ames Laboratory construction	Exit rods: 38.1 mm long
	Mean rod bias -65 V dc on both entrance
	and exit rods
Channeltron electron multiplier	Ion deflection plate: +250 V
Model 4830A	Detector housing aperture: -250 V
Galileo Electro-Optics Corp.	CEM bias voltage: -3000 V
Daly detector	
Photo multiplier tube	PMT bias voltage: 550 V
Model 9924B EMI	target bias voltage: 18 kV
	output pulse width 30 ns (fwhm)
Counting electronics	
Model 1763 preamplifier	Maximum count rate, capability 20 MHz
Model 1762 amplifier-discriminator	pulse width 40 ns
Photochemical Research Associates	TTL output
Multichannel Analyzer	
Model 66 with 20 MHz dual-input	Dwell time/channel: 50 μs
multichannel scanning option	Channels: 4096
Nuclear Data Inc.	

Table II. Continuum background measurements

Sampler Status	DC bias on mass filter (V)	Integrated continuum background (count s^{-1})[a] Channeltron detector	Daly detector
Closed	-1	0.3	3
Open to ICP	-1	0.4	4
Open to ICP	+50	0.4	4

[a]Counting time approx. 10 min. while scanning over m/z = 166 to 200.

Deionized distilled water was nebulized.

Table III. Sensitivity and detection limits determined by Channeltron electron multiplier

Element	sensitivity,[a] counts s^{-1} mg L^{-1}	sensitivity,[b] counts s^{-1} mg L^{-1}	detection limits[a] ng L^{-1}
^{59}Co	1380000	1170000	1
^{63}Cu	1130000	858000	1
^{64}Zn	390000	302000	5
^{89}Y	2100000	1770000	0.9
^{98}Mo	495000	409000	4
^{103}Rh	2780000	2540000	0.7
^{133}Cs	4070000	4070000	0.5
^{165}Ho	6440000	2770000	0.3
^{208}Pb	2500000	1580000	0.8
^{238}U	2150000	736000	0.9

[a]Single element condition: ion lens voltage adjusted to maximize ion signal separately for each group of elements.

[b]Multielement conditions: Ion lens voltages adjusted to maximize ion signal for Cs^+ only.

Table IV. Sensitivity and detection limits determined by Daly detector

Element	sensitivity,[a] counts s^{-1} mg L^{-1}	detection limits ng L^{-1}
^{59}Co	1050000	6
^{63}Cu	467000	10
^{64}Zn	235000	20
^{89}Y	2180000	3
^{98}Mo	520000	10
^{103}Rh	5440000	1
^{140}Ce	3250000	2
^{165}Ho	9550000	0.6
^{205}Tl	2510000	2
^{208}Pb	1680000	4

[a]Ion lens voltages adjusted to maximize ion signal for Ho^+ only.

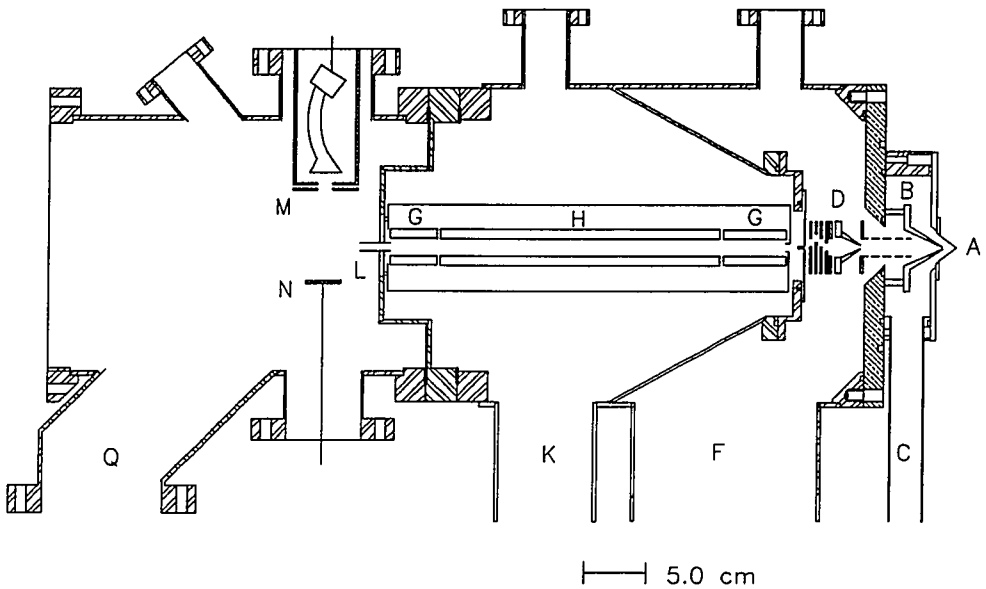

Figure 1. Schematic diagram of MS (ICP not shown): (A) sampler; (B) skimmer; (C) port to rotary pump; (D) ion lens (see Figure 2); (F) port to diffusion pump (1600L s^{-1}); (G) RF-only quadrupoles; (H) quadrupole mass analyzer; (K,Q) ports to turbomolecular pumps (400L s^{-1}); (L) ion exit lens; (M) Channeltron electron multiplier; (N) deflection plate.

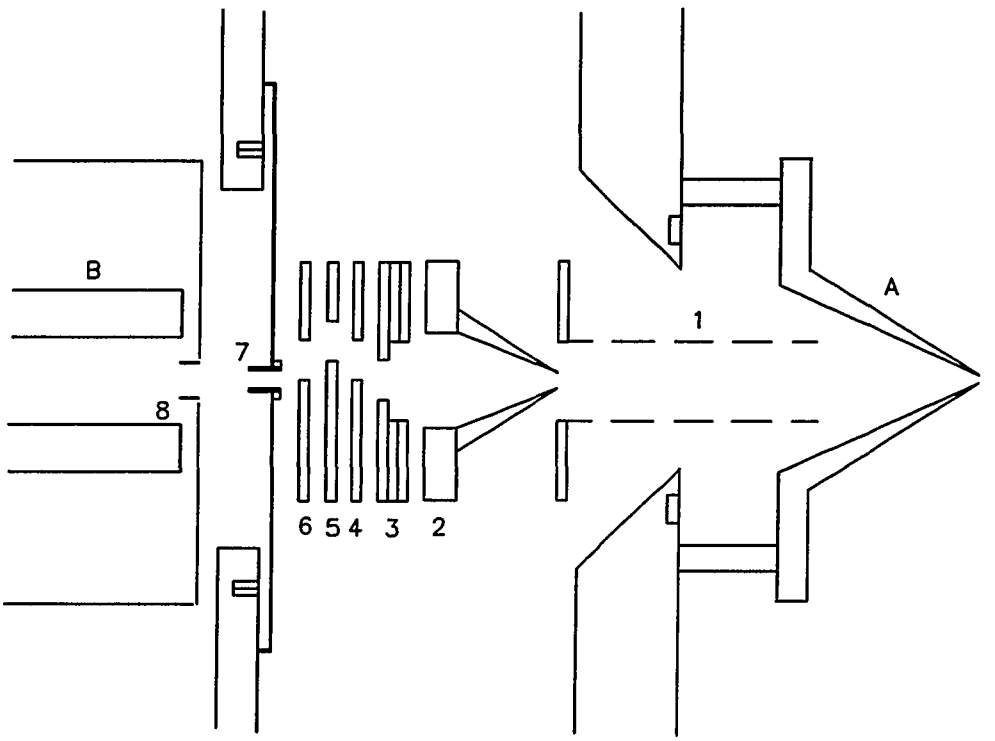

Figure 2. Schematic diagram of ion lens system: (A) skimmer (grounded); (B) RF only quadrupole at entrance to mass filter; (1) perforated cylinder, first electrode of ion lens; (2) copper cone, second electrode of ion lens; (3-6) stainless steel plates, third to sixth electrode of ion lens; (7) differential pump orifice (DPP); (8) ELFS lens.

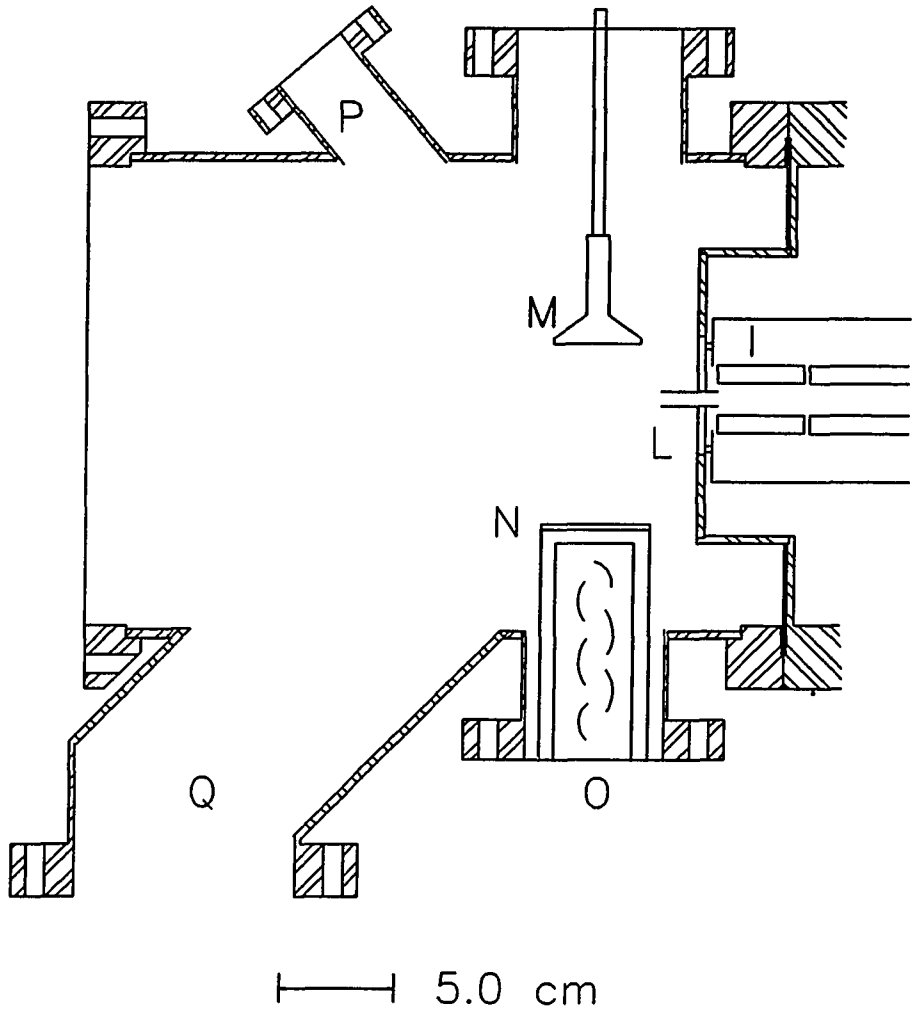

Figure 3. Schematic diagram of Daly detector and detector chamber: (I) exit FR only rods; (L) exit ion lens; (M) polished Al target; (N) scintillator with grounded metal film; (O) photomultiplier tube; (P) port to ion gauge; (Q) port to turbo pump.

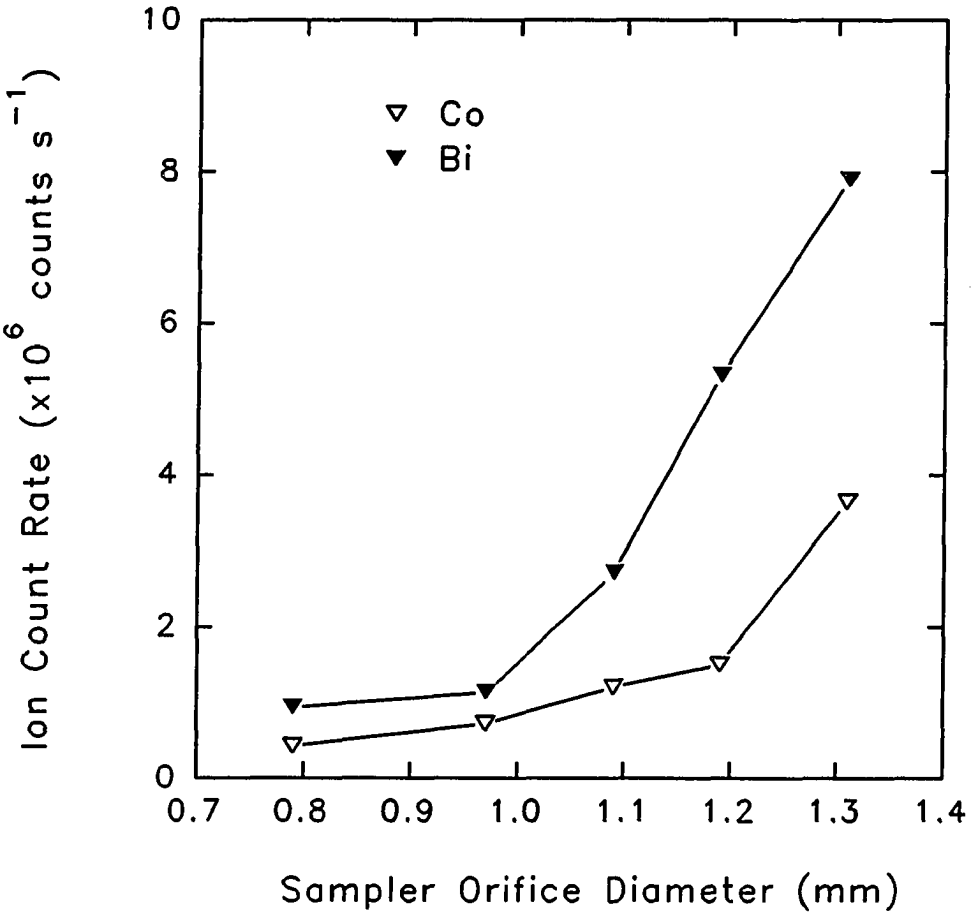

Figure 4. Ion count rates as a function of sampler orifice diameter. The separation between sampler and skimmer was optimized separately for each size sampling orifice diameter as described in the text.

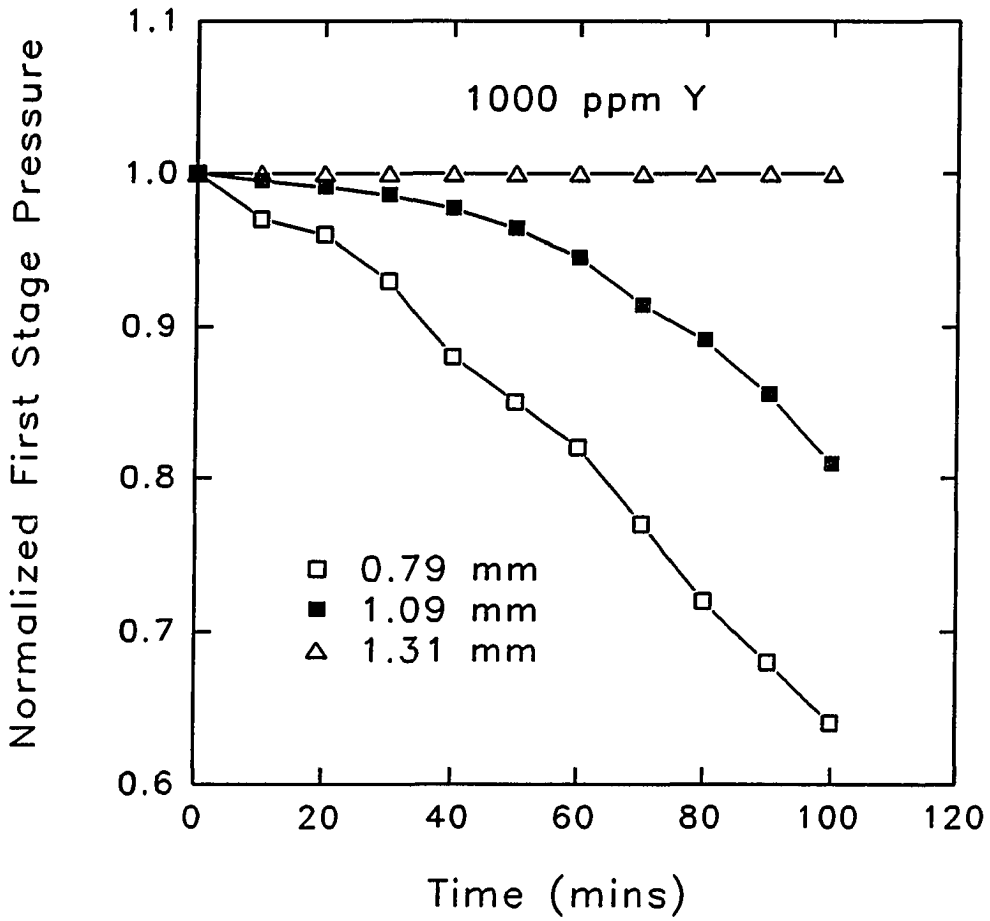

Figure 5. Normalized interface pressure as a function of time for continuous nebulization of 1000 ppm Y at sampling orifice diameter of 0.79 mm (□), 1.09 mm (■) and 1.31 mm (▽).

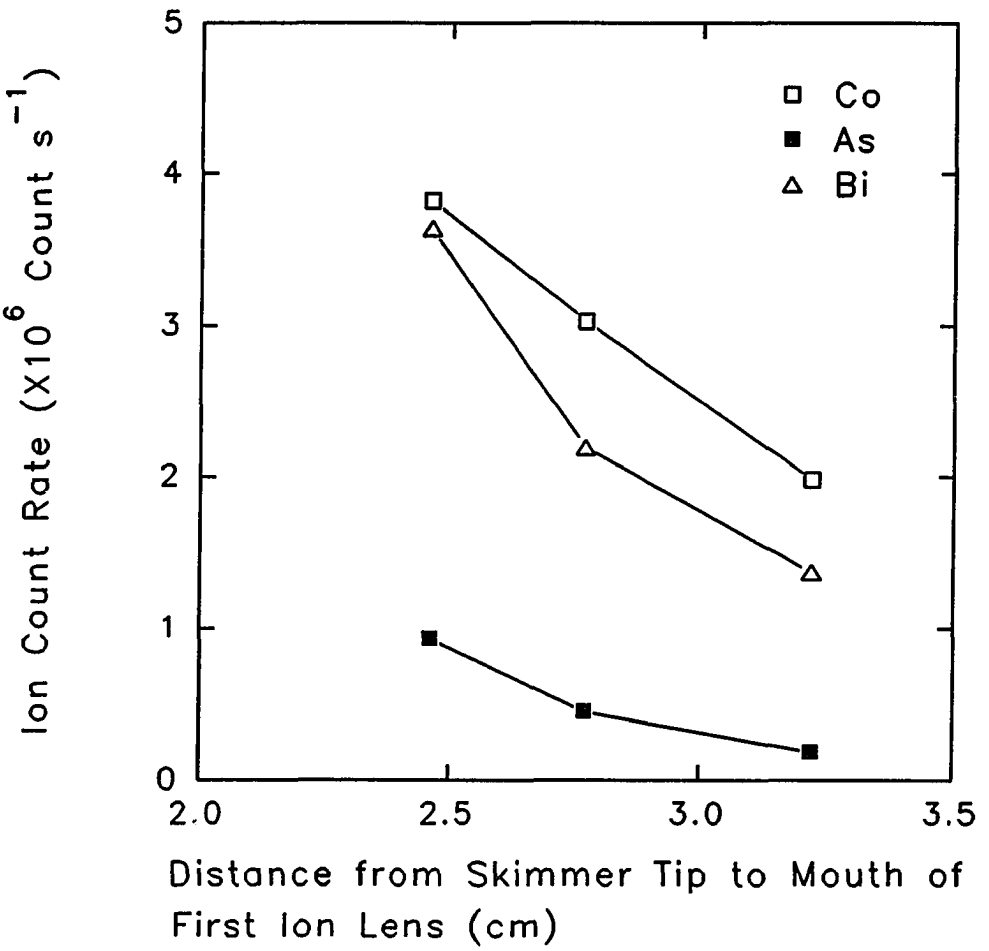

Figure 6. Ion count rates as a function of separation between skimmer tip and entrance to first ion lens.

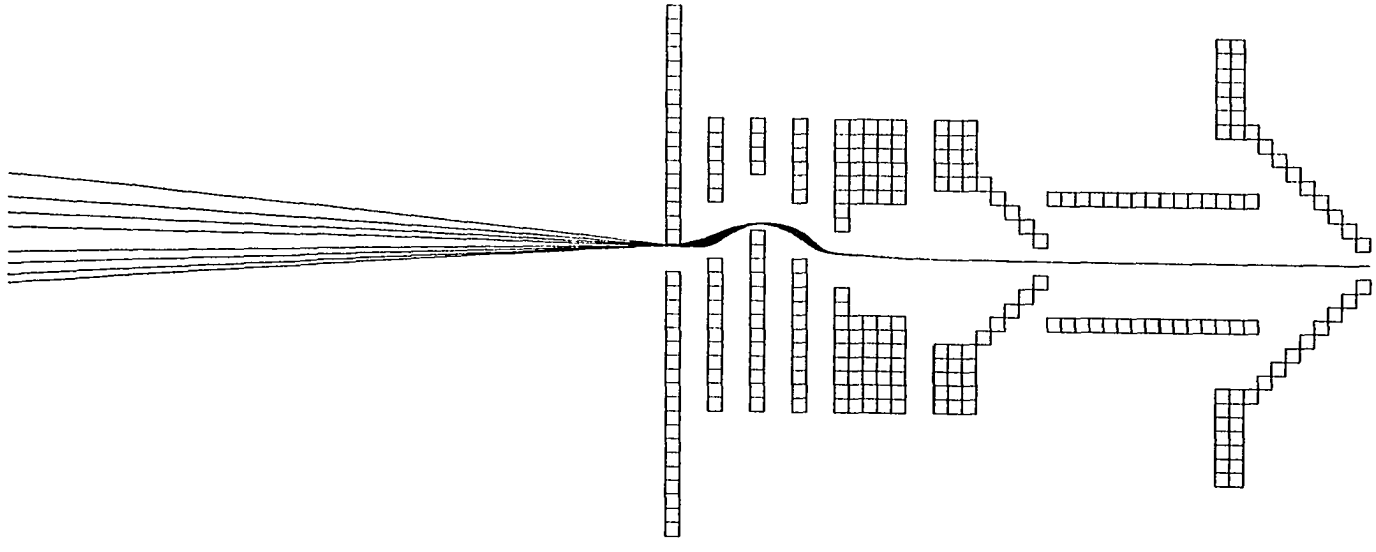

Figure 7. Trajectories for ions of varying kinetic energies. The skimmer is at the far right, and the differential pumping aperture is at the far left. The highest trajectory is from the 4 eV ions, and the lowest trajectory is from the 11 eV ions.

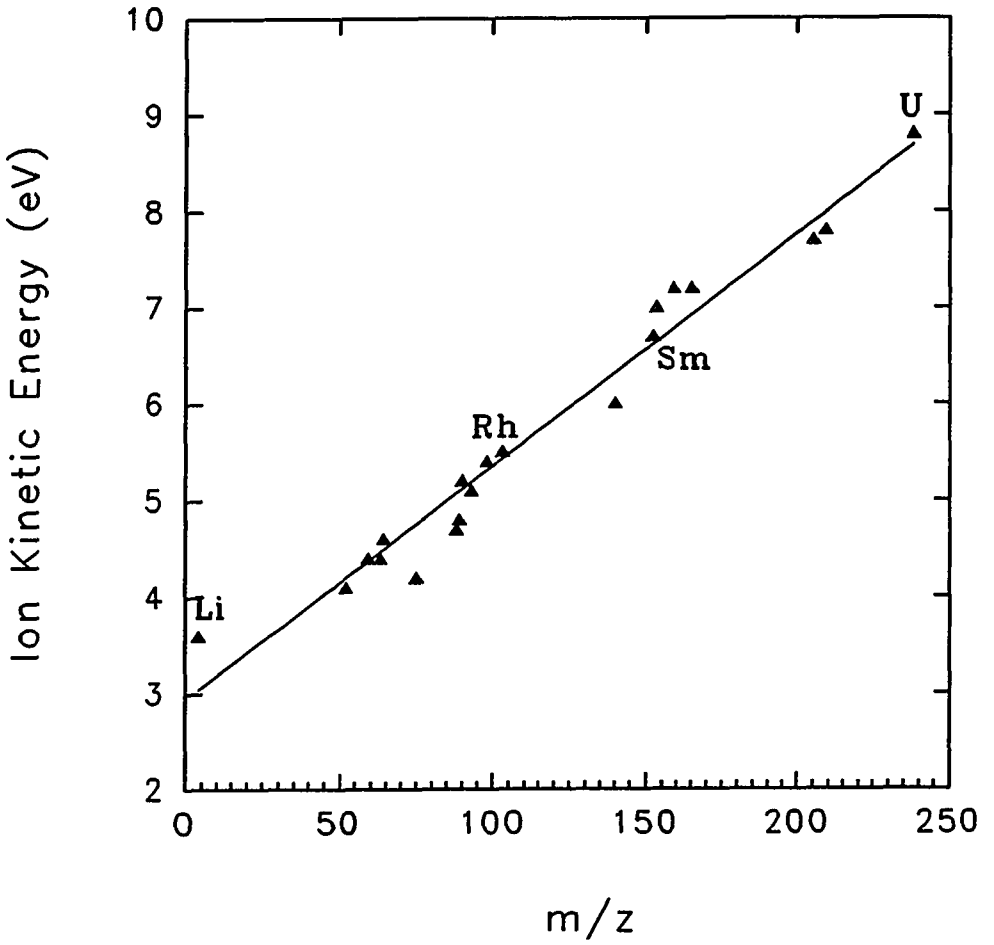

Figure 8. Maximum Ion kinetic energies as a function of atomic mass.

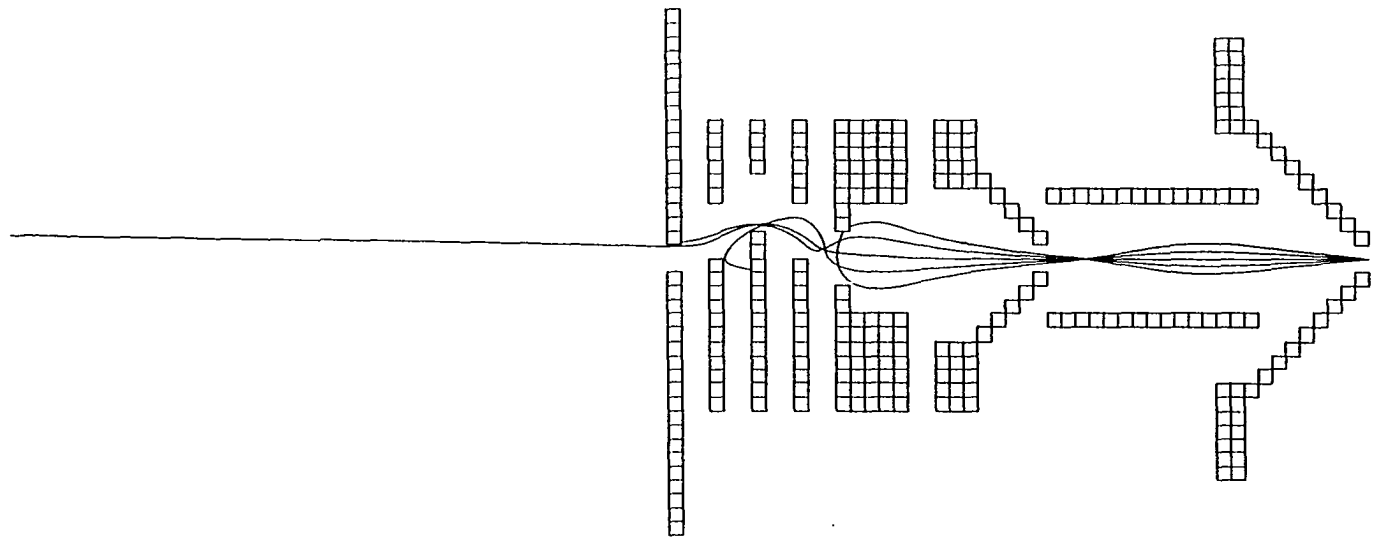

A

Figure 9. Ion trajectories for 7 eV ion with different exit angles and radial positions leaving the skimmer. In A), the exit angles are -6°, -3°, 0°, +3°, +6°. In B), the radial spacing between trajectories is 1.6 mm. Both figures show that only the ion that enters precisely on axis (0^0) passes through the lens.

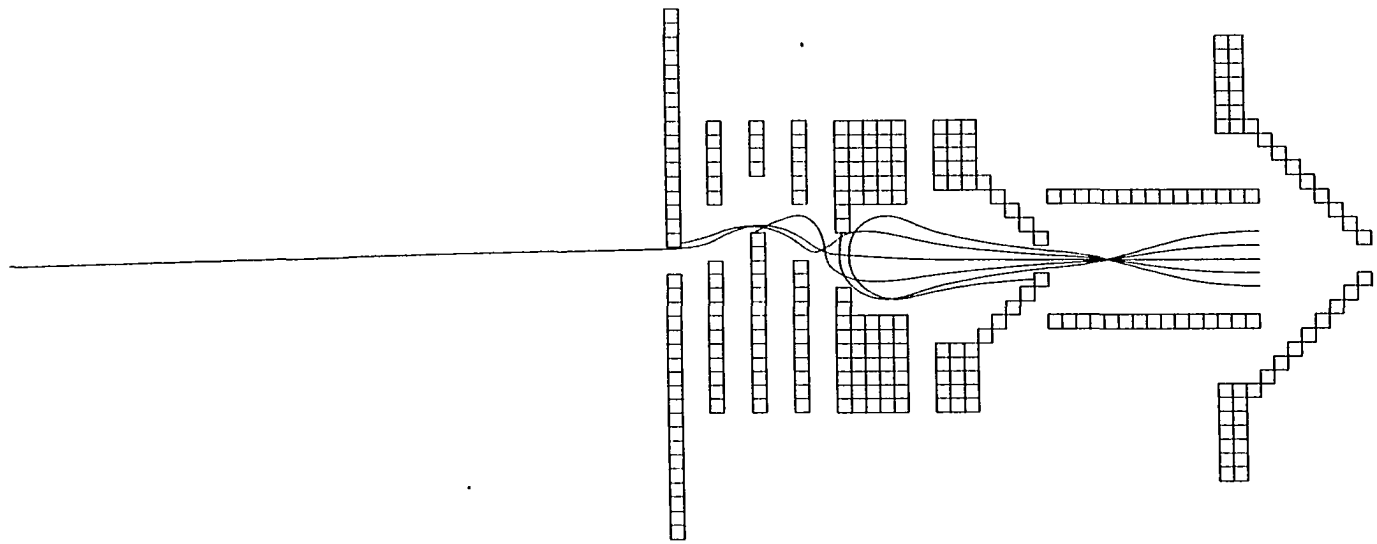

B

Figure 9. (continued)

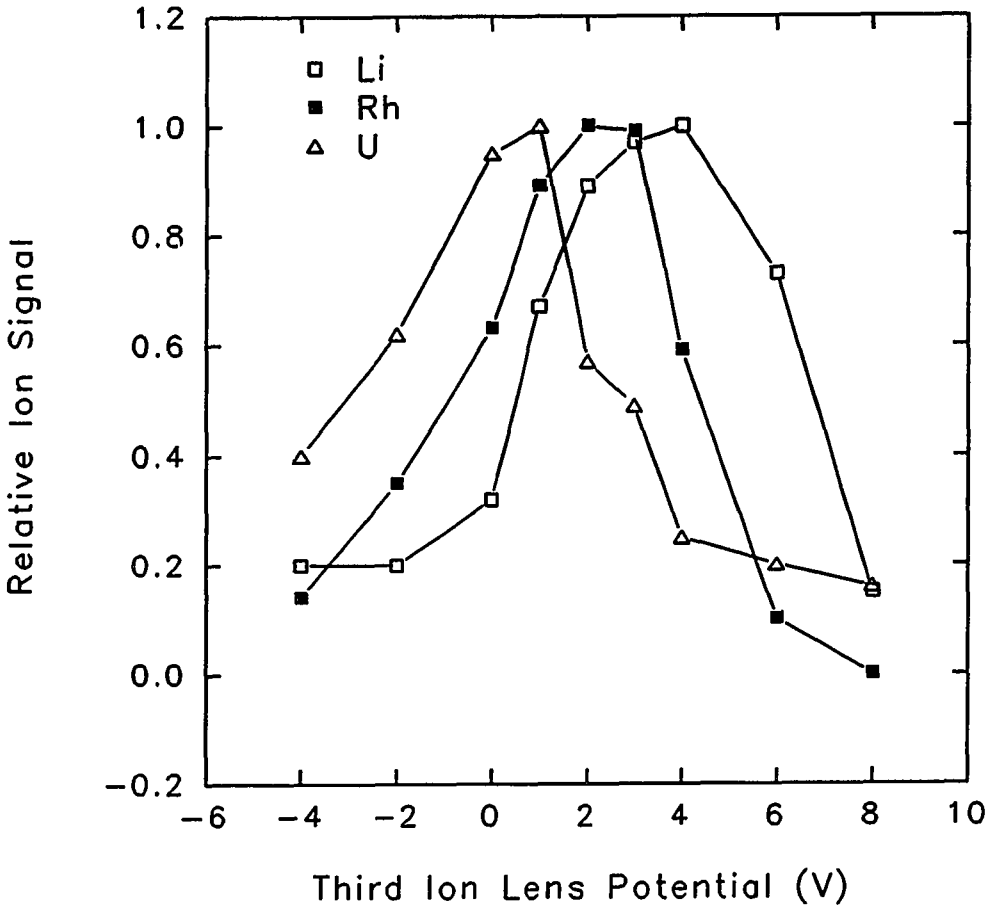

Figure 10. Normalized ion signals as a function of V_3 (see Figure 2) for Li^+, Rh^+, and U^+.

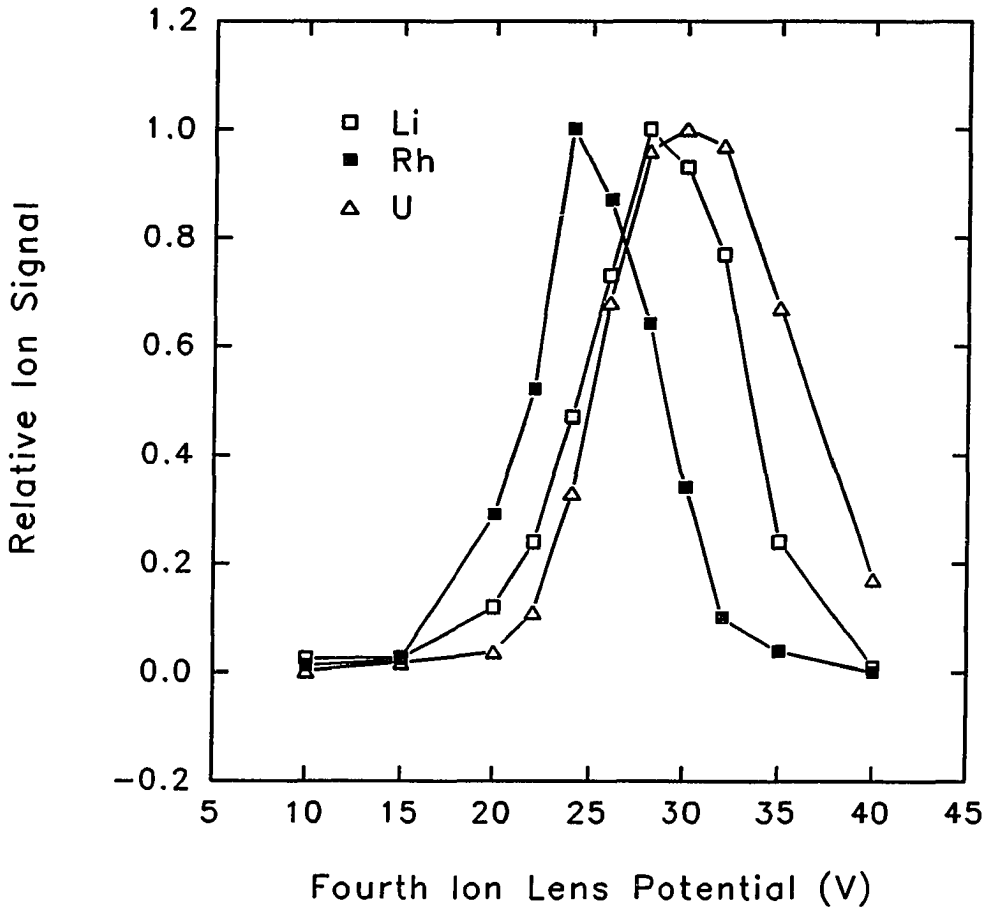

Figure 11. Normalized ion signals as a function of V_4 for Li^+, Rh^+, and U^+.

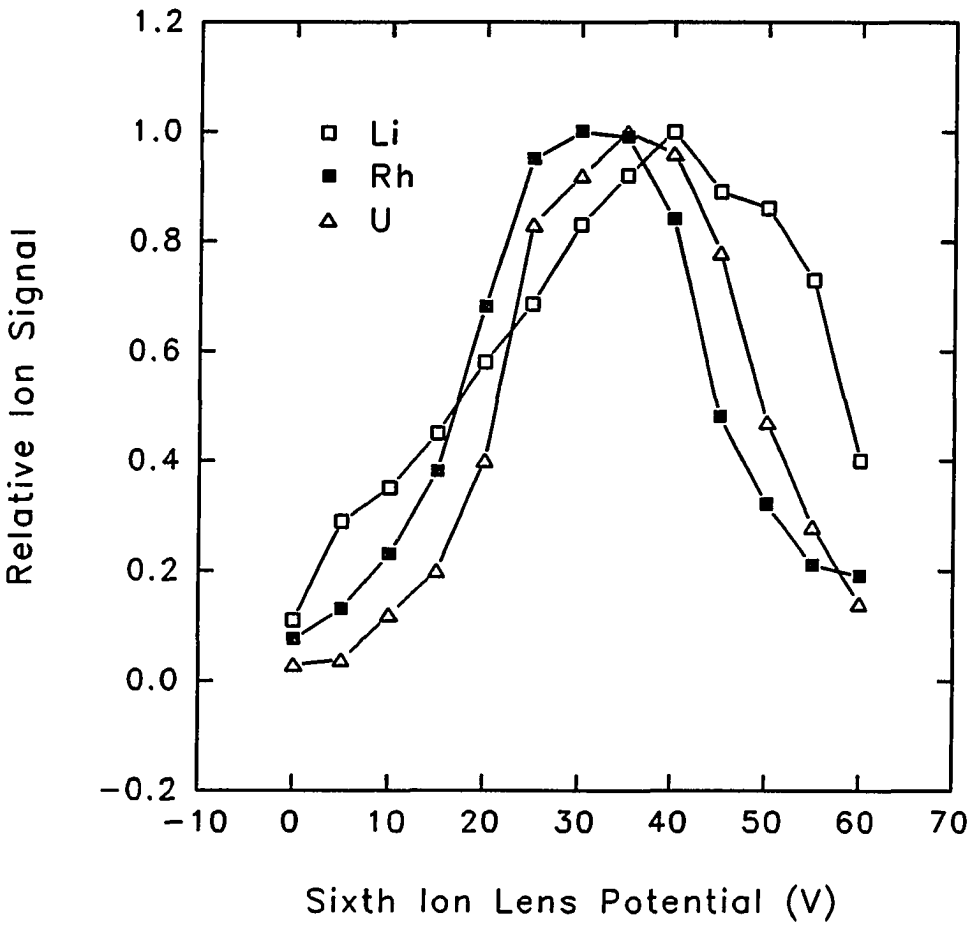

Figure 12. Normalized ion signals as a function of V_6 for Li^+, Rh^+, and U^+.

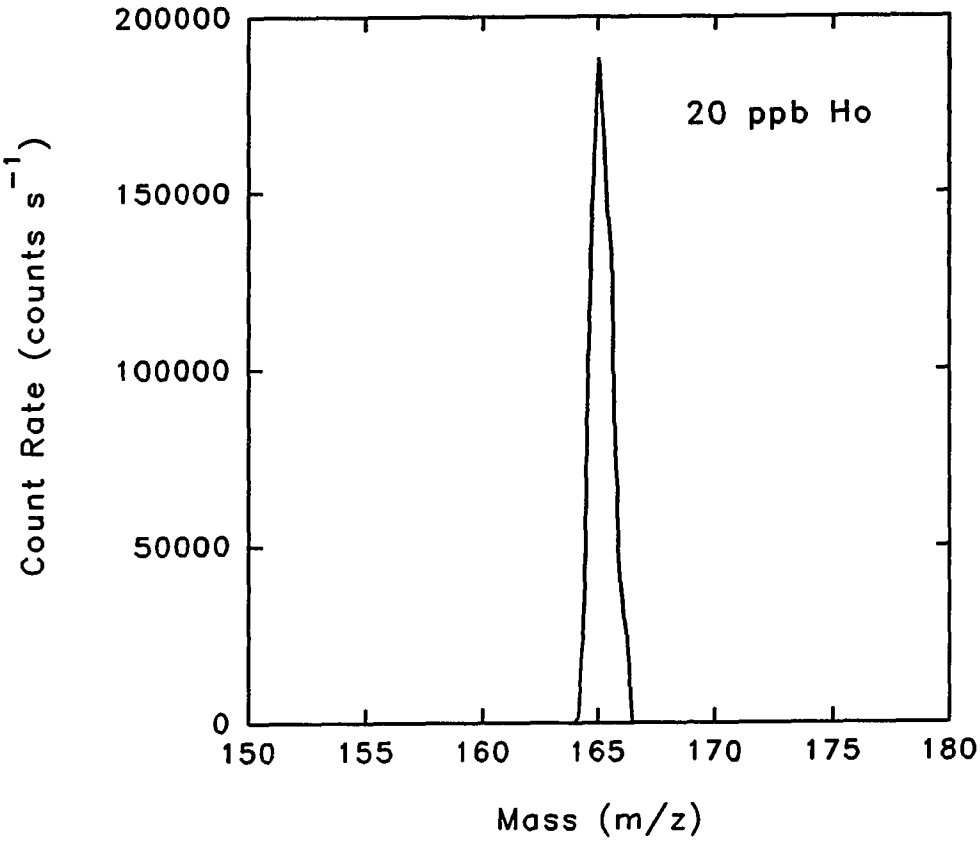

Figure 13. Mass spectrum of Ho at 20 ppb with Channeltron detector.

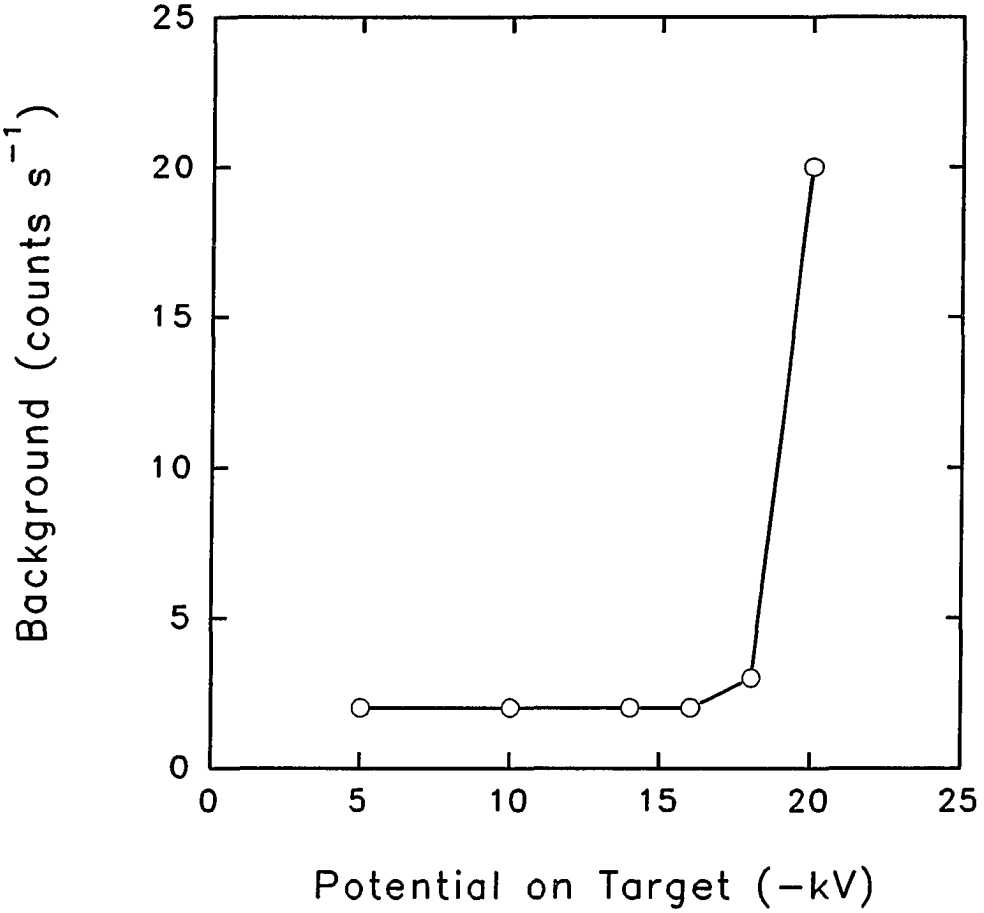

Figure 14. Background as a function of target potential with Daly detector.

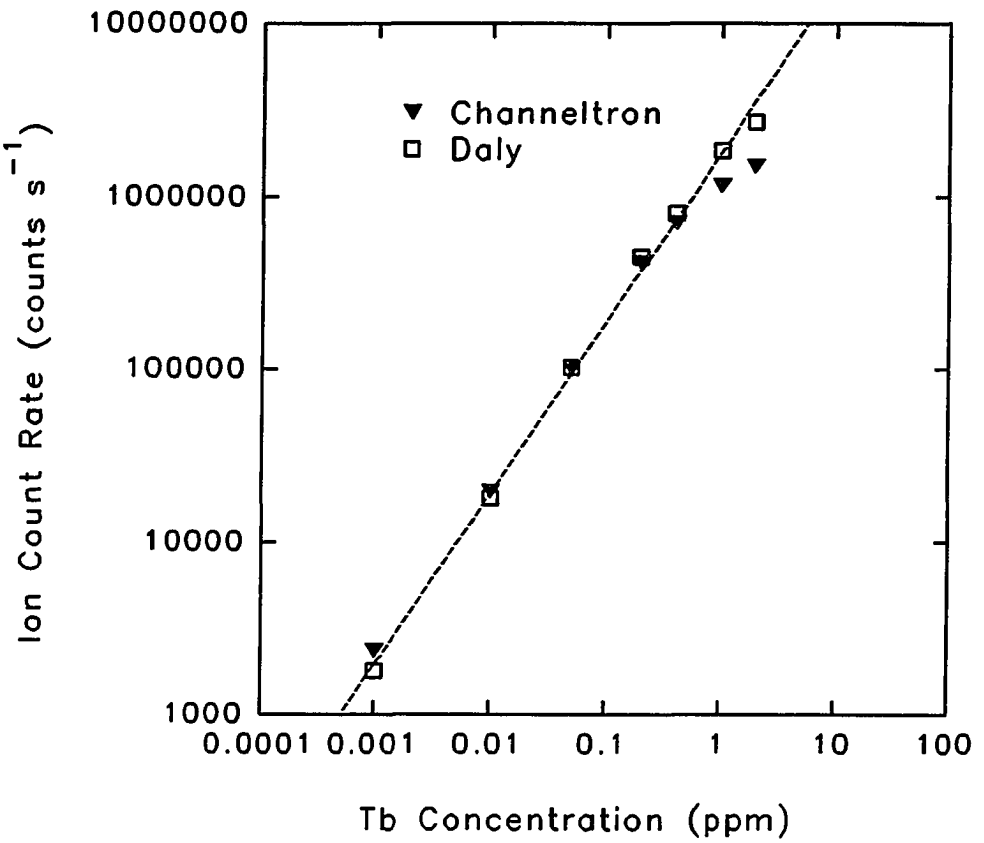

Figure 15. Calibration curves for $^{159}Tb^{+}$ with Daly detector (□) and channeltron electron multiplier (▼). The dashed line represents the extrapolation of the linear section for Daly detector. The gain of the photomultiplier tube was adjusted to bring the linear sections of the two curves into coincidence.

PAPER II.

INDUCTIVELY COUPLED PLASMA-MASS SPECTROMETRY WITH AN ENLARGED SAMPLING ORIFICE AND OFFSET ION LENS

II. POLYATOMIC ION INTERFERENCES AND MATRIX EFFECTS

INTRODUCTION

Although ICP-MS is a highly successful method for elemental and isotopic analysis, some elements still cannot be determined readily in important samples because of interferences. For example, polyatomic ions such as ArO^+, ArN^+, Ar_2^+, ClO^+, and $ArCl^+$ hamper determination of Fe, Se, V and As. These interfering species can be attenuated somewhat by tactics such as mixed gas plasmas (1-5), removal of solvent (1,2,6-11), and polishing the inside of the sampling cone (12). A high-resolution MS (13,14) or a collision cell (15-17) can also be used for this purpose, with the expense associated with the additional hardware necessary.

ICP-MS also suffers from matrix interferences, in which the matrix concentration affects the analyte signal. Generally, the analyte signal is suppressed as the matrix concentration increases (6,18-21), although signal enhancements can sometimes be observed (22). The extent of the interference depends on the plasma operating conditions and the atomic masses of both the matrix and analyte ion. Usually, the interference problem is worst for a light analyte ion in the presence of a heavy matrix ion (19). Thus, the most severe matrix interference is that of uranium matrix on lithium analyte. Gillson et al. (23) and Tanner (24) attribute the matrix interferences mainly to space-charge effects that disperse the ion beam and cause loss of ions behind the skimmer and in the ion lens. Presently, this space charge effect is the most cogent explanation of the matrix interference problem.

Reasonable methods of diagnosing and compensating for interferences due to either polyatomic ions or matrix effects are available. For example, the interference of $^{40}Ar^{35}Cl^+$

on $^{75}As^+$ can sometimes be estimated by measuring the abundance of $^{40}Ar^{37}Cl^+$ and applying the appropriate isotopic correction to the total signal at m/z = 75. Internal standardization is employed routinely to correct for matrix interferences; standard additions and isotope dilution can also be employed for this purpose (11,25). As a general rule, the compensation provided by these methods is more reliable if the extent of the interference is less severe in the first place.

The first paper in this duo described the performance and characterization of a new ion lens system for ICP-MS (26). The present paper shows that this same ICP-MS device has relatively low levels of many troublesome polyatomic ions. Minor adjustments to the lens voltages also reduce the severity of matrix effects substantially. These latter results are compared with those of Ross and Hieftje, who found that matrix effects were greatly reduced by removing the ion lens between the skimmer and differential pumping orifice (27).

EXPERIMENTAL

ICP-MS Instrumentation

The ICP-MS device and its performance are described in the companion paper (26). Conditions particular to the present paper are noted in Table I. Only the Channeltron detector was used.

As shown in Figure 1, the same physical arrangement of ion lens electrodes was used throughout. Three different sets of lens voltages were evaluated. These three configurations differed mainly in the voltages applied to the first cylinder (V_1) and the second electrode of ion lens, the copper cone (V_2). The lens voltages for each lens configuration (Figure A, B, or C) are listed in Table 2. Lens A (A, Figure 1) was used throughout the companion paper and for the studies of background spectra in the present paper. The first cylinder was biassed at +3 V and the voltages applied to the other electrodes were adjusted to maximize Y^+ signal. For lens B (B, Figure 1), the first cylinder was grounded and the other voltages were re-adjusted to maximize Y^+ signal again. The optimum voltages for lens B were only slightly different from those for lens A. Finally, for lens C (C, Figure 1), both the first cylinder and the cone were grounded. Many of the other lenses then required substantial adjustments to the applied voltages to re-maximize the ion signal.

After the optimum lens voltages were found in this manner for each configuration, the aerosol gas flow rate was re-adjusted to maximize Y^+ signal. As shown in Table I, each of the three lens configurations required slightly different aerosol gas flow rates. With the load coil geometry used with this device, the plasma potential and ion kinetic energy varied

somewhat with aerosol gas flow rate, which probably caused the interdependence of aerosol gas flow rate and lens voltages.

Solutions, Solvents and Standards

Standards were prepared by diluting aliquots of commercial stock solutions (1000 ppm, Fisher) with distilled, deionized water (18 MΩ, Barnstead). In matrix effect studies, the analyte concentration was deliberately kept rather high (1 ppm) to minimize possible contamination from impurities in the matrix elements. Blank solutions containing the matrix without analyte were analyzed; contamination was negligible. The 1% HNO_3 and 1% HCl were prepared by diluting ultra pure acids (Ultrex II, reagent grade, J. T. Baker) in distilled, deionized water. The lead matrix was so-called "common lead," i.e., the isotope ratios were $^{207}Pb/^{206}Pb \sim 1/1$, $^{208}Pb/^{206}Pb \sim 2/1$.

Matrix Effect Studies

The analyte elements (Co, Y and Cs) and the matrix elements (Sr, Tm and Pb) were chosen because they are efficiently ionized in the plasma and they have significantly different atomic masses. The mass analyzer was scanned repetitively in multichannel mode through a mass window 30 m/z units wide spanning each analyte peak. Thus, a separate set of scans was obtained for each analyte in each matrix. The solutions were analyzed in the following order: analyte only, analyte + matrix, analyte only. The third step (i.e., re-analysis of the solution containing only analyte) was continued until the analyte signal recovered to its original value, which took approximately two minutes. The process was repeated 6-8 times

successively for each analyte in each matrix; the average matrix effects are reported below. The mass analyzer was then adjusted to the appropriate m/z window for the next analyte, and the process was repeated.

In this fashion, matrix effects were measured for each analyte in each matrix under each lens configuration (see Figure 1 and Table II). All the results reported subsequently in Figures 9-11 were obtained successively on one day without turning the plasma off. The entire sequence of matrix effect experiments was repeated on three separate days, with consistent results.

RESULTS AND DISCUSSION

Polyatomic Ions from Deionized Water and HNO_3 Solutions

Background spectra from m/z = 42 to 85 are shown for deionized water and 1% HNO_3 in Figures 2 and 3. The lower frame in each figure is merely plotted with a more sensitive vertical scale so that weak peaks are evident. The weaker peaks appear noisy in the expanded frames because only a few counts are recorded in each channel for many of them.

Inspection of Figures 2 and 3 shows that the usual polyatomic ions are not very intense with this ICP-MS instrument. The worst one is $^{40}Ar_2^+$ at m/z = 80, and it is only ~ 5000 counts s^{-1}. The minor isotope peaks of Ar_2^+ are not clearly distinguishable. Peaks at m/z = 44 (probably CO_2^+) and m/z = 84 (probably $^{84}Kr^+$) are next in abundance to Ar_2^+. From deionized water $^{40}Ar^{16}O^+$ is only ~200 counts s^{-1}. The 1% HNO_3 is a bit impure, as peaks from ClO^+ (m/z = 51 and 53), $^{55}Mn^+$, Cu^+ (m/z = 63 and 65), and perhaps $^{75}As^+$ and/or $^{40}Ar^{35}Cl^+$ are seen. For either solvent, the absolute levels of these polyatomic ions are far below those usually seen on most other ICP-MS devices. For reference, the spectrum of Fe at 0.5 ppm is shown in Figure 4. Compared to the blank spectrum (Figure 3), both $^{54}Fe^+$ and $^{56}Fe^+$ are easily seen at this level.

Polyatomic Ions from HCl and NaCl Solutions

Chlorine in any form in the sample generally leads to the troublesome polyatomic ions ClO^+ and $ArCl^+$. Background spectra from 1% HCl and 0.25% NaCl (the equivalent

of 0.1 % Na) are shown in Figures 5 and 6. Note that these samples are being introduced with an ultrasonic nebulizer, and the desolvation system does not remove either HCl or NaCl. $ArCl^+$ is barely observable from either solution, and $^{35}Cl^{16}O^+$ is only 200 - 400 counts s^{-1}. The Cu^+ observed from both solutions could be from Cu impurity or possibly from Cu^+ ablated from the conical ion lens, which is made from copper. In the spectrum from 0.25% NaCl, the ratio of the peak at m/z = 63 to that at m/z = 65 is too high for Cu^+, so there is probably some $ArNa^+$ present at ~ 100 counts s^{-1}. A curious peak at m/z = 62 is attributed tentatively to Na_2O^+, the sodium analog of water.

Spectra of As at 0.5 ppm in 1% HCl (Figure 7) and Cu and Co at 1 ppm in 0.25% NaCl are provided in Figures 7 and 8. In Figure 7B, $^{40}Ar^{37}Cl^+$ is not distinguishable from background, even though 1% HCl is being introduced with an ultrasonic nebulizer. Some $^{40}Ar^{35}Cl^+$ (~ 150 counts s^{-1}) is probably evident in Figure 8B. Again, these common polyatomic ions containing chlorine are observed only at quite low levels with this device.

Comparison of Polyatomic Ion Levels to Usual Values

A rigorous comparison of the levels of polyatomic ions seen in Figures 2 - 8 to those seen in other quadrupole ICP-MS devices is difficult for several reasons. First, many of the weak peaks shown in Figures 2 - 8 are probably at least partly due to metal impurities in the solvents rather than polyatomic ions. Second, polyatomic ion levels with any ICP-MS instrument are highly sensitive to operating conditions and the methods used for nebulization and solvent removal.

For these reasons, the following discussion compares polyatomic ion levels obtained

recently in two papers that used an ultrasonic nebulizer with conventional desolvation, i.e., heating at ~140 °C followed by condensation at ~0 °C. This nebulizer and desolvator are the same as those used in the present work. In one paper, Xe is added to attenuate polyatomic ions (5). In the other paper, cryogenic desolvation is employed for the same purpose (9). In either case, the count rates and background-equivalent-concentrations (BECs) cited in Tables III and IV relate to the "control" values, i.e., those measured from a "normal" ICP without these additional ways to attenuate polyatomic ions. The BEC is the solution concentration of analyte that yields a net signal for M^+ of the same magnitude as that for the interfering polyatomic ion. A Sciex ELAN Model 250 with upgraded ion optics is used for the comparative data derived from refs. (5) and (9). In general, the ICP operating conditions are selected to yield maximum M^+ signal in each case.

The count rates observed for four of the most troublesome polyatomic ions (ArN^+, ArO^+, ClO^+ and $ArCl^+$) are compared to those seen from our Sciex ELAN instrument in Table 3. For the present work, the total count rates at m/z = 54, 56, 51 and 75 are reported and are assumed to be solely due to the polyatomic ions. Table III shows that the levels of polyatomic ions seen in the present work are indeed much lower than those seen when a comparable nebulizer and desolvator are used on our Sciex ELAN instrument.

BEC values for the two instruments are given in Table IV. The BEC values are particularly useful for comparison because they account for both the background and the analyte signals. In general, the BEC values seen in the present work are superior to those from ref. (5). However, the measurements in ref. (5) were performed with a home-made ultrasonic nebulizer (28), which was similar in principle but did not yield as intense an

aerosol as the commercial nebulizer used in the present work and in ref. (9). The BEC values from the present work are comparable to or perhaps somewhat worse than those from ref. (9). Although the absolute levels of polyatomic ions are quite low for the instrument described in the present work and the companion paper (26), the count rates for analyte ions are also lower than would usually be expected when an ultrasonic nebulizer is employed. The BEC values reported for ref. (9) in the far right column of Table IV are among the best values obtained with commercial instruments. The higher values from ref. (5) are more typical.

A detailed comparison of the BEC values in Table IV with those obtained on commercial instruments with the usual pneumatic nebulizers is even more questionable, so only some typical examples are cited. Recent desolvation studies by Lam and McLaren (1), Tsukahara and Kubota (10), and Jakubowski et al. (7,8) report BEC values for $^{56}Fe^{+}$ of 74 - 190 ppb with a spray chamber at 0 - 30 C. These BECs improve to 14 - 55 ppb with a desolvation system like that used in the present work. Evans and Ebdon report data that correspond to a BEC of 140 ppb As in 1% HCl with a spray chamber cooled to 5 °C and no additional substances (e.g., N_2, O_2 or organic solvent) added to the plasma (29). Jarvis et al. (11) list BECs for a VG PQ2 with a cooled spray chamber. These values are cited for Co and are corrected below for isotopic abundance for Fe and for the ionization efficiency of As (estimated to be 30% (11)). With these corrections, the values of Jarvis et al. correspond to BECs of 200 ppb Fe at m/z = 54 and 90 ppb Fe at m/z = 56 in 1% HNO_3. In 1% HCl, BEC values of 230 ppb V and 120 ppb As are estimated (11).

Either of these values with pneumatic nebulizers are substantially poorer than our

BECs from Table IV. At any rate, the instrument described in the present work yields very low levels of polyatomic ions and BECs that are at least as good as the best values produced by typical commercial instruments based on quadrupoles. Newfangled tricks like adding N_2 or Xe (1,3-5,29) or cryogenic desolvation (2,9) could attenuate some of the interfering ions to still lower levels, if indeed they are due to polyatomic ions and are not simply metal impurities from the solvents. As described in the companion paper (26), the background at higher m/z values (i.e., above ~ m/z = 80) is also very low (~ 0.4 counts s^{-1}) for the device described in the present work.

Metal Oxide Ions

Under the conditions that yield maximum M^+ signal, refractory metal oxide ions are fairly abundant, i.e., the count rate for MO^+ is 10% of that for M^+ for M = La and U. Moving the sampling position slightly downstream to 15 mm and decreasing the aerosol gas flow rate from 1.30 L min^{-1} to 1.1 L min^{-1} reduces the MO^+/M^+ ratios substantially to the values shown in Table V. This adjustment of operating conditions induces only a minor sacrifice of 10% to 20% loss of M^+ signal. The values of 0.5% for MoO^+/Mo^+ and ~1% for LaO^+/La^+ and UO^+/U^+ are quite typical of ICP-MS devices with this type of desolvation (i.e., heating at 140 °C followed by cooling at ~0 °C) (1,7,9,10).

The general observation that weakly-bound polyatomic ions like $ArCl^+$ and ArO^+ are at quite low levels while refractory oxide ions like LaO^+ and UO^+ are at usual levels is interesting. Hieftje (30) has suggested that the high degree of spatial selectivity of the lens discriminates against ArO^+, $ArCl^+$, etc. If these weakly-bound ions are not present in the

plasma but are created by reactions during the extraction process in the boundary layer inside the edge of the sampler or skimmer, they would not be particularly abundant along the central axis of the beam leaving the skimmer. In contrast, many other ICP-MS devices block photons with a solid baffle along the center line. Such lenses accept only ions that leave the skimmer off-center (31). Perhaps the off-center section of the beam is enriched in polyatomic ions made in the boundary layer; these weakly-bound polyatomic ions are therefore more abundant in spectra from these devices.

Vaughan and Horlick conclude that metal oxide ions are made largely during the extraction process, but their study merely proves that extra metal oxide ions can be seen if the sampling orifice is too small (32). The author's view is that refractory metal oxide ions like LaO^+ and UO^+, which have dissociation energies of 8 to 9 eV, are not completely dissociated in the plasma (33-35). These ions pass through the sampler and skimmer just like the atomic analyte ions and are not rejected preferentially by the lens. Hence, the spatial selectivity of the offset ion lens does not discriminate against MO^+, and the levels of MO^+ seen in the present work are typical of those seen on most ICP-MS devices.

Matrix Interferences

These experiments are performed under conditions that yield maximum Y^+ signal for each lens configuration. The sampling position is 11 mm. Each lens requires a slightly different value of aerosol gas flow rate, as shown in Table 1. The measured interference effects are plotted for each analyte and matrix for the three lens configurations (A, B, and C, Figure 1) in Figures 9 - 11. Again, a highly-efficient ultrasonic nebulizer is used. The

high rate of introduction of matrix with this nebulizer would be expected to induce substantial matrix effects (36). In each case, the analyte signal is suppressed severely with lenses A and C, whereas little or no suppression is seen with lens B. For example, Sr and Tm at 10 mM do not cause measurable interference on any of the three analytes with lens B. Lead at 10 mM suppresses Co^+ and Y^+ signal by only 20% (Figures 9 and 10) and causes little interference on the heavier Cs^+ (Figure 11).

Sensitivities and detection limits with the three lenses are given in Table VI. Lens A yields the best sensitivity but is highly vulnerable to matrix effects. Grounding the first cylinder (lens B) involves only a modest sacrifice in sensitivity and detection limits, and matrix effects are minimal. The basic reasons why lenses A and B should result in substantially different matrix effects are not clear at this time. The two configurations differ mainly by only +3 V on the first cylinder (V_1, Figure 1), with only minor differences in the voltages applied to the other electrodes. The extent of matrix effects does not simply increase with the total transmission, because the transmissions of lenses A and B are not that different, and lens C has both poor transmission (i.e., poor sensitivity in Table VI) and bad matrix effects.

The matrix concentrations (10 mM) in the present work are the same as those used by Ross and Hieftje, who introduced samples with a conventional pneumatic nebulizer (27). The small matrix effects observed with lens B are considered comparable to their results with no lens in the second stage, when the differences in rate of transport of matrix from the two nebulizers are considered. The measures taken to reduce matrix effects (i.e., grounding the first lens, rather than removing all the lenses) are quite different in our study.

Effect of Matrix on Lens Voltages

At times, we have observed that introduction of a matrix element can affect the apparent voltage applied to the first lens (37). A similar phenomenon is seen in the present work with lens A. During nebulization of a blank solution, V_1 is set to +3 V and the other lenses are adjusted to maximize signal. When a matrix solution is added, the apparent voltage on lens 1 decreases, as shown in Table VII. If the matrix effect is measured without changing the power supply setting that feeds lens 1, analyte signals are suppressed substantially (Figure 12). If the voltage output of the power supply is re-adjusted to read +3 V with the matrix present, the effect of matrix on analyte signal is not severe, as also shown in Figure 12. The matrix effects on Co^+ and Y^+ signal can also be alleviated in much the same way. The deviation of apparent voltage on lens 1 is greatest for the heavier matrix element (Pb in Table VII), which again agrees roughly with our previous observations (37).

This procedure could prove useful in that it allows use of the more sensitive lens A configuration with minimal matrix effects. Caruso and co-workers have reported at length on a successful tactic for mitigating matrix effects, which they call matrix tuning. The ion lens voltages are adjusted to maximize analyte signal with the matrix actually present. This adjustment of lens voltages is sometimes done during nebulization of the actual sample of interest, rather than a standard (38,39). This procedure differs in detail from our method of resetting lens 1 to its original voltage with the matrix present. Nevertheless, both approaches mitigate matrix effects significantly, perhaps for similar basic reasons. All these instrumental modifications for attenuating matrix effects require much more fundamental and applied study before they are understood properly.

CONCLUSION

This paper and its companion (26) describe a quadrupole ICP-MS device with the following attributes: low levels of polyatomic ions, minimal matrix interferences, low background, and high tolerance to plugging from deposited solids. The analyte sensitivity is ~10X lower than that expected from a commercial instrument with an ultrasonic nebulizer. Experiments to test these performance figures for the analysis of difficult samples with this ICP-MS device are under way in our laboratory.

LITERATURE CITED

1. Lam, J. W.; McLaren, J. W. J. Anal. At. Spectrom. 1990, 5, 419-424.
2. McLaren, J. W.; Lam, J. W.; Gustavsson, A. Spectrochim. Acta, Part B 1990, 45B, 1091-1094.
3. Lam, J. W.; Horlick, G. Spectrochim. Acta, Part B 1990, 45B, 1313-1325.
4. Ebdon, L.; Evans, E. H.; Barnett, N. W. J. Anal. At. Spectrom. 1989, 4, 505-508.
5. Smith, F. G.; Wiederin, D. R.; Houk, R. S. Anal. Chem. 1991, 63, 1458-1462.
6. Houk, R. S.; Fassel, V. A.; Flesch, G. D.; Svec, H. J.; Gray, A. L.; Taylor, C. E. Anal. Chem. 1980, 52, 2283-2289.
7. Jakubowski, N.; Feldman, I.; Stuewer, D. Spectrochim. Acta, Part B 1992, 47B, 107-118.
8. Jakubowski, N.; Feldman, I.; Stuewer, D.; Berndt, H. Spectrochim. Acta, Part B 1992, 47B, 119-129.
9. Alves, L. C.; Wiederin, D. R.; Houk, R. S. Anal. Chem. 1992, 64, in press.
10. Tsukahara, R.; Kubota, M. Spectrochim. Acta, Part B 1990, 45B, 581-589.
11. Jarvis, K. E.; Gray, A. L.; Houk, R. S. Handbook of Inductively Coupled Plasma Mass Spectrometry; Blackie: Glasgow, 1991, pp. 16, 44, 132, and 164-171.
12. Hutton, R. C. U.S. Patent 4760253, 1988.
13. Bradshaw, N.; Hall, E. F. H.; Sanderson, N. E. J. Anal. Atomic Spectrom. 1989, 4, 801-803.
14. Morita, M.; Ito, H.; Uehiro, T.; Otsuka, K. Anal. Sci. (Japan) 1989, 5, 609-610.

15. Rowan, J. T.; Houk, R. S. Appl. Spectrosc. 1989, 43, 976-980.

16. King, F. L.; Harrison, W. W. Int. J. Mass Spectrom. Ion Processes 1989, 89, 171-185.

17. Duckworth, D. C.; Marcus, R. K. Appl. Spectrosc. 1990, 44, 649-655.

18. Olivares, J. A.; Houk, R. S. Anal. Chem. 1986, 58, 20-25.

19. Tan, S. H.; Horlick, G. J. Anal. Atom. Spectrom. 1987, 2, 745-763.

20. Gregoire, D. C. Appl. Spectrosc. 1987, 41, 897-903; Spectrochim. Acta, Part B 1987, 42B, 895-907.

21. Kawaguchi, H.; Tanaka, T.; Nakamura, T.; Morishita, M.; Mizuike, A. Anal. Sci. (Japan) 1987, 3, 305-308.

22. Beauchemin, D.; McLaren, J. W.; Berman, S. S. Spectrochim. Acta, Part B 1987, 42B, 467-490.

23. Gillson, G. R.; Douglas, D. J.; Fulford, J. E.; Halligan, K. W.; Tanner, S. D. Anal. Chem. 1988, 60, 1472-1474.

24. Tanner, S. D. Spectrochim. Acta, Part B 1992, 47B, accepted.

25. Thompson, J. J.; Houk, R. S. Appl. Spectrosc. 1987, 41, 801-806.

26. Hu, K.; Clemons, P. S.; Houk, R. S. J. Amer. Soc. Mass Spectrom. 1992, submitted.

27. Ross, B. C.; Hieftje, G. M. Spectrochim. Acta, Part B 1991, 46B, 955-962.

28. Bear, B. R.; Fassel, V. A. Spectrochim. Acta, Part B 1986, 41B, 1089-1113.

29. Evans, E. H.; Ebdon, L. J. Anal. Atomic Spectrom. 1989, 4, 299-300.

30. Hieftje, G. M., Winter Conf. on Plasma Spectrochemistry, San Diego, CA, January, 1992, Paper PL-6.

31. Vaughan, M. A.; Horlick, G. Spectrochim. Acta, Part B 1990, 45B, 1301-1311.

32. Vaughan, M. A.; Horlick, G. Spectrochim. Acta, Part B 1990, 45B, 1289-1299.

33. Douglas, D. J. Fundamental Aspects of ICP-MS, in ICPs in Analytical Atomic Spectrometry, 2nd ed., A. Montaser and D. Golightly, Eds., VCH: New York, 1992.

34. Longerich, H. P. J. Anal. Atomic Spectrom. 1989, 4, 491-497.

35. Kubota, M.; Fudagawa, N.; Kawase, A. Anal. Sci. (Japan) 1989, 5, 701-706.

36. Tarr, M. A.; Zhu, G.; Browner, R. F. Appl. Spectrosc. 1991, 45, 1424-1432.

37. Crain, J. S.; Houk, R. S.; Smith, F. G. Spectrochim. Acta, Part B 1988, 43B, 1355-1364.

38. Wang, J.; Shen, W. L.; Sheppard, B. S.; Evans, E. H.; Fricke, F. L.; Caruso, J. A. J. Anal. Atomic Spectrom. 1990, 5, 445-449.

39. Sheppard, B. S.; Shen, W. L.; Caruso, J. A. J. Amer. Soc. Mass Spectrom. 1991, 2, 355-361.

Table I. Operating conditions (see also ref (26))

ICP Conditions	
Forward power	1.4 kW
Aerosol gas flow rate[a]	lens A[b] 1.30 L min^{-1}
	lens B[b] 1.25 L min^{-1}
	lens C[b] 1.20 L min^{-1}
Sampling position	13 mm from downstream end of load coil, on center
MS Condition	
Mean DC bias:	
on mass analyzer	-1.0 V
on RF only rods	-65 V
Bias voltages on Channeltron	
sensitivity measurements	-3000 V
matrix effect measurements	-2700 V

[a]These represent the aerosol gas flow rates that yield max. Y^+ signal.

[b]See Figure 1 for diagrams of lenses.

Table I. continued

Data Acquisition	
Background spectra	Multichannel scanning (11)
(Figs. 2-8)	1000 sweeps
	4096 channels from m/z = 42 to 85
	Dwell time 50 μs per channel
Matrix effect studies	See text
Solutions	
Matrix effect studies	1 ppm each analyte
	One matrix element per solution
	at 10 mM
Sensitivity meas.	0.5 ppm Co, Y
	0.2 ppm Cs
Metal oxide meas.	1 ppm Mo
	0.2 ppm La
	0.5 ppm U

Table II. Ion lens potentials for the various lens system[a]

	Ion Lens Potential (V)							
System[b]	V_1	V_2	V_3	V_4	V_5	V_6	V_7	V_8
A	+3	-240	-55	+2.0	-200	+14	-240	-200
B	ground	-240	-61	+3.0	-200	+13	-240	-210
C	ground	ground	-20	+28	-225	+28	-230	-230

[a]Each ion lens voltage was optimized for obtaining maximum Y^+ signals.

[b]Ion lens systems A, B, and C are shown in Figure 1.

Table III. Comparison of count rates for polyatomic ions to other ICP-MS work with ultrasonic nebulization and conventional desolvation[a]

		Count rates (counts s^{-1})		
Interferant	Solution	present work	Ref. (5)	Ref. (9)
$^{40}Ar^{14}N^+$	DDW	60	14,100	1,000
$^{40}Ar^{16}O^+$	DDW	200	72,800	12,000
$^{35}Cl^{16}O^+$	1% HCl	400	24,000	50,000
$^{40}Ar^{35}Cl^+$	1% HCl	150	890	1,200

[a]Aqueous samples, heater temp. ~140 °C, condenser temp. ~0 °C.

Table IV. Comparison of BECs to those obtained in other ICP-MS work with ultrasonic nebulization with conventional desolvation[a]

Analyte	Interferant	BEC (ppb) Present work	Ref. (5)	Ref. (9)
$^{54}Fe^+$	$^{40}Ar^{14}N^+$	4	100	0.8
$^{56}Fe^+$	$^{40}Ar^{16}O^+$	0.7	35	0.7
$^{51}V^+$	$^{35}Cl^{16}O^{+b}$	1.8	15	4
$^{75}As^+$	$^{40}Ar^{35}Cl^{+b}$	1.8	1.4	0.3

[a]Aqueous samples, heater temp. ~140 °C, condenser temp. ~0 °C.

[b]Analyte and interferant measured during nebulization of 1% HCl.

Table V. Sensitivity and MO^+/M^+ ratios for elements that form refractory oxides

Element	M^+ sensitivity, counts s^{-1} mg L^{-1}	Signal ratio MO^+/M^+, %
$^{98}Mo^+$	180000	0.5
$^{139}La^+$	3450000	1.0
$^{238}U^+$	1230000	1.2

Table VI. Analyte sensitivities and detection limits measured with the various lens systems[a]

	Sensitivities (counts mg L^{-1})			Detection limit (ng L^{-1})		
System[b]	Co	Y	Cs	Co	Y	Cs
A	1200000	1900000	3600000	2	1	0.5
B	1000000	1200000	2500000	2	2	0.8
C	180000	480000	1000000	10	4	2

[a]Each system was optimized for maximum Y^+ signal using the conditions listed in Table I and Table II.

[b]Ion lens systems A, B, and C are shown in Figure 1.

Table VII. Influence of matrix element on apparent voltage applied to lens 1

Matrix	Apparent voltage on lens 1[a] (V)
None	+3.0
Sr[b]	+2.5
Tm	+2.0
Pb	+1.0

[a]Measured from output meter on power supply to lens 1.

[b]Matrix elements present at 10 mM.

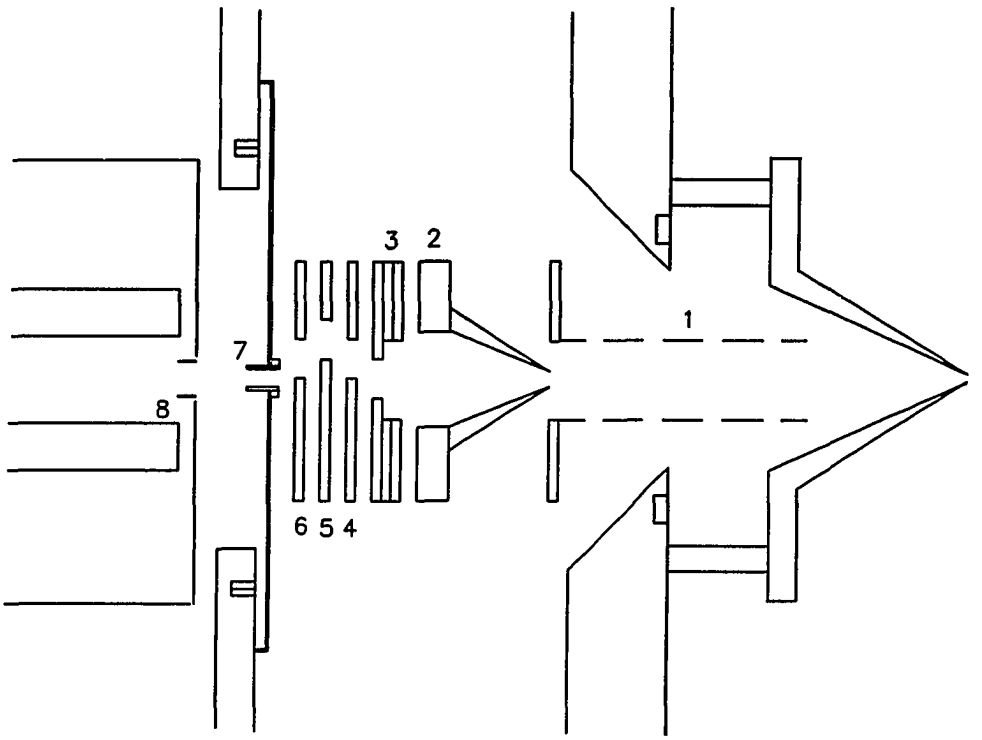

A

Figure 1. Ion lens configurations. The skimmer is at the far right, and the entrance RF-only rods are at the far left. 1: perforated cylindrical electrode, 2: conical electrode, 3-6: electrodes with circular apertures, 7: differential pumping aperture, 8: ELFS entrance to RF-only rods. (A) all ion lens biased; (B) first electrode of ion lens grounded; (C) first and second electrodes of ion lens grounded.

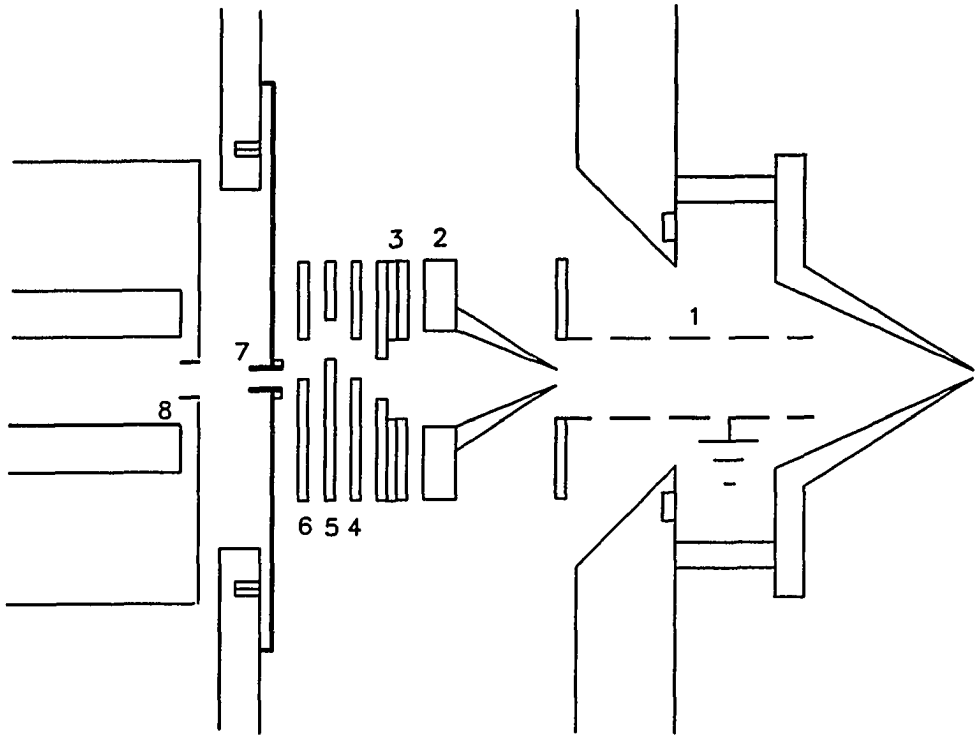

B

Figure 1. (continued)

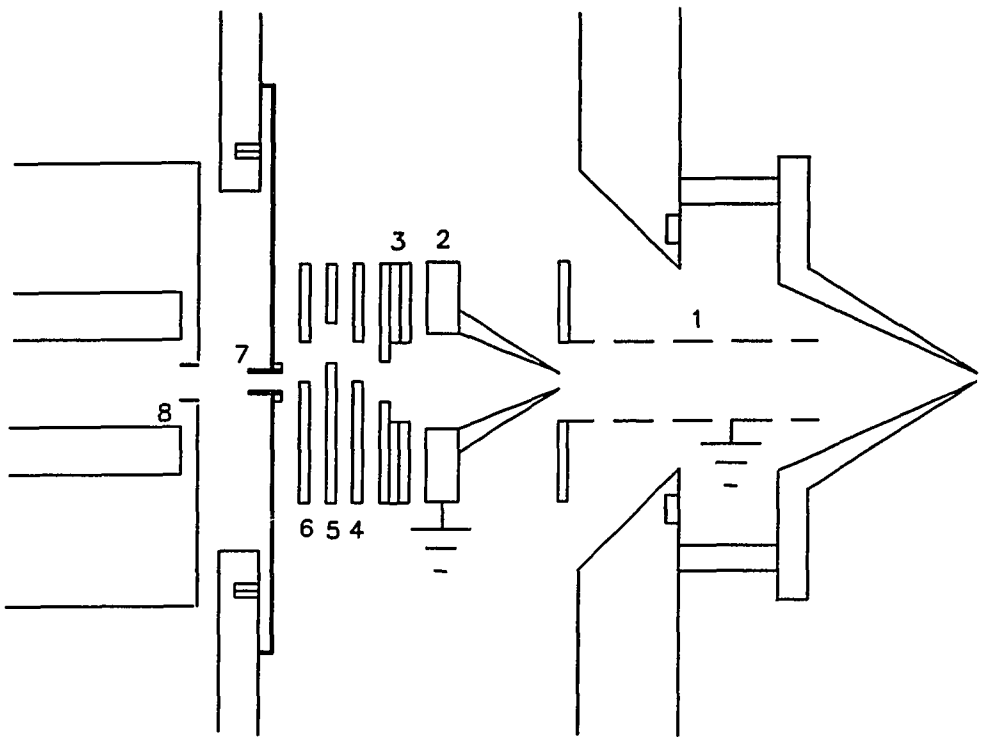

C

Figure 1. (continued)

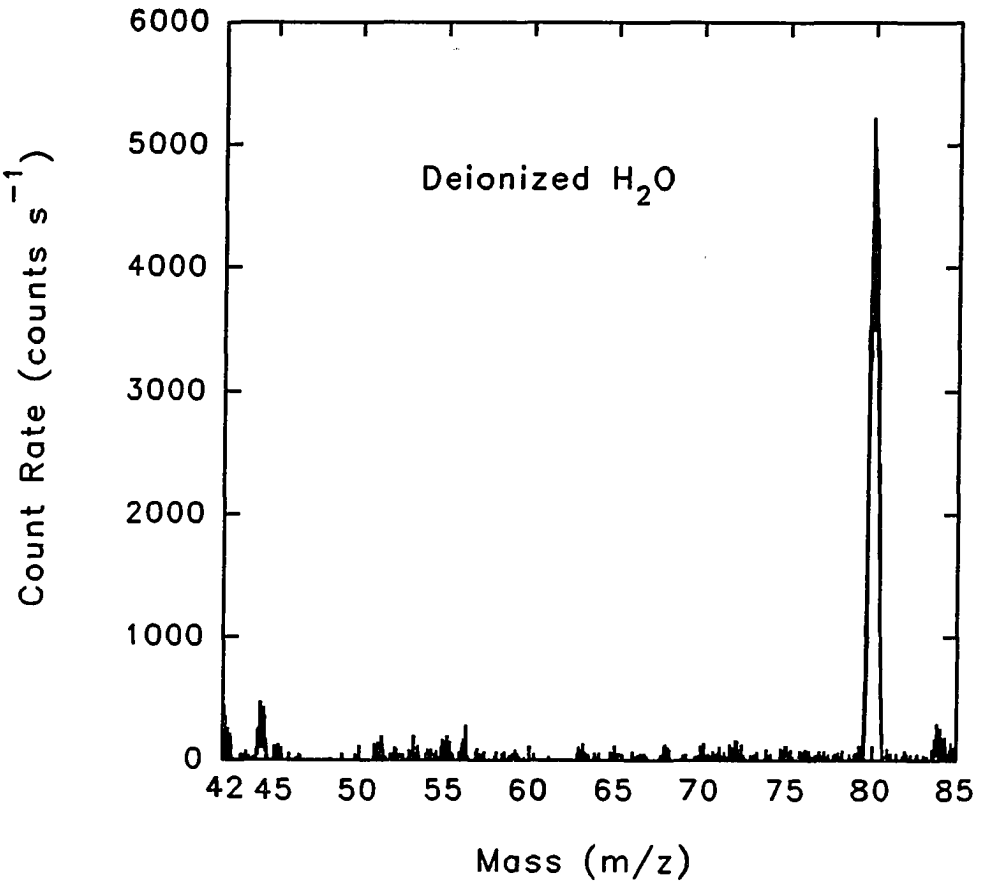

A

Figure 2. Background spectra obtained during nebulization of deionized distilled water for m/z = 42 to 85. The A is the raw spectrum, and the B is scale expanded 10 times.

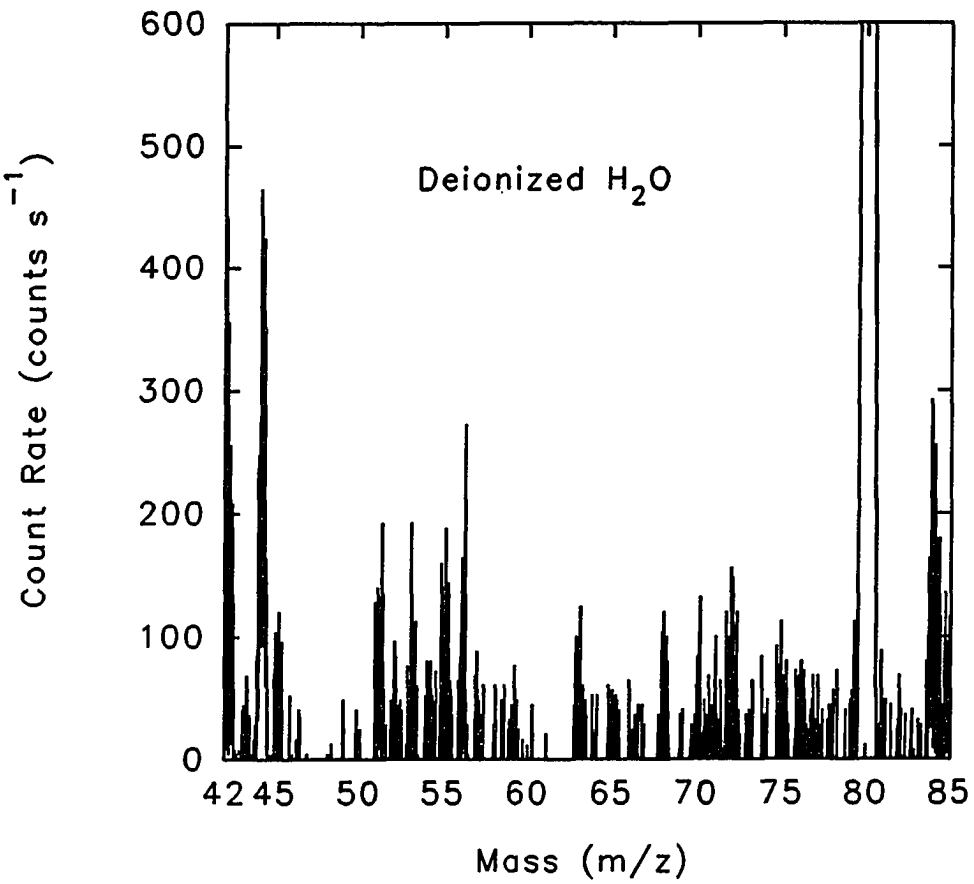

B

Figure 2. (continued)

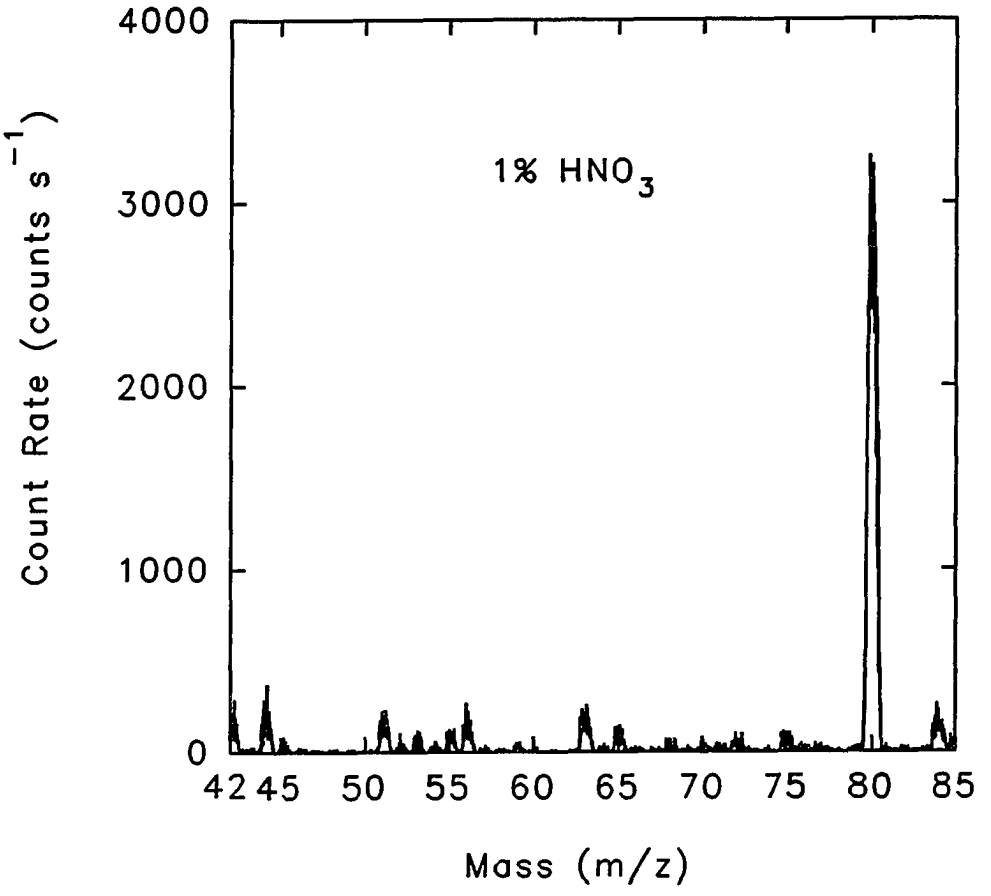

A

Figure 3. Background spectra obtained during nebulization of 1% HNO_3.

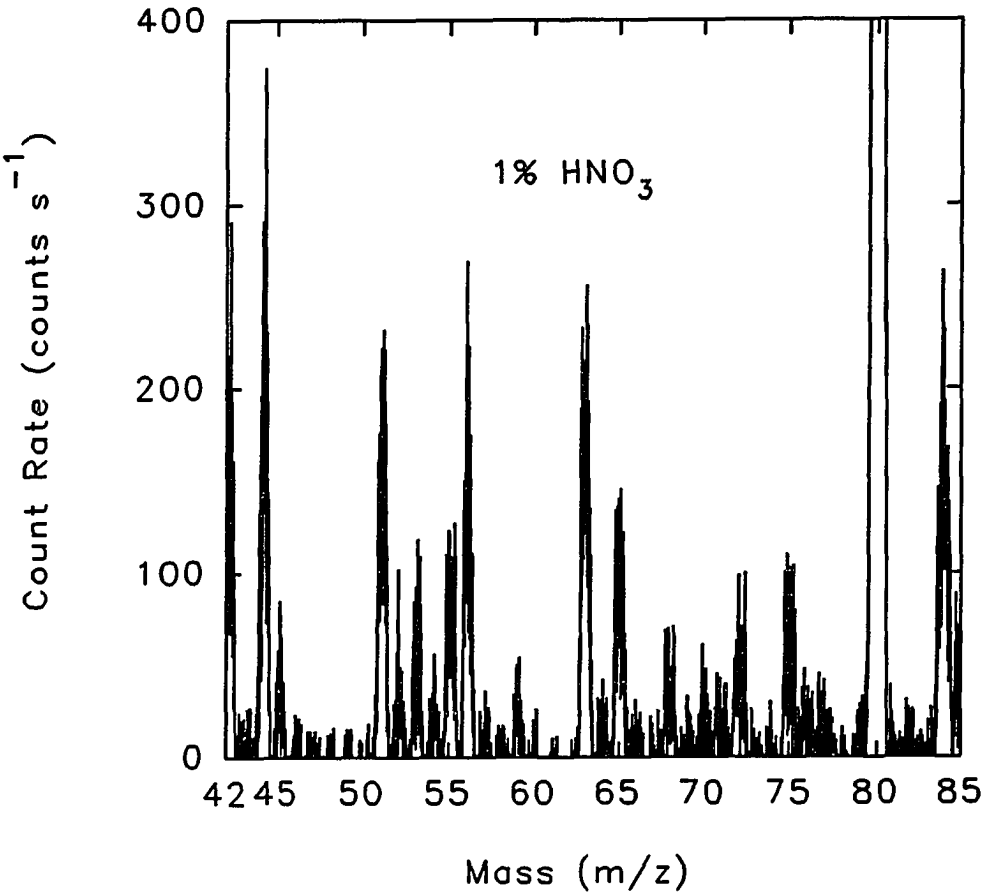

B

Figure 3. (continued)

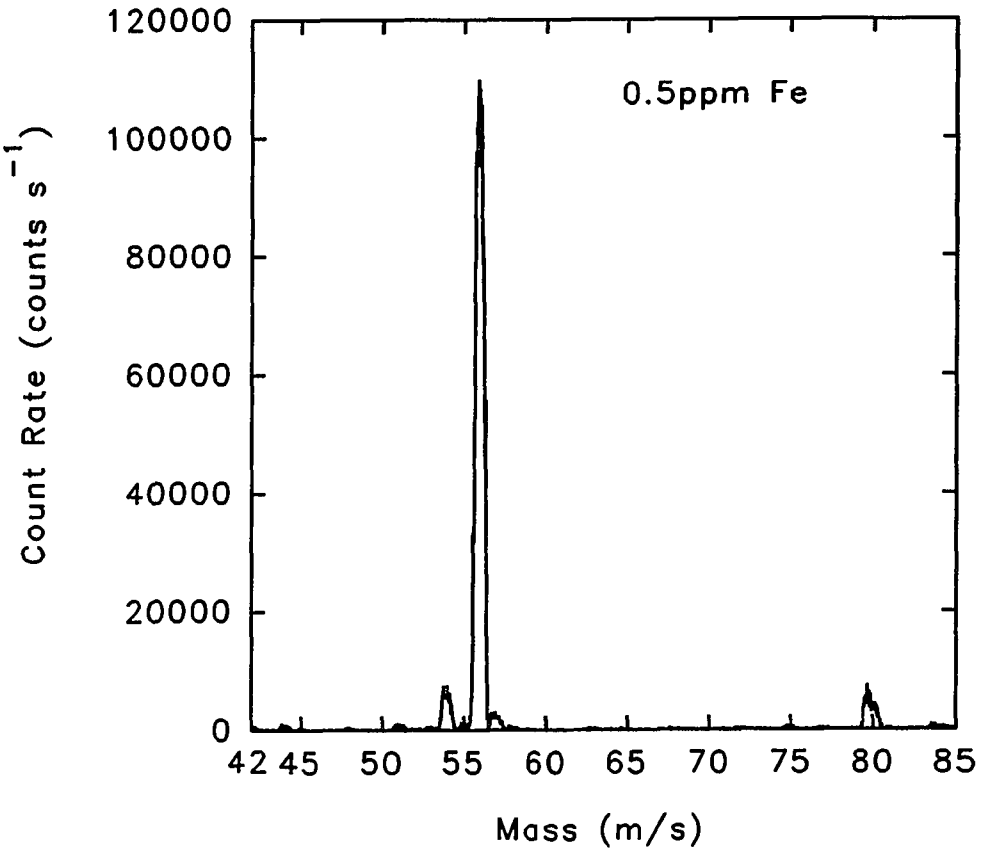

Figure 4. Mass spectrum from 0.5 ppm Fe in 1% HNO_3.

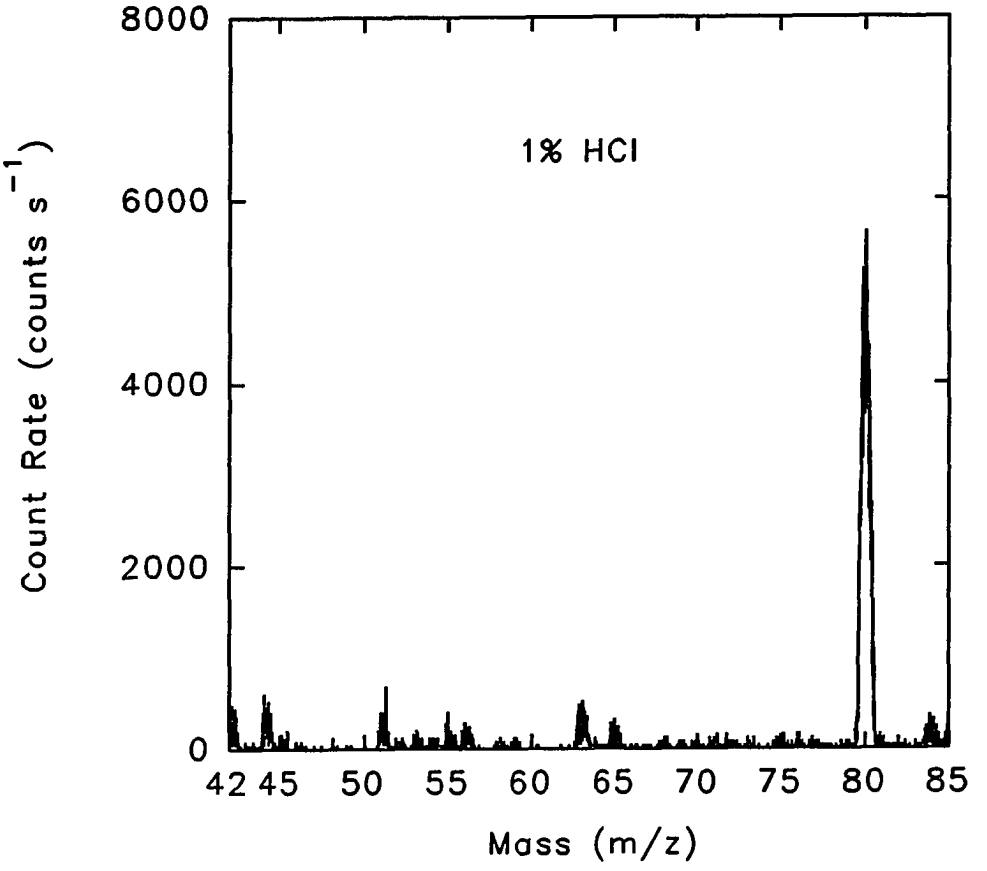

A

Figure 5. Background spectrum from 1% HCl.

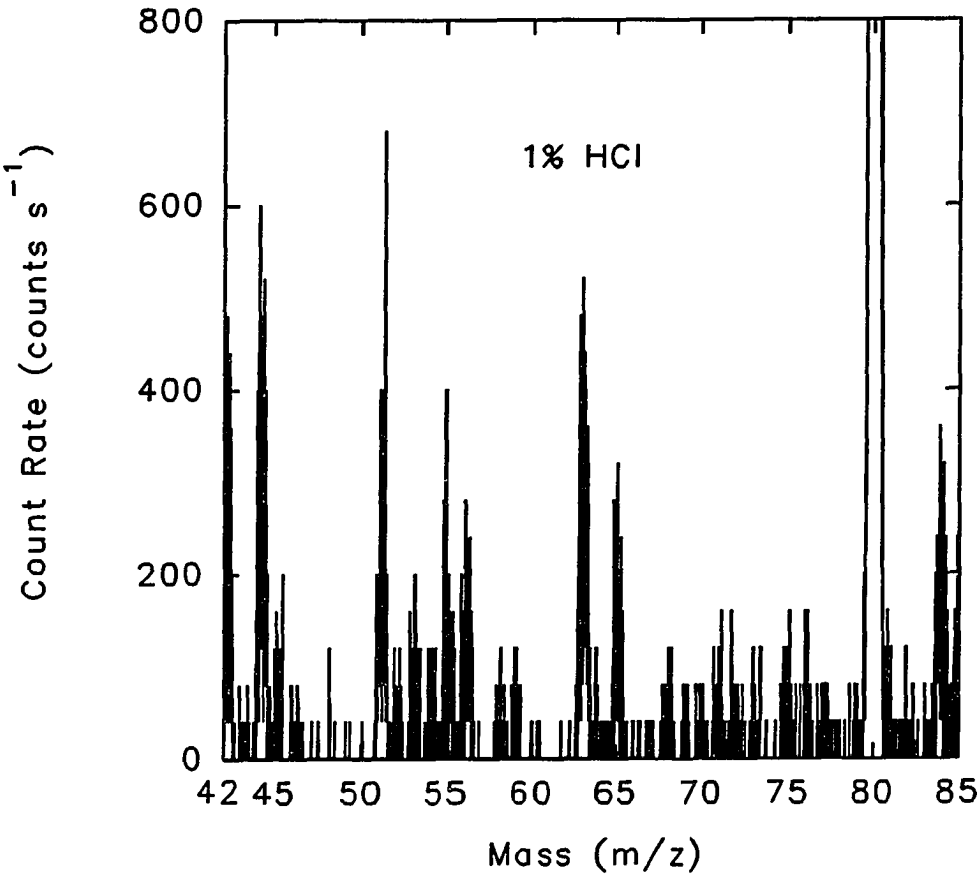

B

Figure 5. (continued)

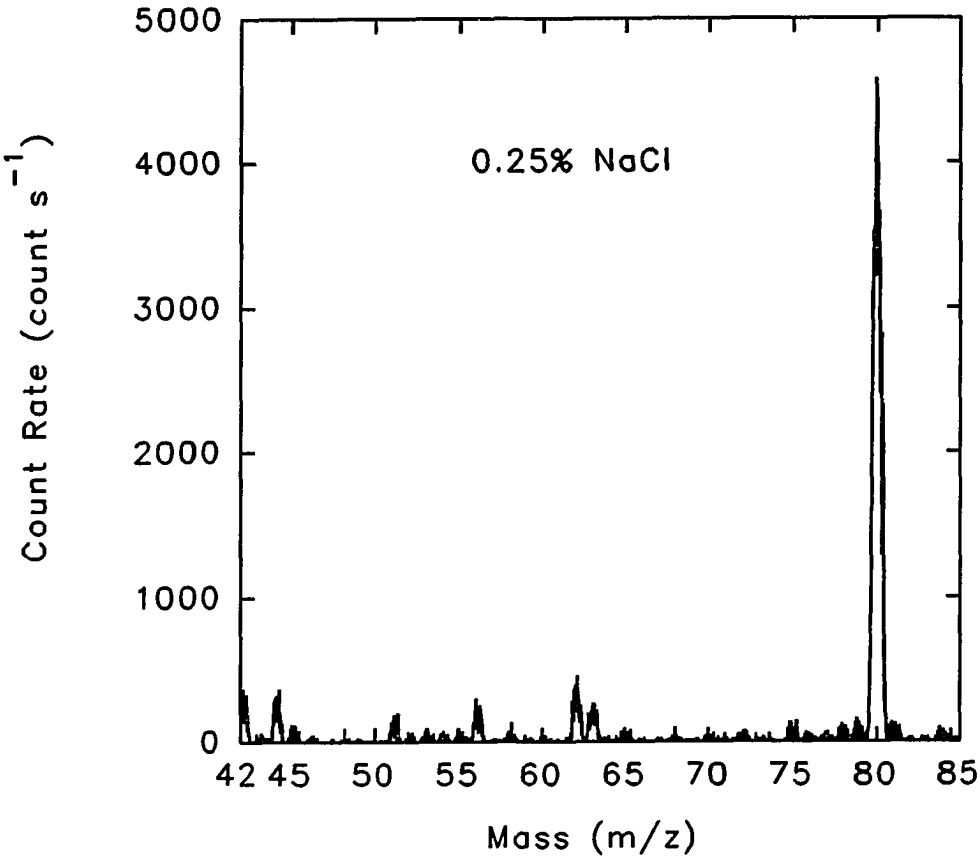

A

Figure 6. Background spectrum from 0.25% NaCl (0.1% Na) in 0.1% HNO_3.

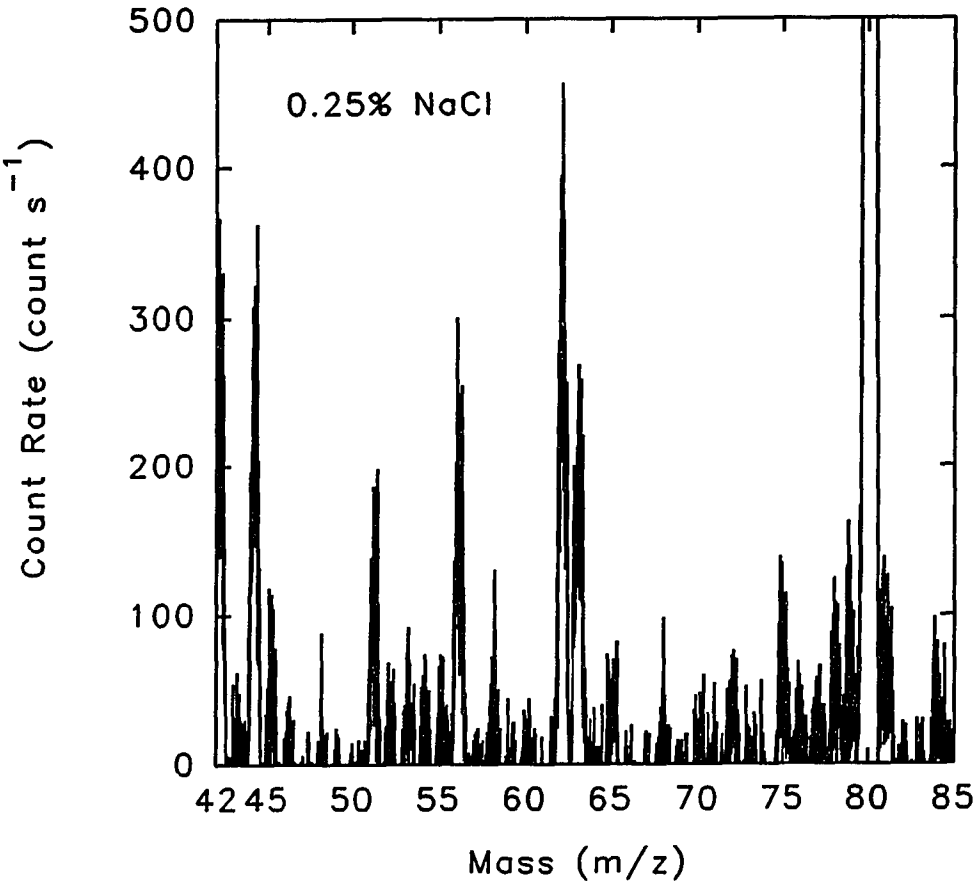

B

Figure 6. (continued)

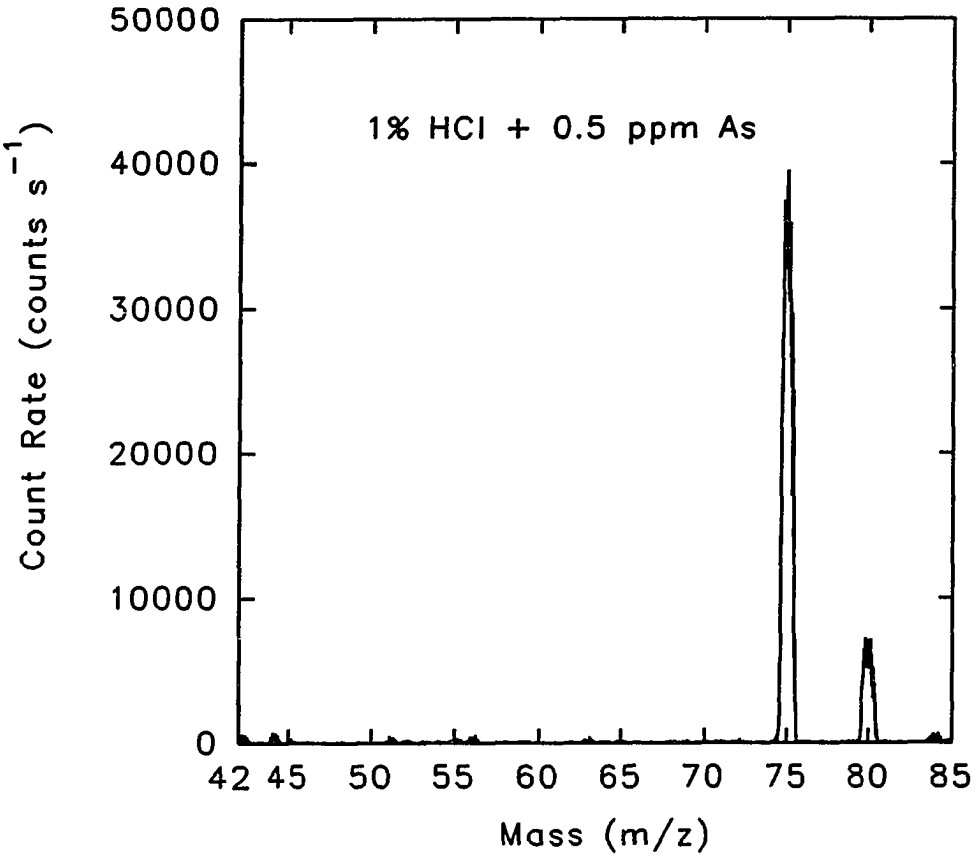

A

Figure 7. Mass spectrum from 0.5 ppm As in 1% HCl.

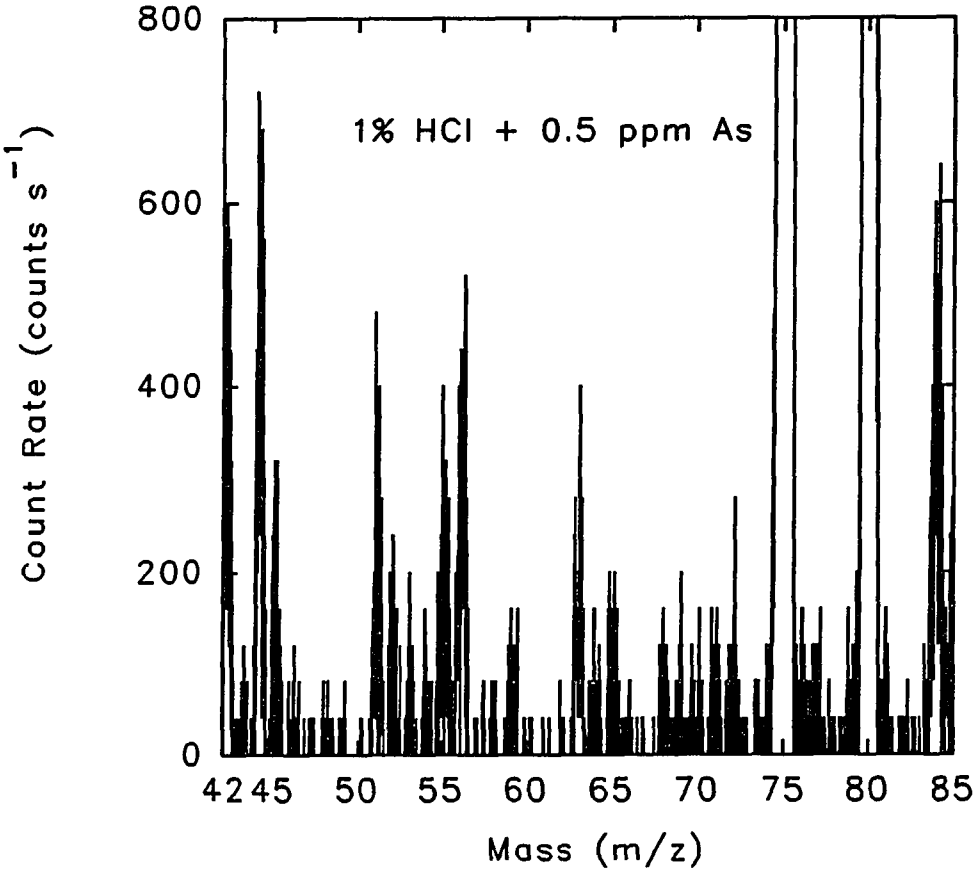

B

Figure 7. (continued)

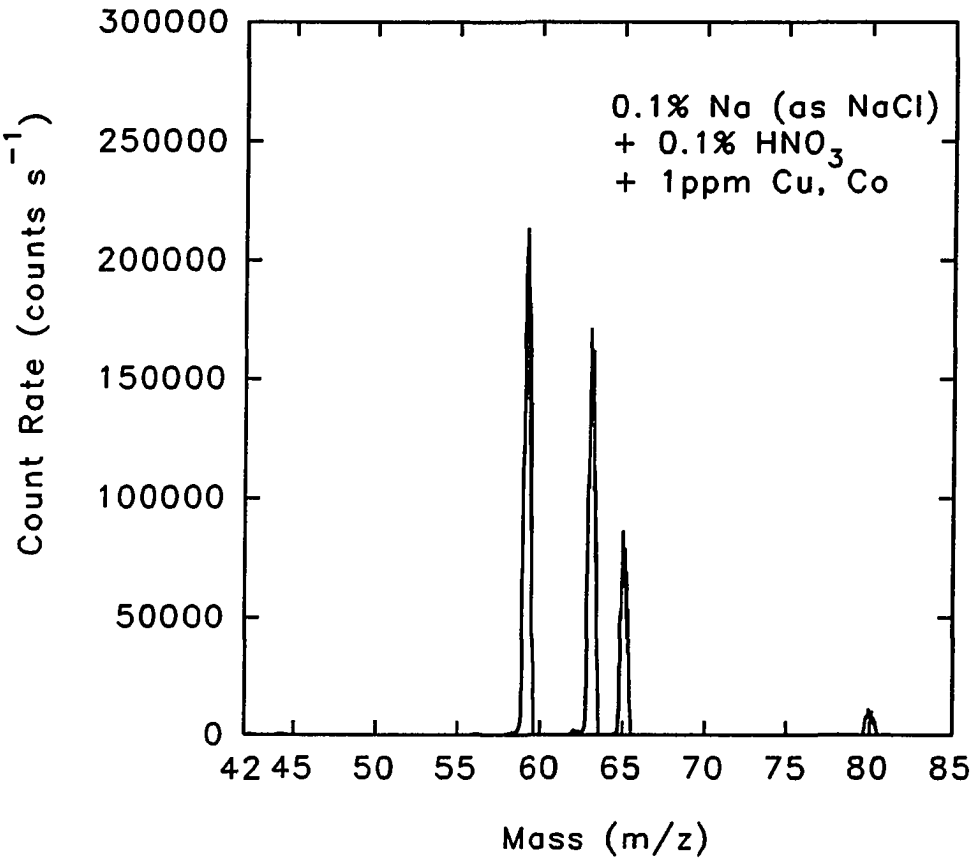

A

Figure 8. Mass spectrum from 1 ppm Co and 1 ppm Cu in 0.25% NaCl (0.1% Na).

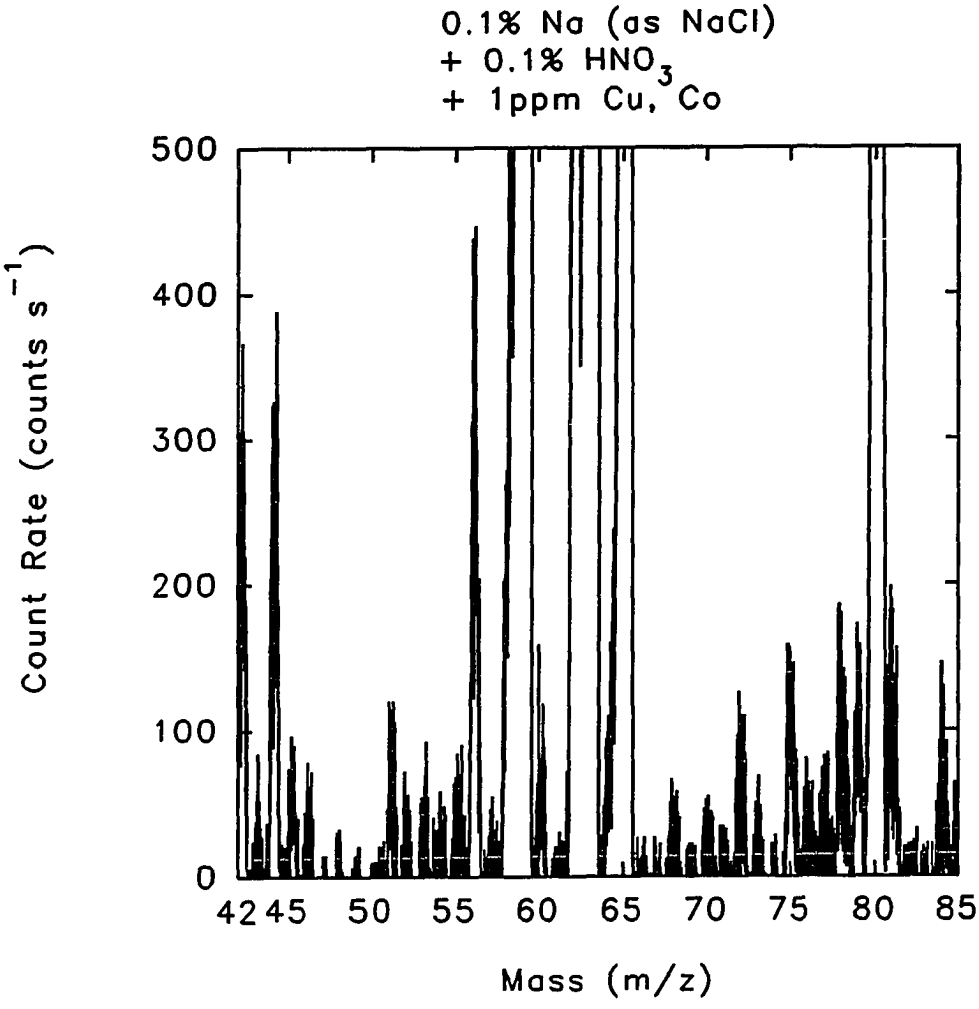

B

Figure 8. (continued)

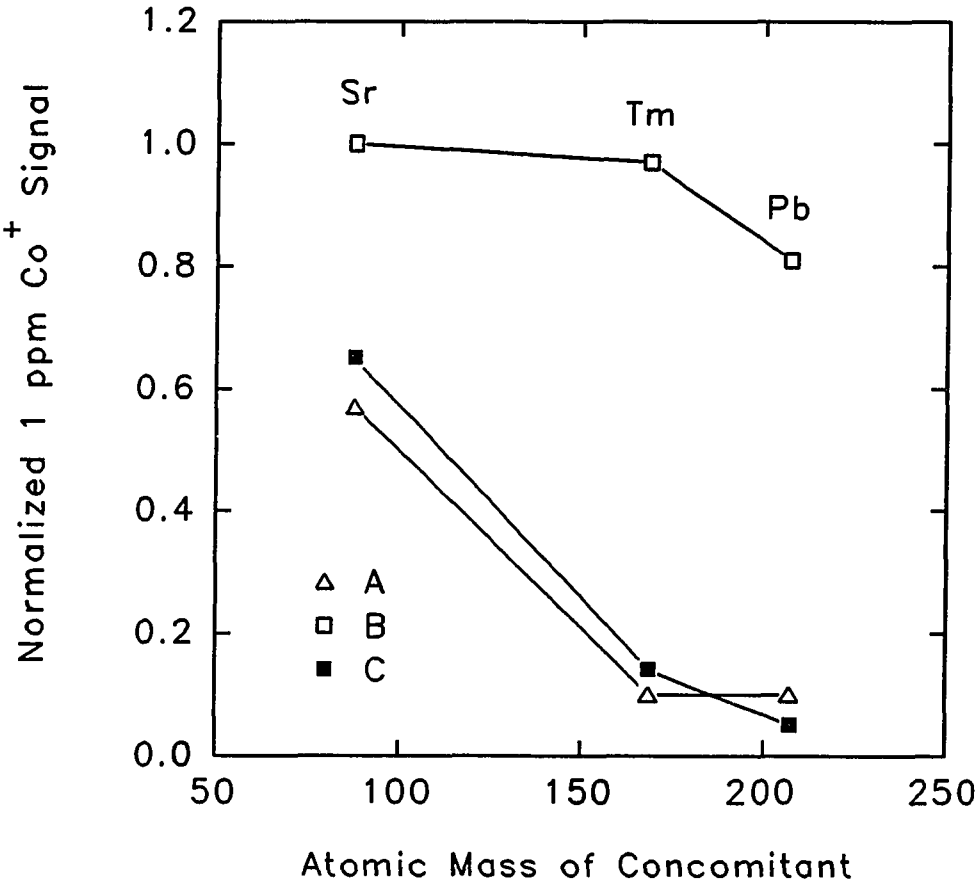

Figure 9. Matrix effect results: normalized Co^+ signal for 1 ppm Co in the presence of Sr, Tm or Pb, each at 10 mM. (△): lens A; (□): lens B; (■): lens C.

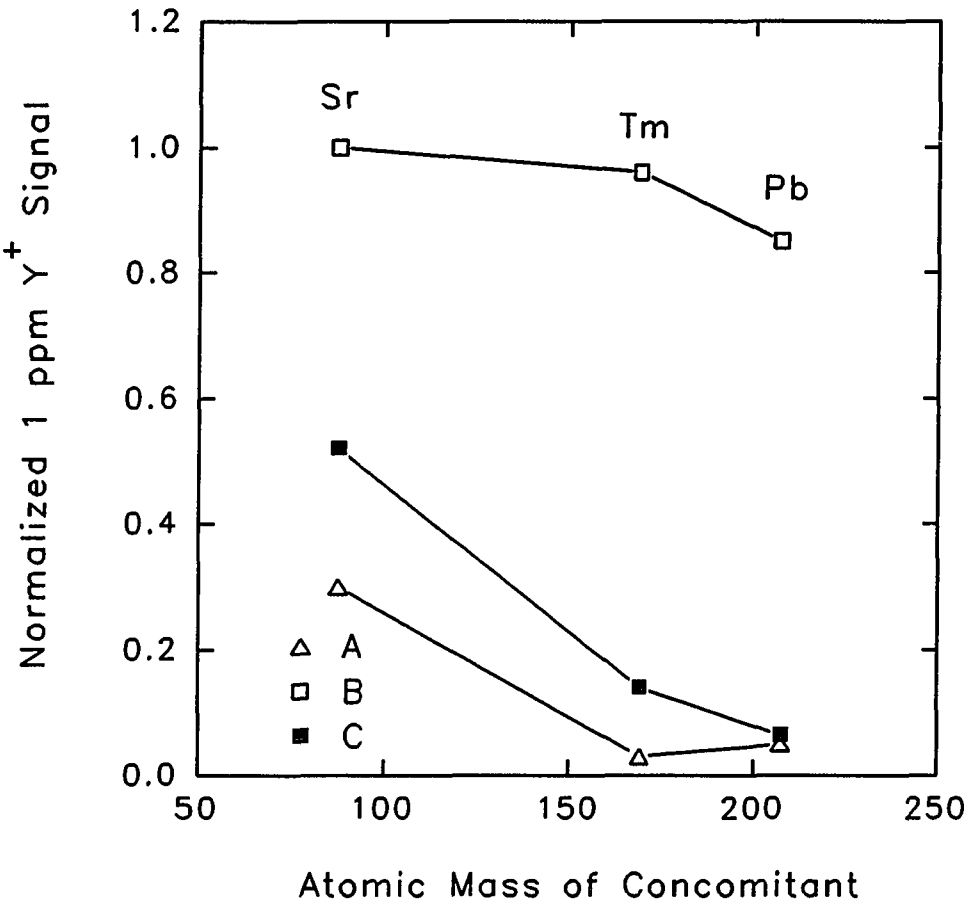

Figure 10. Normalized Y^+ signal for 1 ppm Y in the presence of Sr, Tm or Pb, each at 10 mM. (△): lens A; (□): lens B; (■): lens C.

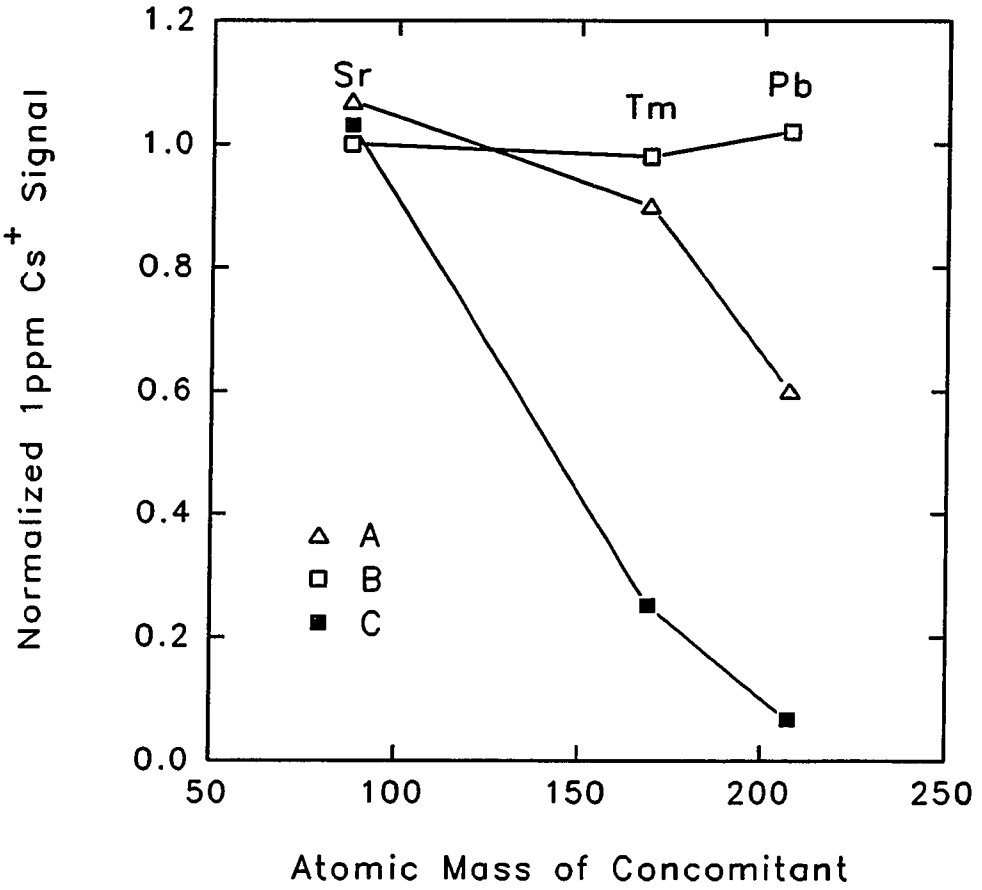

Figure 11. Normalized Cs^+ signal for 1 ppm Cs in the presence of Sr, Tm or Pb, each at 10 mM. (△): lens A; (□): lens B; (■): lens C.

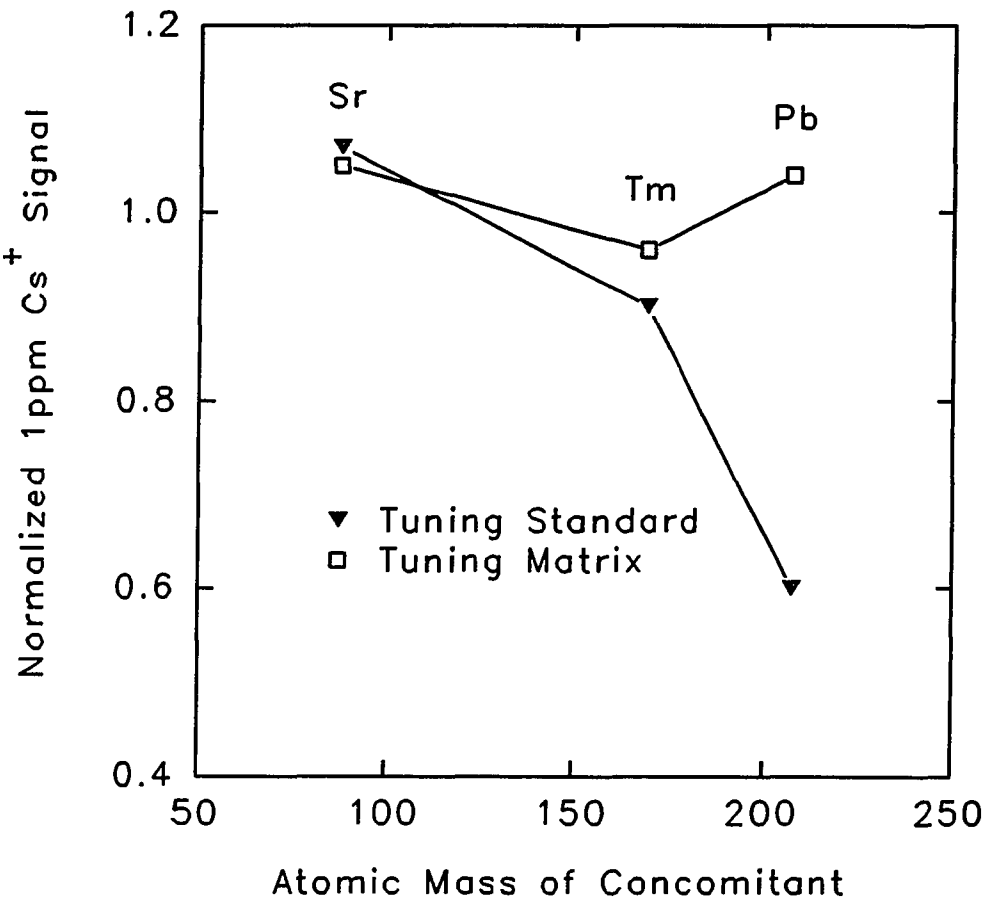

Figure 12. Normalized Cs^+ signal for 1 ppm Cs in the presence of Sr, Tm or Pb, each at 10 mM. (▾): lens 1 power supply not adjusted when matrix present; (□): lens 1 power supply re-adjusted to +3.0 V output when matrix present. See text for explanation.

PAPER III.

FLOATING INTERFACE FOR INDUCTIVELY COUPLED PLASMA MASS SPECTROMETRY

INTRODUCTION

Although inductively coupled plasma mass spectrometry (ICP-MS) has very low detection limits for most elements (1 - 50 ng L^{-1}), it still suffers ion loss from inefficient collection and transmission of ions. The sensitivity of current commercial ICP-MS systems is ca. $1x10^6$ - $1x10^8$ counts s^{-1} ppm^{-1}. For an element of mass 100 this corresponds to the introduction of 10^8 - 10^6 atoms of an element to the plasma to detect one ion. This low efficiency derives largely from the relatively poor transmission of the ion optics due to severe space charge effects and partially from the limited transmission of the skimmer and mass filter. Space charge problems are also believed to cause matrix interference effects. It has generally reported that heavy analyte ions are suppressed less severely than light ones and heavy matrix ions suppress analyte signals more extensively than light matrix ions (1-5).

The space charge limit (I_{mas} in μA) for an ion current focused through a cylinder of diameter D (cm) and length L (cm) is given by

$$I_{max} = 0.9(m/z)^{1/2}V^{3/2}(D/L)^2 \qquad 1$$

where m/z is the mass to charge ratio of the ion (^{12}C = 12) and V is the ion energy (eV) (6). This equation suggests that accelerating the ions to higher energies would improve ion transmission and attenuate mass discrimination by overcoming the space charge problem. Conventionally, the metal interface cones through which the ions are extracted are connected to ground potential. Electrically floating one or both of these cones at various potentials could accelerate the ions and, therefore, improve the ion transmission. Bradshaw et al (7) and Morita et al (8) applied the same high voltage, about 4 - 5 kV, to both the sampling and

skimmer cones. A magnetic sector mass analyzer was used and high resolution was achieved, so that polyatomic ions might be separated from analyte ions. Sensitivity was also improved with these instruments (9). Turner accelerated ions to high kinetic energy behind the skimmer by using another metal cone at -2 kV (10). He reported that sensitivities of low mass ions increased compared with other ICP-MS instruments; most elements with different masses had comparable molar sensitivities. Turner also stated that matrix effects were minimized with this interface arrangement. Douglas applied a RF voltage on the sampling and skimmer plates (11). Arcing at the sampler orifice can be eliminated by grounding the sampler and applying an RF bias to the skimmer orifice. It was also found that the signal to noise ratio was improved by a factor of approximately 2 by correct RF biasing of the skimmer plate (11).

In the present work, modest DC voltages (10 - 50 V) are applied to the sampler or skimmer cones. Ion transmission and calibration linearity are improved, and mass discrimination is greatly reduced by these arrangements. In another experiment, the injection tube of the torch is made of metal instead of the usual quartz. Ion transmission is also improved substantially when a negative voltage is applied to the injector tube.

EXPERIMENTAL

ICP-MS Apparatus

A schematic diagram of the ICP-MS instrument used in this work is shown in Figure 1. This instrument and some components have been described in detail elsewhere (12-15). The operating conditions are identified in Table I. Sample solutions were nebulized with a continuous flow ultrasonic nebulizer (16, 17). The solutions were delivered with a peristaltic pump (Gilson Model Minipuls 2) at a rate of 1.5 ml min^{-1}. The aerosol was desolvated in a pyrex heating tube at 140 °C followed by a condenser at 0 °C. RF-only quadrupoles were not used. Ions were detected with a Channeltron electron multiplier (Model 4830A Galileo Electro-Optics Corp.).

Interface

A typical ICP-MS sampling interface is shown in Figure 2. The sampling cone was made from nickel. The orifice was enlarged to 1.31 mm diameter from the usual 1.0 mm. The diameter of the skimmer orifice was also 1.31 mm. The angles and other dimensions of the sampler and skimmer were described elsewhere (12). The distance between the sampler orifice and skimmer orifice was 11 mm. At this position, the skimmer tip was 2/3 of the way from the sampling orifice to the onset of the Mach disk, which yielded optimum sensitivity, as seen previously by Douglas and French (18).

Three specific arrangements for floating parts of the interface have been studied. In Figure 3A, the same DC bias voltage was applied to both the sampler and skimmer (sampler

& skimmer biased together). This arrangement was the same as that described in ref. 7 and ref. 8. Figure 3B shows a second arrangement (sampler floating & skimmer biased) in which the sampler was allowed to float, i.e. the sampler was not connected to ground or to any voltage source, and a DC bias voltage was applied to the skimmer. In a practical ICP-MS apparatus, the sampler is usually cooled by water supplied through water cooling lines, and the sampler is thus connected to ground through the water cooling lines, which have an electrical resistance of ~ 20 MΩ. Because of the relatively high resistance, for all practical purposes the sampler was not connected to ground, and therefore floats.

Figure 3C shows a third floating arrangement of sampling interface (sampler grounded & skimmer biased) in which the sampler is grounded and the DC bias voltage was applied only to the skimmer. The skimmer was bolted to the main vacuum chamber by Nylon bolts and was insulated at its base with a teflon spacer. The sampler flange was bolted to the expansion chamber in the same way. The sampler and skimmer were insulated from each other except that both shared the same cooling water line (20 M Ω resistance to ground). Cooling water was circulated through the skimmer to keep it from melting.

There were two ways to ground both sampler and skimmer flanges. The sampler and skimmer could be bolted directly to vacuum system with stainless steel bolts, which was not convenient for switching from a grounding pattern to one of the floating patterns. Alternatively, the sampler and skimmer flanges were grounded to the vacuum chamber with copper wires (5 - 10 cm long) at four opposite positions.

When a DC voltage was applied to the plasma torch injector, a stainless steel injector tube was used, instead of the usual glass tube. A schematic diagram of this special torch is

shown in Figure 4. The outside and inside diameters of the injector tube were 3.2 mm and 2.0 mm, respectively.

Ion Lens

The ion lens used on this ICP-MS instrument was slightly different from that used on the instrument described in ref. 13. This modified ion lens is shown in Figure 5. Ions passing the skimmer (A, Figure 5) entered the first stainless steel cylinder (1, Figure 5). Numerous holes were drilled in the side wall of the cylinder, so that neutral atoms could be evacuated. The second and the third electrodes (2 and 3, Figure 5) of the lens were stainless steel cylinders also, but the inside diameter of the second electrode was 2.5 cm, twice that of the third electrode. A small conical photon stop (7, Figure 5) was placed on center after the second cylinder. The fourth electrode of the ion lens (4, Figure 5) was tapered, the entrance was 12.7 mm diameter and the exit was 6.4 mm diameter. Finally, ions passed through the differential pumping orifice (5, Figure 5) which was a tube 2.50 mm diam. x 6.4 mm long. The voltages applied to each electrode are identified in Table 1. Ions were transmitted better through this modified ion lens than our previous ion lens (12-14), which was shown by better analyte sensitivity for analytical purposes and better ion beam intensity for ion deposition.

Data Acquisition

Detection limits were measured by the procedure described in ref. 13. The detection limits represented the solution concentration necessary to yield a net peak height equivalent

to 3 times the standard deviation of the background. Signals were measured in the multichannel scanning mode (19). The dwell time was 50 μs address^{-1} for 4096 addresses over a mass window 20 m/z units wide. Fifty such sweeps were averaged. The mass analyzer was operated at unit mass resolution. Sensitivity, detection limits, and mass discrimination were measured by pulse counting. A preamplifier (Model 1763) and a amplifier-discriminator (Model 1762) (Photochemical Research Associates) were used for ion counting.

At higher ion signal levels, ion current was measured for determination of calibration curves. The analog output of the electron multiplier was fed to a current-to-frequency converter (Model 151, Analog Technologies Inc.). The TTL pulses from the converter were carried to the input of a multichanner analyzer. The number of pulses in the train were counted by the analyzer with a dwell time of 50 μs. In order to compare dynamic linear ranges fairly, the ion current from 20 ppm Co for each system was adjusted to nearly equal sensitivity by adjusting the detector bias voltage.

Voltages on the sampler and skimmer were measured with a voltmeter (Model ME-550 Digital Multimeter, SOAR Corporation, Japan). Ion kinetic energies were measured by applying a positive stopping voltage as the mean DC bias to the quadrupole mass filter (20-22). The stopping voltage necessary to attenuate the ion signal to 5% of the original signal level was measured and is referred to as "maximum ion energy" subsequently. Unfortunately, the highest DC bias voltage for the quadrupole mass filter was only 15 volts. Ion kinetic energies above 15 eV could not be measured with this ICP-MS instrument.

Standards and Solutions

Standard solutions were 0.1 mg L^{-1} of each element unless noted otherwise and were prepared by diluting aliquots of commercial stock solutions (Fisher) with distilled deionized water (18 MΩ, Barnstead).

RESULTS AND DISCUSSION

Sensitivity and Detection Limit

Relative Co^+ sensitivities (assuming ion signal was unity when sampler and skimmer were grounded by copper wires) as a function of the floating potentials are shown in Figure 6. As shown in curve 6A, Co^+ sensitivity was improved modestly by applying the same DC voltages (10 - 20 V) to both sampler and skimmer. The sensitivities were improved by a factor of 6 by floating the sampler and applying a DC voltage of 30 - 40 V to the skimmer (curve 6B). The signals were improved by factor of 5 by grounding the sampler and applying DC voltages (above 20 V) to the skimmer (curve 6C). It is interesting that the ion signals increased two to three times at 0 volts with all these three interface arrangements compared with the signals obtained when both sampler and skimmer were grounded.

The data in Table II were collected under the optimal operation conditions for each interface arrangement. Actually, the ion lens settings, plasma power, and aerosol gas flow rates that yielded maximum Co^+ signal were comparable to each other for all arrangements, which can be seen in Table I. Higher positive voltages (up to 100 V) could be applied to the interface if the ion lens voltages were adjusted to re-optimize ion transmission. However, the Co ion sensitivities shown in Figure 4 and Table II were the best sensitivities we could get. For either floating interface, sensitivities were in the range $4.0 \times 10^6 \sim 6.0 \times 10^6$ counts s^{-1} ppm^{-1} and detection limits were in the range 10 - 20 ng L^{-1} (pptr). Both sensitivity and detection limit of Co^+ were improved by a factor of 4 to 6 with either floating interface arrangement. The best arrangement was perhaps the one with the floating sampler

and biased skimmer, which improved ion signal by a factor of 6. The interface arrangement did not affect the background, which was 150 ± 20 counts s^{-1} in all cases.

Linear Dynamic Range

Figure 7 shows that the linear dynamic range for Co^+ was improved when the sampler was floated and the skimmer was biased (Figure 3B) compared to the performance of a conventional grounded interface (Figure 2). It is noted that the relative signal for Co^+ with the grounded interface was much smaller and rolled over at a solution concentration of 80 ppm. The Y-intercept of this curve did not pass through zero, as the curve probably has already rolled over at 20 ppm. The curve obtained with the sampler floating and skimmer biassed (Figure 3B) by 30 V was linear to at least 100 ppm. Similar improvements in linear dynamic range were obtained with the interfaces shown in Figure 3A and 3C (sampler & skimmer biased together and sampler grounded & skimmer biased) as well. Figure 7 also shows that the linear dynamic range was extended when the floating voltage was raised from 10 V to 30 V. The sensitivity for Co^+ with the floating potential of 10 volts with floating interface B (sampler floating & skimmer biased) was only linear to about 60 ppm, while the curve obtained with the bias potential of 30 volts was linear to at least 100 ppm (see Figure 7). Similar observations could be seen with the interface shown in Figure 2A (sampler & skimmer biased together). However, the linear dynamic range obtained with the sampler grounded and skimmer biased (Figure 3C) was not influenced by the voltage applied to the skimmer if the voltage was above 20 volts. The curves with this bias system were linear to at least 100 ppm if the bias voltages were above 20 volts.

Mass Discrimination

Mass discrimination is a common problem for multielement determinations in ICP-MS. This discrimination can be shown by expressing ion sensitivity in terms of atomic concentrations rather than weight concentrations. The signals, i.e., sensitivities of Co^+, Rh^+, and Ho^+ in terms of atomic concentrations, are shown in Table III. These three analyte elements were chosen because they are efficiently ionized in the plasma, they are all monoisotopic, and they have significantly different atomic masses. The sensitivity of a heavy element (Ho) was about 4 times higher than that for a light element (Co) when both sampler and skimmer were grounded. This 4x difference in sensitivity is quite common in many ICP-MS instruments. Mass discrimination was greatly reduced in this instrument with the sampler floating and skimmer biased by 30 V, as shown by the similar sensitivities for $^{59}Co^+$, $^{103}Rh^+$, and $^{165}Ho^+$ in the last line of Table III. This result shows that the signal for any element might reflect the behavior of all the others, so that a single element can serve as an internal standard for all the others. This will make internal standardization and calibration for multielement semi-quantitative analysis much easier. Similar reductions in mass discrimination also were seen in other floating interface arrangements.

Ion Energy

Ion energies of Co, Rh, and Ho increased as the interface was floated. The influence of voltage applied to both sampler and skimmer together on Co ion energy is shown in Table IV. It is shown that the ion kinetic energy increased with floating potential. It is interesting that the ion energy with interface grounded directly to the vacuum chamber was different

from that grounded through the power supply (0 V). Perhaps this was a reason that ion sensitivities increased when the interface was grounded through the power supply (0 V points, Figure 6). This also shows that the ion kinetic energy, and perhaps the plasma potential, is affected by different ground configurations.

Measured Potential on Sampler and Skimmer

In these experiments, voltages were applied to the interface from an adjustable DC power supply. The actual potentials on the sampler and skimmer were measured by a voltmeter. Figure 8 shows that the potentials measured on the sampler were the same as the voltages applied when the sampler and skimmer were biased together (A, Figure 8), and were about 6 volts less positive than the applied voltage when the sampler was floated and the skimmer was biased (B, Figure 8). Figure 9 shows that the potentials measured on the skimmer were the same as the applied voltages except at zero voltage with either sampler and skimmer biased together or sampler floating and skimmer biased. The measured potentials on the sampler was always zero (C, Figure 8) and was about +10 V on the skimmer (C, Figure 9) when the sampler was grounded and skimmer was biased regardless of the voltage applied to the skimmer. Perhaps this was why the ion signal change with this arrangement was different from the others (C, Figure 6). The signal did not change with applied voltages above $\sim +20$ V (Figure 6) with this interface arrangement.

It is noted in Figure 8 that the measured potentials were not zero when the applied voltages were zero on the sampler in arrangement A (sampler & skimmer biased together) and arrangement B (sampler floating & skimmer biased). One possible reason was that the

sampler potential was affected by the plasma when the sampler was not grounded. When the applied voltages were higher than the potentials induced by the plasma, the sampler voltage would be controlled by applied voltages. This was also why the skimmer potential measured was not at zero when applied voltage was zero in the arrangement A and B.

Peak Shape and Matrix Effects

The shapes of ion signal peaks became broadened and split as the floating voltage increased. Increasing the bias voltage of the quadrupole rods to more positive values would improve the shapes of ion peaks and prevent splitting. Matrix effects were slightly improved, but were not as desirable as hoped.

Effect of Voltage on Aerosol Injection Tube

The Co^+ sensitivity as a function of voltage applied to the metal aerosol injector tube is shown in Figure 10. Both the sampler and skimmer were grounded at this time. The experiment was initiated with the injector tube grounded (0 V) through its power supply. At 0 V, the Co^+ signal was similar to that obtained with a standard quartz injector tube. Signal decreased when a positive voltage was applied to the injection tube. Ion signal grew slightly as a negative voltage was applied. The signal increased substantially at voltages more negative than -300 V, but at potentials more negative than -360 volts, a strong discharge occurred between the injector tube and sampler. Sensitivity for Co^+ could be improved by 60% with -350 V applied to the injection tube. As described above, either applied positive voltages on the interface or negative voltages on the injector tube, or the

plasma, would improve ion transmission, perhaps for similar basic reasons.

Table V shows that the voltage measured on the sampler was strongly affected by the voltage applied to the injector tube when both sampler and skimmer were floated. The measured voltages on the sampler was always 80 volts more positive than that applied to the injector. The measured voltage was -5 V when the injector was floated, which was similar to the normal quartz injector. The potential in the immediate vicinity of the injector tip should be - 85 V if the 80 V difference was also true with the floating injector. Koppenaal and Quinton (23) measured the potentials in a plasma with a Langmuir probe. They reported that the potential values became less negative as the Langmuir probe approached the sampler orifice from the quartz torch and coil region of the plasma. The potential was - 30 V in the immediate vicinity of the aperture and was - 90 V at the end of the torch. The potential difference was 60 V. The difference between the sampler aperture and the torch tip should be larger than 60 V. Our experiments showed a similar trend.

These experiments showed that the ion signal could be affected by applying a voltage to the injector tube. This result is surprising because the injector is outside the plasma and is well upstream ($\sim$40 mm) from the sampling orifice. While the observed increase in ion signal is certainly welcome, the underlying reasons are not at all clear. Further experiments, such as plasma potential measurements with a floating Langmuir probe (23-25), are necessary to clarify the fundamental reason for the observed influence of injector voltage on ion signal and to determine if this is a general phenomenon.

CONCLUSION

This paper describes three different floating arrangements of the sampling interface. Sensitivity can be improved by a factor of 4 to 6, therefore, detection limits are improved also. The linear dynamic range of a calibration curve was extended. Mass discrimination was greatly reduced. All these experiments were just empirical. Perhaps further improvements are possible if some understanding of the underlying reasons can be developed. Further research combining different floating arrangements with different ion optic modifications, such as grounding one or two ion lens electrodes (26), or offset ion lens (26,27), would reduce space charge effects, and hence eliminate matrix effects. Deeper research with applying voltage on the injector tube and changing the injector tube position would further improve sensitivity and detection limits, and may give us some fundamental information about the ICP-MS interface.

LITERATURE CITED

1. Gillson, G. R.; Douglas, D. J.; Fulford, J. E.; Halligan, K. W.; Tanner, S. D. Anal. Chem. 1988, 60, 1472-1474.
2. Tan, S. H.; Horlick, G. J. Anal. Atom. Spectrom. 1987, 2, 745-763.
3. Crain, J. S.; Houk, R. S.; Smith, F. G. Spectrochim. Acta, 1988, 43B, 1355-1346.
4. Beauchemin, D.; McLaren, J. W.; Berman, S. S. Spectrochim. Acta, 1987, 42B, 467-490.
5. Kawaguchi, H.; Tanaka, T.; Mizuike, A. Spectrochim. Acta Part B 1988, 43B, 955-962.
6. Pierce, J. R. Theory and Design of Electron Beam, 2nd Ed. Van Nostrand, New York, 1954.
7. Bradshaw, N.; Hall, E. F. H.; Sanderson, N. E. J. Anal. Atom. Spectrom. 1989, 4, 801-803.
8. Morita, M.; Ito, H.; Uehiro, T.; Otsuka, K. Anal. Sci. (Japan), 1989, 5, 609-610.
9. Kim, C. K; Seki, R.; Morita, S.; Yamasaki, S. I.; Tsumura, Akito; Takaku, Y.; Igarashi, Y.; Yamamoto, M. J. Anal. Atom. Spectrom. 1991, 6, 205-209.
10. Turner, P. J. In Applications of Plasma Source Mass Spectrometry, 1991, Holland, G.; Eaton, A. N. Eds.; Thomas Graham House. Science Park. Cambridge.
11. Douglas, D. J. U. S. Patent Document, Patent #: 4 482 026.
12. Olivares, J. A.; Houk, R. S. Anal. Chem. 1985, 57, 2674-2679.
13. Huang, L. Q.; Jiang, S. J.; Houk, R. S. Anal. Chem. 1987, 59, 2316-2320.

14. Crain, J. S.; Houk, R. S.; Eckels, D. E. Anal. Chem. 1989, 61, 606-612.

15. Scott, R. H.; Fassel, V. A.; Kniseley, R. N.; Nixon, D. E. Anal. Chem. 1974, 46, 75-80.

16. Olson, K. W.; Haas, W. J., Jr.; Fassel, V. A. Anal. Chem. 1977, 49, 632-637.

17. Bear, B. R.; Fassel, V. A. Spectrochim. Acta, Part B 1986, 41B, 1089-1113.

18. Douglas, D. J.; French, J. B. J. Anal. Atom. Spectrom. 1988, 3, 743-747.

19. Jarvis, K.E.; Gray, A. L.; Houk, R. S. Handbook of Inductively Coupled Plasma Mass Spectrometry; Blackie: Glasgow, 1991.

20. Olivares, J. A.; Houk, R. S. Appl. Spectrosc. 1985, 39, 1070-1077.

21. Fulford, J. E.; Douglas, D. J. Appl. Spectrosc. 1986, 40, 971-974.

22. Chambers, D. M.; Hieftje, G. M. Spectrochim. Acta Part B 1991, 46B, 761-784.

23. Koppenaal, D. W.; Quinton, L. F. J. Anal. Atom. Spectrom. 1988, 3, 667-672.

24. Gray, A. L.; Houk, R. S.; Williams, J. G. J. Anal. Atom. Spectrom. 1987, 2, 13-20.

25. Houk, R. S.; Schoer, J. K. Crain, J. S. J. Anal. Atom. Spectrom. 1987, 2, 283-286.

26. Hu, K.; Houk, R. S. J. Amer. Soc. Mass Spectrom. 1992, Submitted.

27. Hu, K.; Clemons, P. S.; Houk, R. S. J. Amer. Soc. Mass Spectrom. 1992, submitted.

Table I. Optimal operation condition for the ICP-MS system

Component	Operation conditions
Plasma forward power	1.30 kW
Plasma reflected power	< 5 W
Plasma argon gas flow	17 L min^{-1}
Auxiliary argon gas flow	0
Aerosol argon gas flow	1.30 L min^{-1}
Sampling position	13 mm from load coil, on center
Expansion chamber pressure	2.35 torr
Second stage pressure	$5x10^{-4}$ torr
Third stage pressure	$2x10^{-5}$ torr
Ion lens setting	
first cylindrical lens	-250 V
second cylindrical lens	-10 V
third cylindrical lens	-30 V
fourth cylindrical lens	-170 V
photon stop	-14 V
differential pumping orifice	-100 V
ELFS lens	-20 V
ion exit lens	-150 V

Table I. continued

Ion deflecting plate	+700 V
Detector housing aperture	- 250 V
Channeltron electron multiplier	
pulse counting	-3000 V
ion current	-2500 V
Quadrupole rod mean dc potential	+1.0 V

Table II. Co sensitivity and detection limit in floating interface systems and grounding interface system

Interface arrangement	Sensitivities (counts s^{-1} ppm^{-1})	Detection limit (ppb)
Sampler & skimmer grounded (Fig. 2)	$1.0x10^6$	0.060
Sampler & skimmer biased together (Fig. 3A)	$4.0x10^6$	0.015
Sampler floating & skimmer biased (Fig. 3B)	$6.0x10^6$	0.010
Sampler grounded & skimmer biased (Fig. 3C)	$5.0x10^6$	0.012

Table III. Measured element sensitivities expressed in terms of atomic concentration.

	Sensitivities (counts s^{-1} mM^{-1})		
Interface arrangement	Co	Rh	Ho
Sampler & skimmer grounded (Fig. 2)	$5.6x10^7$	$8.5x10^7$	$2.2x10^8$
Sampler floating & skimmer biased (Fig. 3B)[a]	$3.5x10^8$	$3.3x10^8$	$3.0x10^8$

[a]The voltage applied to the skimmer was +30 V.

Table IV. Influence of voltages applied to both sampler & skimmer together on Co ion kinetic energies

Interface arrangements	Co ion energies (eV)
Sampler & skimmer grounded (Fig. 2)	4.4
Sampler & skimmer biased (V) (Fig. 3A)	
0	7.4
10	11.0
>20	>15

Table V. Influence of voltages applied to injection tube on potentials measured on sampler[a]

Injector voltage (V)	Voltage measured on sampler (V)
floating	- 5
- 120	- 40
0	+80
+120	+200

[a]Both sampler and skimmer were floated.

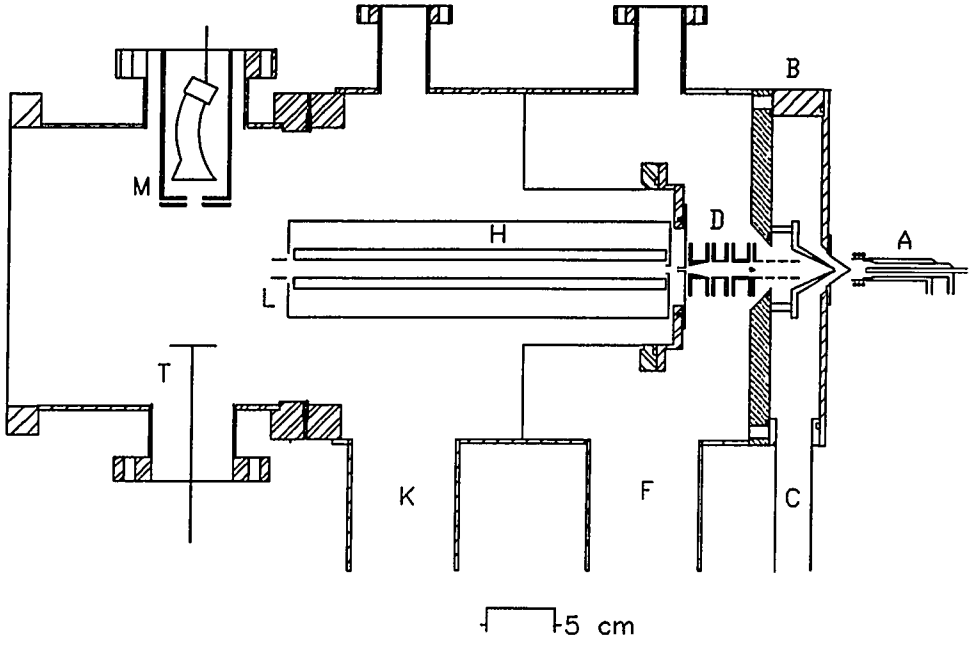

Figure 1. Schematic diagram of ICP-MS instrument: (A) ICP; (B) ion extraction interface; (C) port to rotary pump; (D) ion lens; (H) quadrupole mass analyzer; (F,K) ports to diffusion pumps; (L) ion exit lens; (M) Channeltron detector; (T) ion deflection plate.

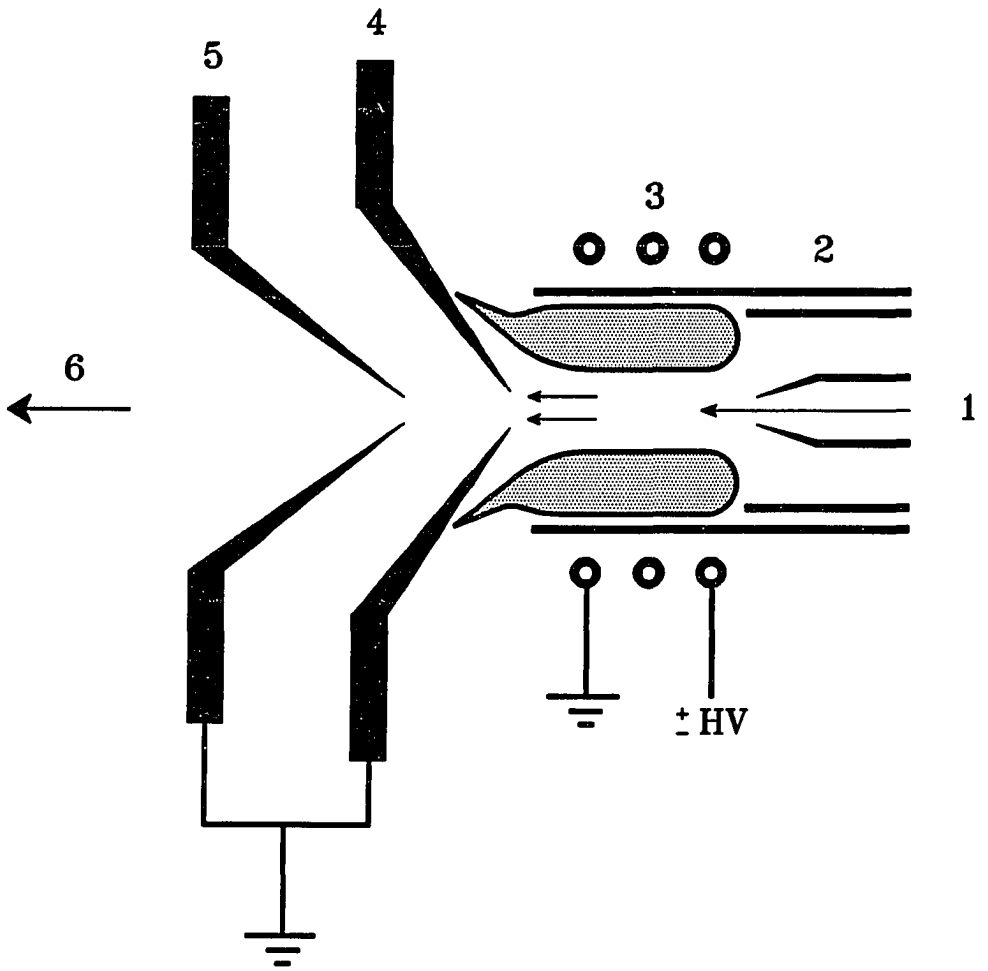

Figure 2. A typical ICP-MS sampling interface (both sampler & skimmer grounded): (1) sample aerosol; (2) ICP torch; (3) load coil; (4) sampler; (5) skimmer; (6) ion beam to mass analyzer.

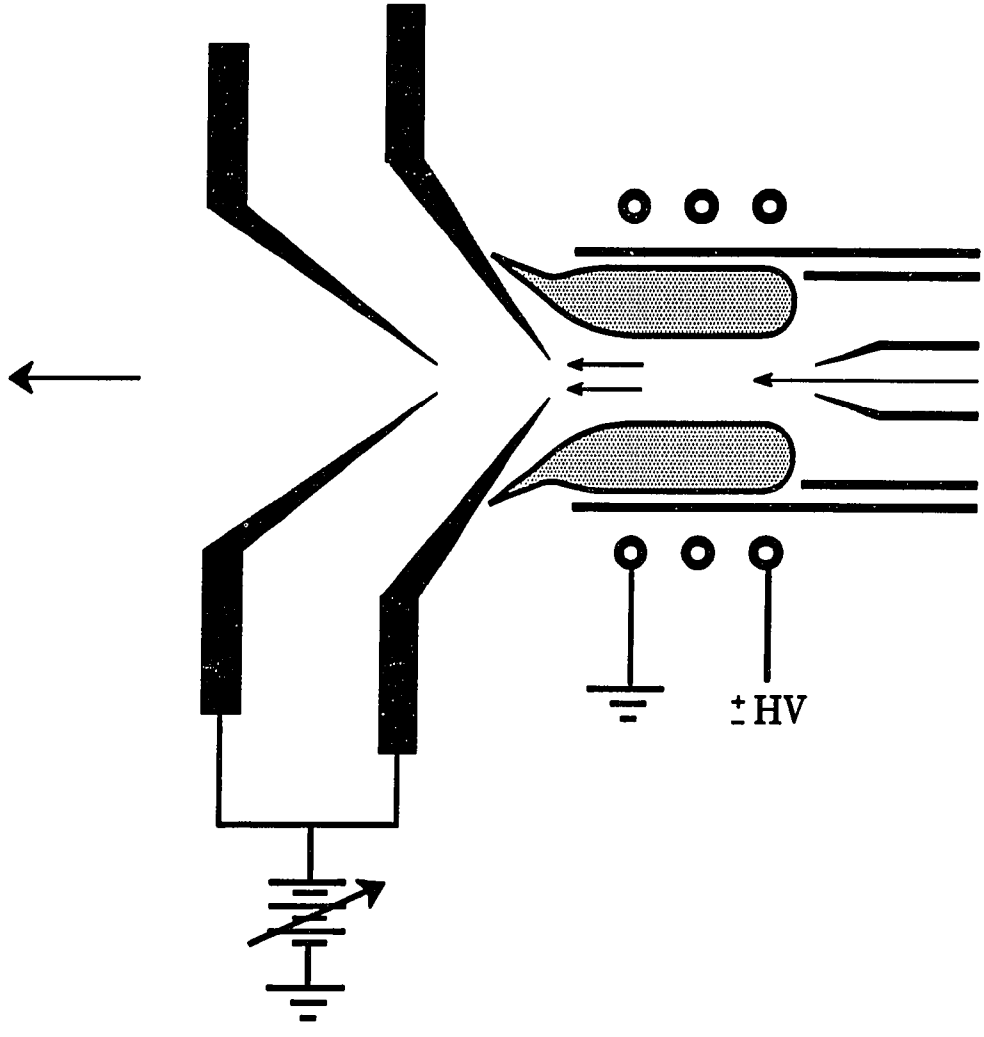

A

Figure 3. Diagrams of floating arrangements of sampling interface: (A) sampler & skimmer biased together; (B) sampler floated & skimmer biased; (C) sampler grounded & skimmer biased.

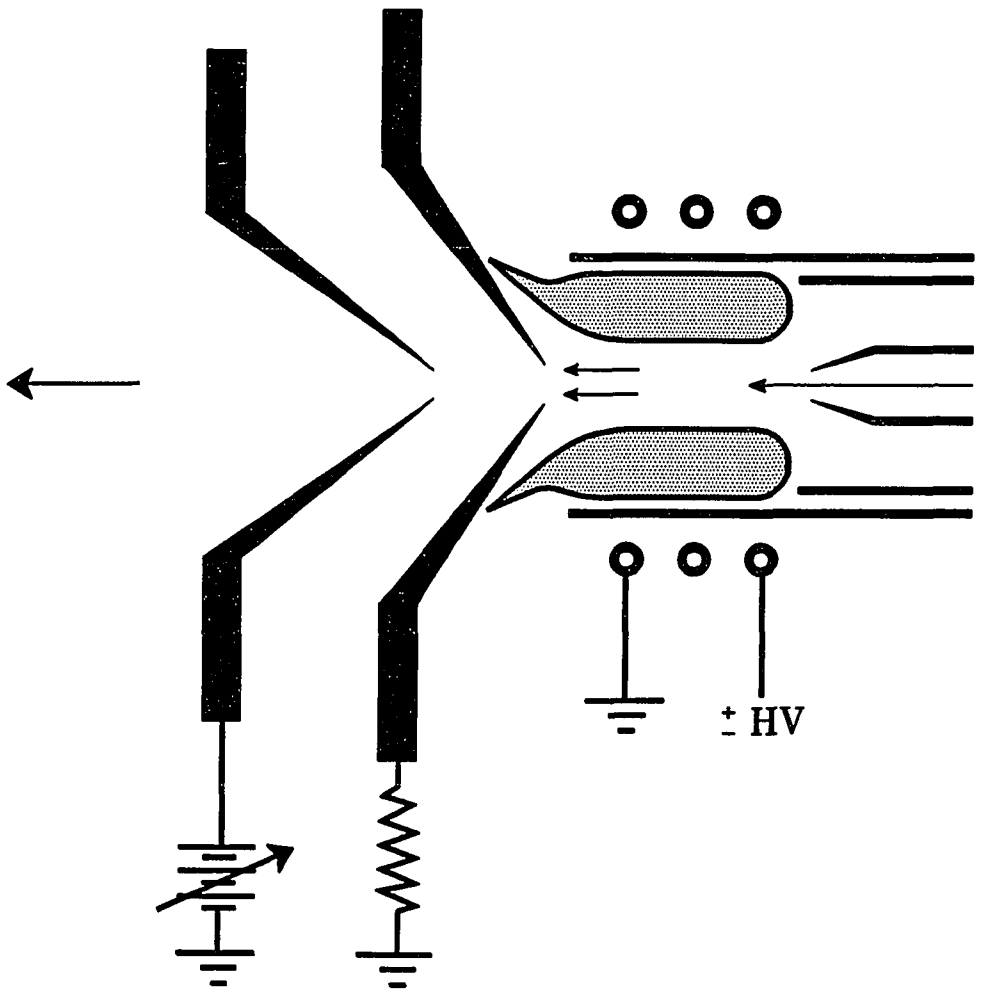

B

Figure 3. (continued)

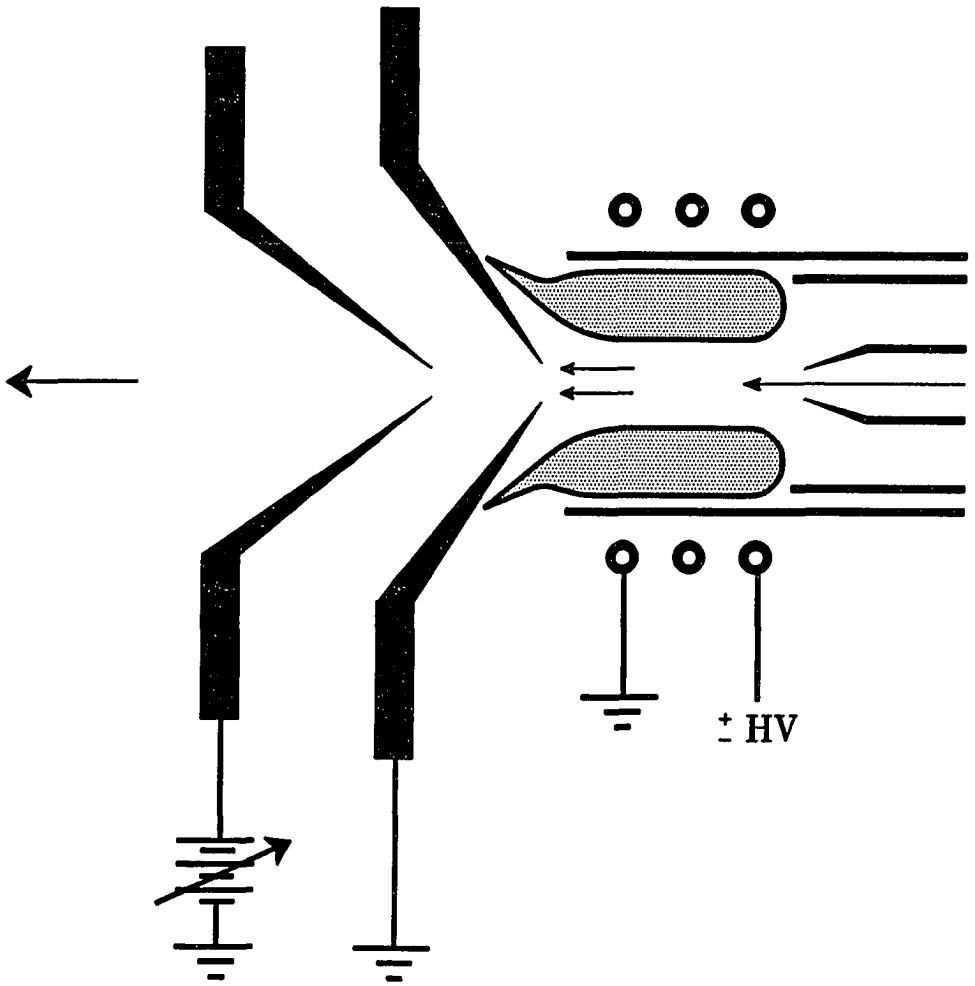

C

Figure 3. (continued)

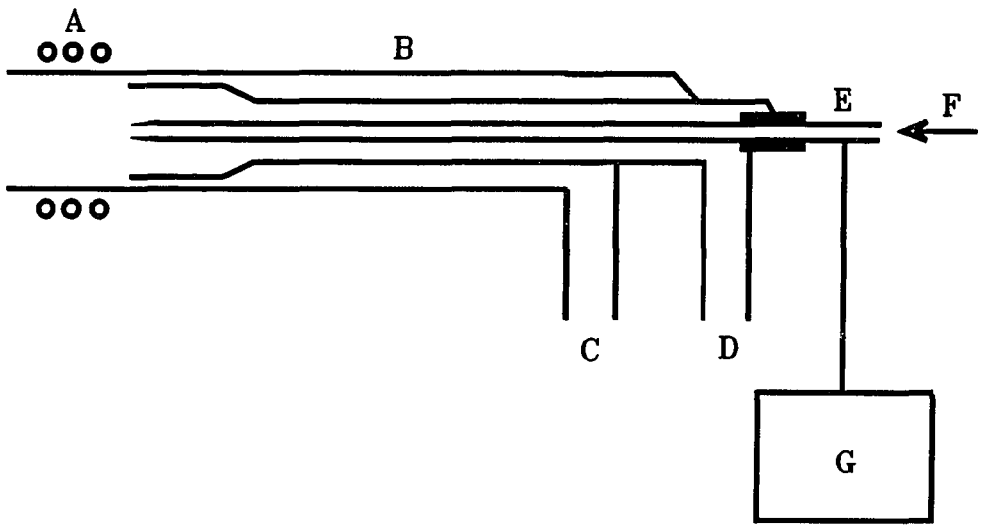

Figure 4. Diagram of ICP torch with a stainless steel injector tube: (A) load coil; (B) ICP torch; (C) plasma gas in; (D) auxiliary gas in; (E) stainless steel injector tube; (F) aerosol gas flow containing sample; (G) DC power supply.

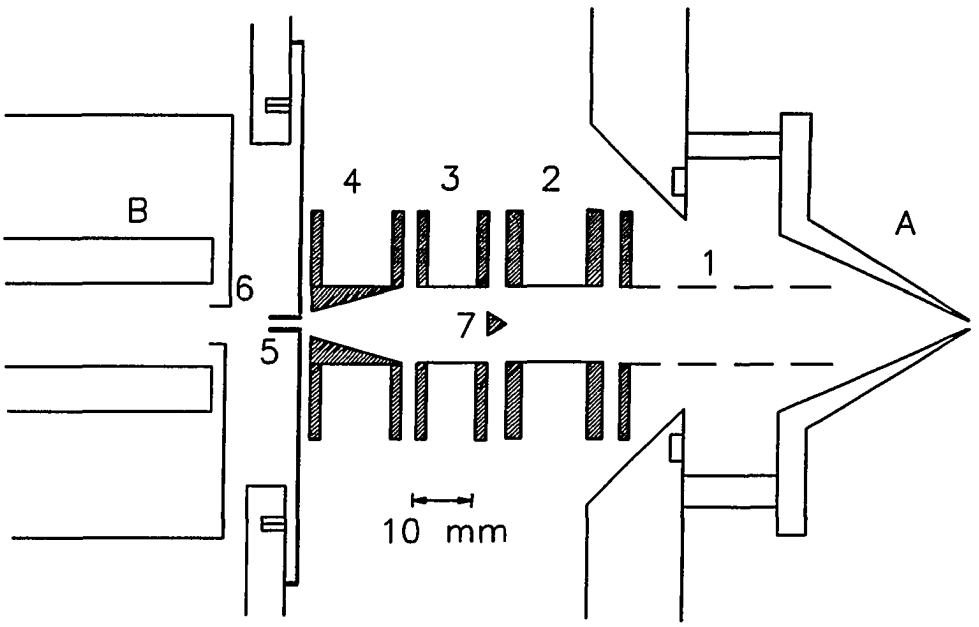

Figure 5. Schematic diagram of ion lens system: (A) skimmer; (B) quadrupole mass analyzer; (1 - 4) first to fourth electrodes of ion lens; (5) differential pumping orifice; (6) ELFS lens into rod housing; (J) quadrupole mass analyzer; (7) photon stop.

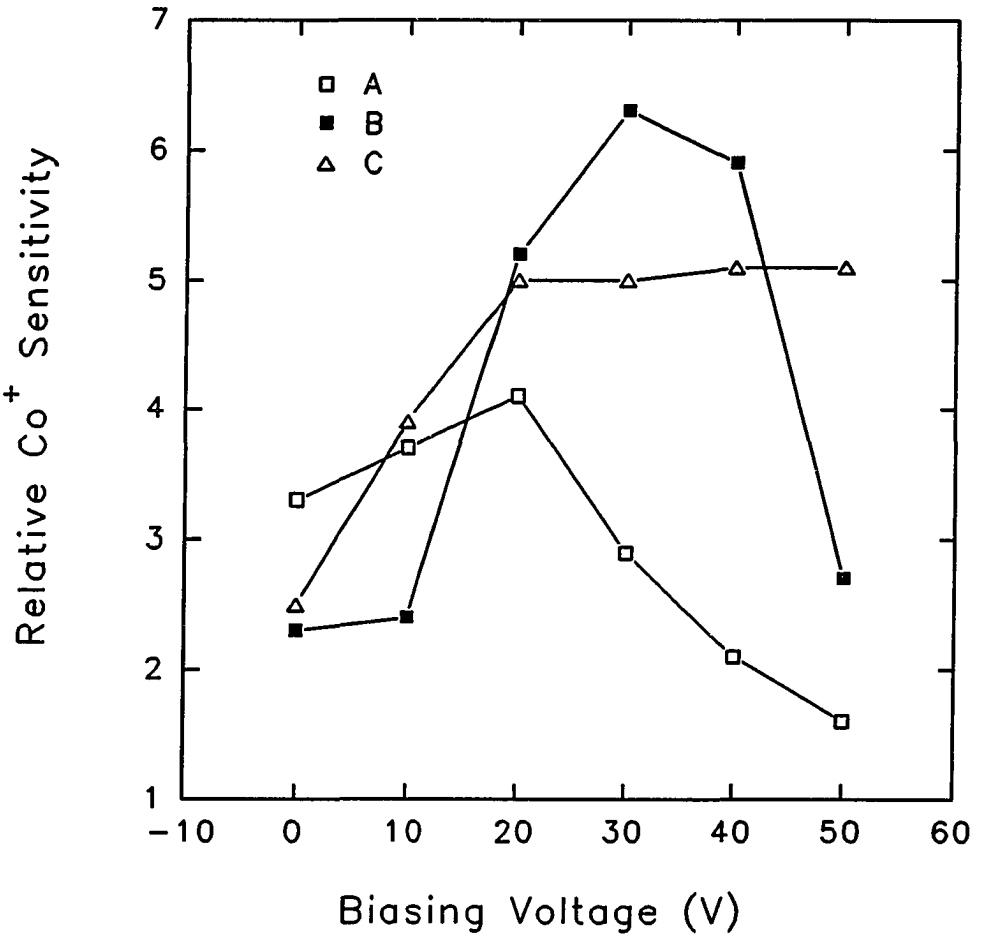

Figure 6. Relative Co ion signal as a function of biassing voltages with interface arrangements of A (sampler & skimmer biased together) (□), B (sampler floating & skimmer biased) (■), and C (sampler grounded & skimmer biased) (△).

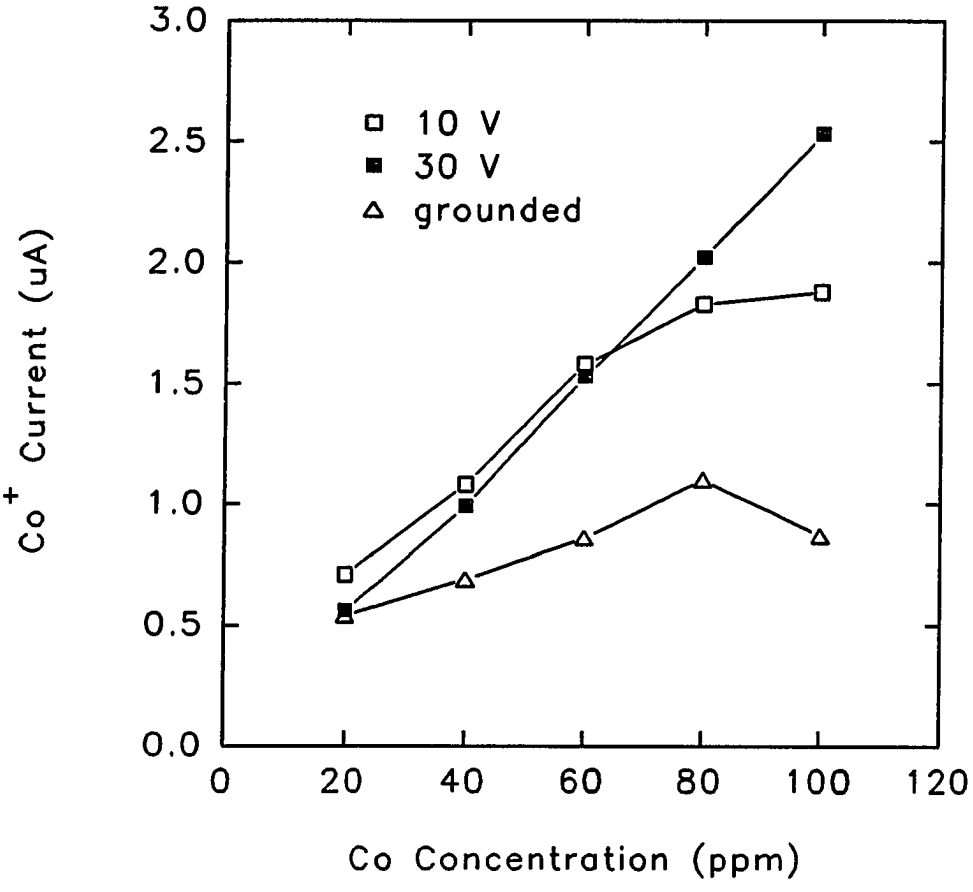

Figure 7. Linear dynamic range for interface arrangement A (sampler floated & skimmer biased) by 10 V (□) or 30 V (■) and conventional interface (sampler & skimmer grounded) (△).

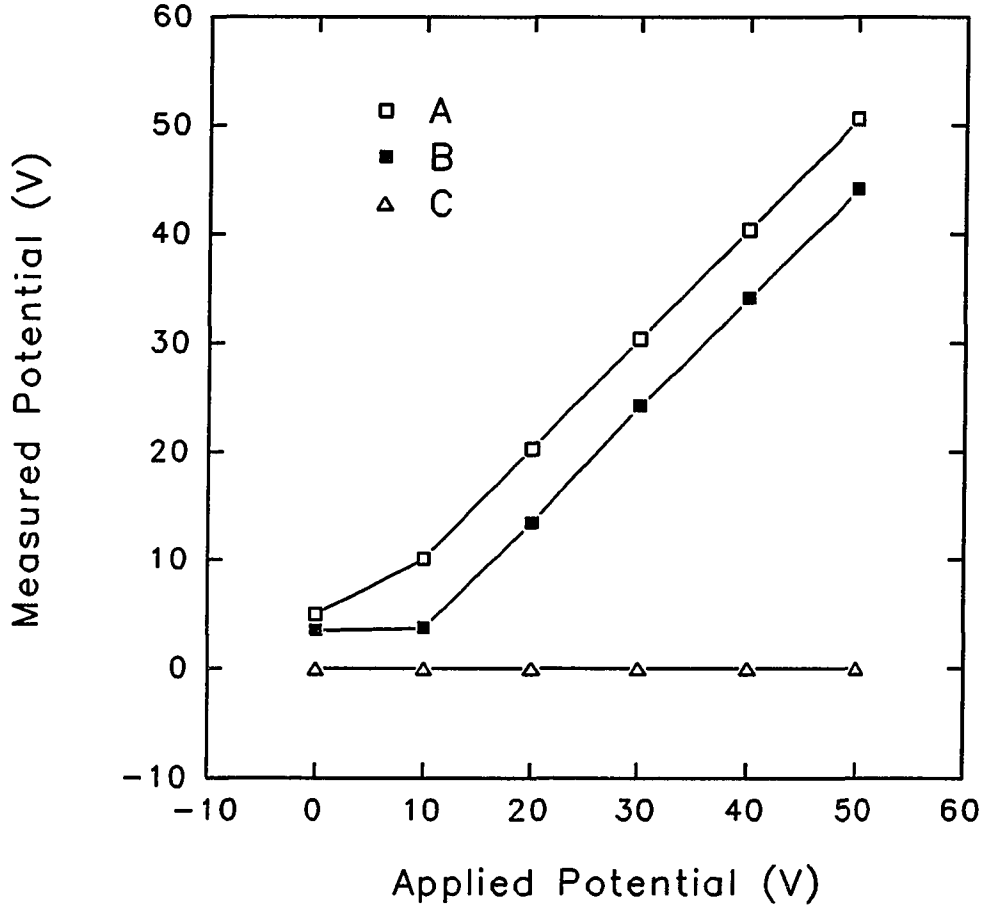

Figure 8. Measured potential on sampler as a function of applied bias potential with interface A (sampler & skimmer biased together) (□), interface B (sampler floating & skimmer biased) (■), and interface C (sampler grounded & skimmer biased) (△).

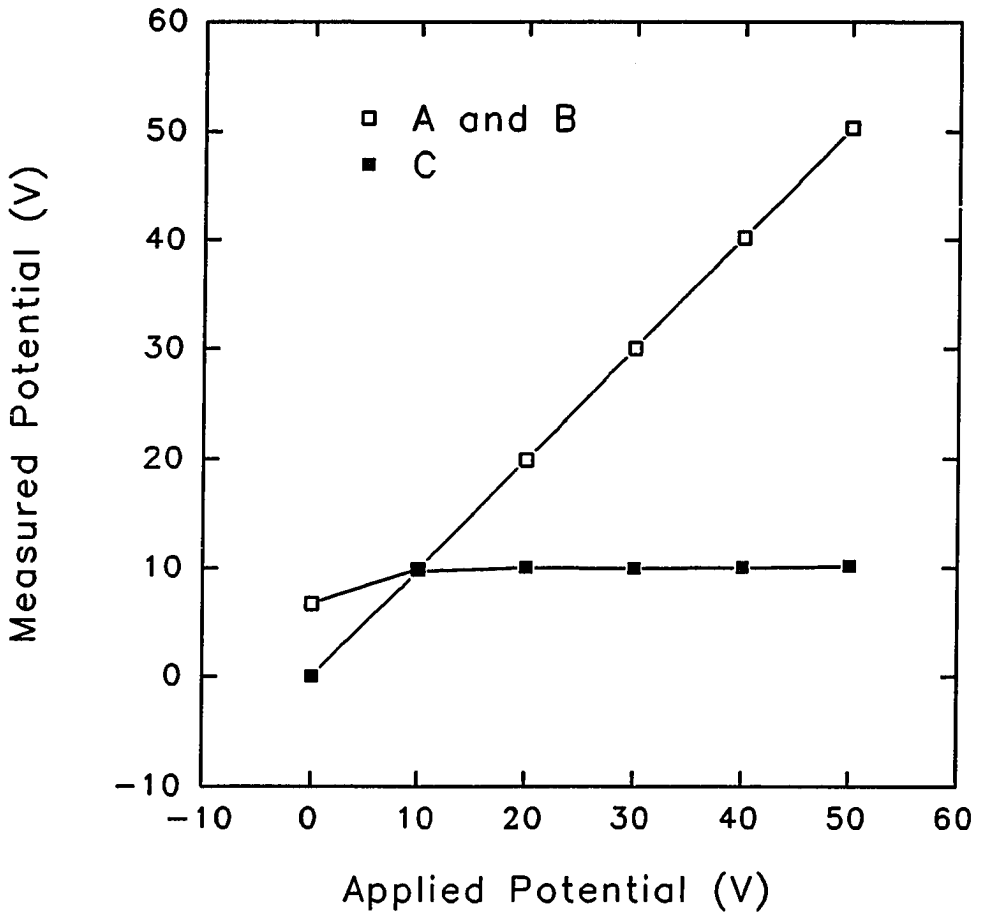

Figure 9. Measured potential on skimmer as a function of applied bias potential with interface A (sampler & skimmer biased together) and interface B (sampler floating & skimmer biased) (□), and interface C (sampler grounded & skimmer biased) (■).

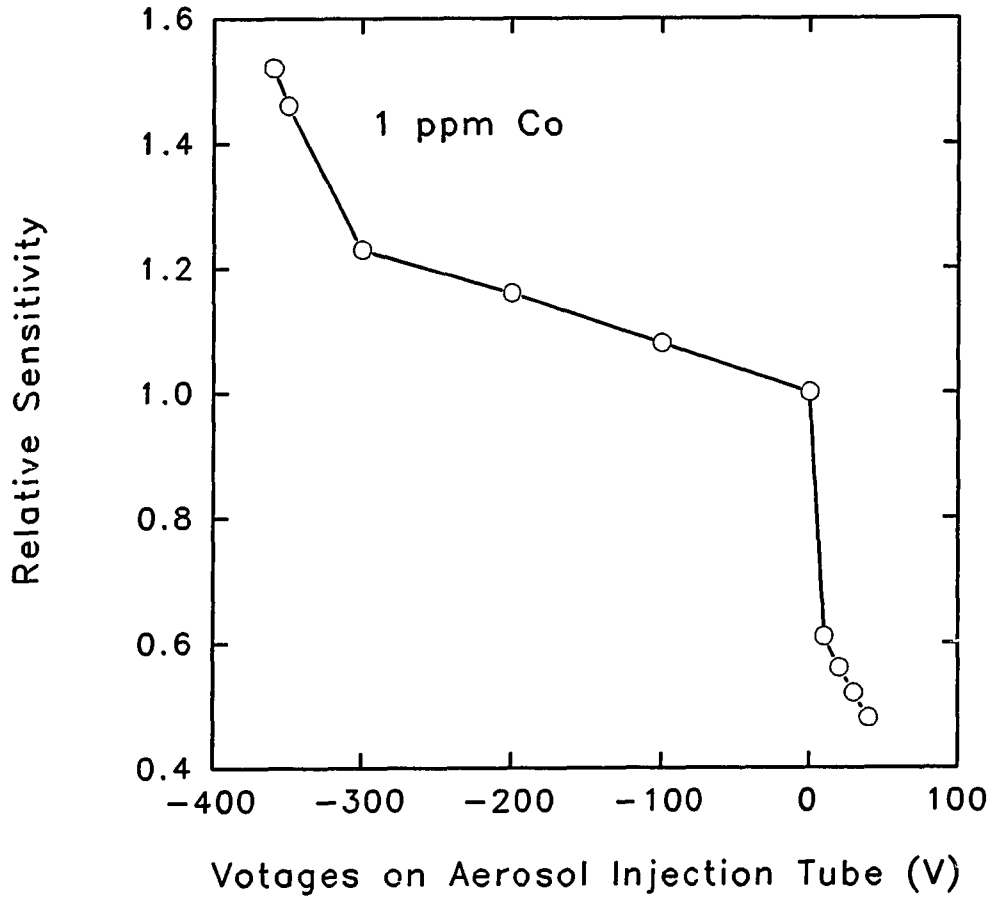

Figure 10. Relative ion signal as a function of voltage applied to aerosol injection tube.

PAPER IV.

INDUCTIVELY COUPLED PLASMA ION SOURCE AND MASS SPECTROMETER FOR ION DEPOSITION OR ION IMPLANTATION

INTRODUCTION

As thin film technology has developed, film characteristics such as purity, defect concentration, adhesion, and the range of materials that can be deposited have been improved by using various deposition techniques. Vacuum evaporation, various modes of sputtering, and ion plating have been well documented as to their suitability for a wide range of thin film applications (1-4). Unfortunately, such techniques also deposit undesirable foreign impurities within the film (5, 6). These impurities may come from the original source of the depositing particles. Another disadvantage of "conventional" techniques is that the energy of the depositing particles is uncontrolled.

Direct ion beam deposition is defined as a film formation method which exploits mass-separated, low-energy metal ion beams of the film constituents. Intensive work has already been reported recently for a variety of materials including metals and semiconductors (7-28). From the application point of view, ion beam deposition with finely controlled stoichiometry is useful for the fabrication of compound semiconductor devices which will be useful as high-speed, high-frequency devices and optoelectronics devices. Similar methods should be useful for the formation of very thin multilayers.

If the ions are accelerated to high ion energies, they penetrate more deeply into the solid target material, and ion implantation occurs. The principles and applications of ion implantation have been investigated and reported in detail elsewhere (29-33).

The basic requirements of an ion beam deposition facility for the production of high-purity, adherent thin films are as follows. First, the ion source should be as clean as

possible to maintain film purity. Second, the arrival energy of the depositing ions should be easily adjustable. Third, the arrival rate of the material to the substrate should be such that the film is deposited within a reasonable time. Finally, the pressure in the target chamber must be sufficiently low that residual gas contamination is minimized during deposition.

The ICP is a versatile, multielement ion source based on an atmospheric pressure plasma. Atomic ions are generated from all the sample constituents at the same time, so mixtures of such ions can be extracted for deposition. Samples of the element(s) to be deposited are generally added to the plasma as aqueous solutions. Thus, the concentration of ions in the plasma can be changed easily by varying the concentration of the element(s) in the solution. Because of the high temperature ($\sim$6000 K) and long residence time, atomic ions from elements that form refractory oxides such as Ta or rare earths are easily made.

The ICP was originally developed for film and crystal growth (34, 35), in which the crystal was grown on a solid probe that was inserted directly into the plasma. All atoms and ions in the ICP were deposited on the substrate at very high deposition rate. Merkle et al. successfully developed a technique utilizing an ICP combined with a low-pressure deposition chamber for deposition of thin films (36). The interface was similar to that used to extract ions for ICP-MS. The substrate was located behind the skimmer, so the deposition rate was not as high as when the substrate was inserted directly into the plasma (34,35). The film deposited with this method had less impurities because the target was in the deposition chamber with at 4×10^{-3} torr. But large amount of impurities extracted from the plasma were still deposited on the substrate and residual gas at this pressure could also cause reaction in

the film.

Since the publication of the first ICP-MS paper in 1980 (37), especially, since the introduction of the first commercial ICP-MS instrument in 1983, the technique has gained rapid and wide acceptance in many analytical laboratories. Because of its sensitivity, minimal interferences, capability for multielement analysis, and analysis of isotope ratios, ICP-MS is used in many disciplines for the analysis of environmental, geological, metallurgical, nuclear, and industrial samples.

One problem for using an ICP as ion source for ion deposition or ion implantation is ion beam intensity. Generally, an ICP-MS instrument can generate a mass-resolved beam of $\sim 10^7$ ions s^{-1} per ppm in solution. If all mass-resolved ions from a 500 ppm solution are deposited on a substrate with area 1 cm^2, 56 hours are needed to deposit just one layer. This is not acceptable for most practical applications. In order to successfully use the ICP-MS as ion source for ion deposition, the ion beam intensity should be raised to a reasonable rate so that the film is built up within a reasonable time.

Usually, an ICP-MS instrument has three stages. Ions are extracted from the atmosphere pressure ICP to the first expansion chamber at a background pressure of a few torr. The ion beam then passes through the second stage at $1x10^{-4}$ torr. The analyzer and detector chamber is kept at 10^{-5} -10^{-6} torr. This pressure is not low enough to maintain film purity and reactions of film components with residual gas might contaminate the thin film.

The present work reports initial experiments in the adaptation of ICP-MS for ion deposition. A solution containing the elements of interest is nebulized. This sample aerosol is desolvated and injected into the ICP, where the sample is vaporized, dissociated, and

ionized. A portion of the plasma is extracted through an interface into a vacuum chamber. Ions are collected by ion optics and sent to a quadrupole mass analyzer, while neutrals are pumped away. This ion beam is then mass selected by the quadrupole mass spectrometer and deposited on the substrate. The mass transmitted can be changed rapidly and easily, so the stoichiometry of the ion mixture deposited on the target can be easily varied.

Thin films can be deposited softly on the surface of the target at a relatively low energy, or ions can be implanted deeply into the target at relatively high energy. In the ICP-MS system, ion energies are initially only a few eV, and the deposition energy can be easily controlled by changing the target bias potential. The instrument is modified to increase the ion intensity to about $5x10^{12}$ ions s^{-1} from a 1000 ppm solution. A four-stage vacuum system is used. The pressure in the deposition chamber is reduced to $1.5x10^{-7}$ torr. The target is kept at this relatively low pressure, so that side reactions of the deposited materials can be minimized.

EXPERIMENTAL

Two ICP-MS ion beam deposition instrument have been studied. First, the original three-stage ICP-MS (33-35) was used for maximizing ion beam intensity and for preliminary ion deposition experiments. Second, a new four-stage ICP-MS ion beam deposition device was constructed based on improvements identified from initial experiments with the old ICP-MS.

Old Instrument

The original ICP-MS, most components, and operating conditions have been described in detail elsewhere (38-41) and in paper III (see Figure 1 and Table I, paper III). The sampler and skimmer orifices were 0.79 mm and 1.09 mm diameter, respectively. The sampler - skimmer spacing was 9 mm. The pressure in the first, second, and ion deposition chamber were 1.2, $1x10^{-4}$, and $4.5x10^{-6}$ torr, respectively. The sampling position was 10 mm. A highly concentrated deposition solution (500 ppm) was nebulized by a continuous flow ultrasonic nebulizer (42,43). The solutions were delivered with a peristaltic pump (Gilson Model Minipuls 2) at a rate of 2.0 ml min^{-1}. The aerosol was desolvated in a pyrex heating tube at 140 °C followed by a condenser at 0 °C. Roughly 10% of the nebulized sample was transported out of the spray chamber. The remaining 90% ran into the drain of the spray chamber. This waste solution was circulated by pumping it back to the main solution container with a peristaltic pump. The ion deflecting plate was replaced by a target for ion deposition or ion implantation. Because the substrate was inserted perpendicular to

the ion exit axis, ions had to be deflected over a long distance (6 cm) to hit the target (see Figure 1, paper III). The ions did not form a collimated ion beam without an RF-only quadrupole after the mass filter and were further defocused as they left the mass analyzer, which complicated the task of steering them onto the target.

Improvement of Interface and Ion Lens for Old ICP-MS Device

To obtain an intense ion beam, a highly concentrated solution was used. Solid condensed from the highly concentrated solution easily plugged the usual 1.00 mm diameter sampler orifice. Drilling the orifice to 1.31 mm diameter prevented this ion condensation problem (44). The ion beam intensity also increased with the larger sampler and skimmer orifices (44).

After extraction through the interface, the ion beam was focused in the ion optics. In order to intensify ion beam, the ion lens was modified (Figure 1). The first, second, third, and fourth electrodes of ion lens were a perforated stainless steel cylinder, a copper cone, a stainless steel cylinder, and a stainless steel tapered cylinder, respectively (1-4, Figure 1). The usual photon stop was removed for improving ion transmission. Some neutrals and photons were blocked by the second electrode, which was a copper cone. The ions then passed a differential pumping orifice (2.5 mm diam. x 6.4 mm long) and were injected into the quadrupole.

New ICP-MS Ion Deposition Device

A new ICP-MS ion deposition instrument was constructed based on the lessons

learned with the old device. A schematic diagram of this new ICP-MS ion beam deposition instrument is shown in Figure 2. A commercial continuous flow ultrasonic nebulizer (Model U-5000, CETAC Technologies, Inc.) was used to nebulize the sample solution. The interface and ion lens were the same as those described above. Most other instrument components in this device were described elsewhere (44). A rigorous treatment of particular components of interest follows. The general operation conditions are identified in Table I.

The quadrupole mass filter used in this work was coupled with both entrance and exit RF only quadrupoles. The schematic diagram of the power connection and coupling of quadrupole filter with RF-only quadrupoles is shown in Figure 3. This component was described in detail elsewhere (44).

As described above, the pressure in the substrate chamber must be sufficiently low that residual gas contamination is minimized if a high purity film is desired. The last stage (ion beam deposition chamber) was pumped with a turbomolecular pump (Model TMP 360V, Leybold Vacuum Products Inc.; Pumping speed, 400 L s^{-1}). A stainless steel tube, 2.54 cm long x 0.625 cm inside diameter served as differential pumping aperture. The pressure in this chamber was lowered to 1.5×10^{-7} torr which was at least 10 times lower than that obtained with general ICP-MS instruments and about 30 times lower than the pressure obtained with the old ICP-MS device described above. One of the other advantages of low pressure in deposition chamber is that a higher target potential can be applied for ion implantation. A Channeltron electron multiplier was used to monitor the ion beam intensity before and after ion deposition.

A substrate interlock chamber for inserting the target was constructed and is shown

in Figure 4. This chamber was pre-evacuated by a mechanical vacuum pump (Model 1402, Welch Scientific Company) before opening to the ion deposition chamber, hence, vacuum was not broken when the target was changed. The target could be changed in 5 - 10 minutes.

Substrate

Generally, a graphite target (0.36 cm^2 surface) was used as the ion deposition substrate because of its softness, low sputtering efficiency at low ion kinetic energy, high ion deposition efficiency, good adherence, and resistance to dissolution in acid. The target was polished with 600-A grit SiC paper (3M) to a final dimension of 6.0 mm diameter x 3.0 cm long. Before a deposition experiment, the substrate was cleaned by the following procedures. The substrate was first immersed in 1% HNO_3 for 1 hour, then immersed in distilled deionized water for 2 hours, then dried. Finally, the substrate was cleaned ultrasonically with acetone and then methanol and then dried again.

A titanium oxide (Ebonex) target (0.25 cm^2) was also used with the old ICP-MS instrument (see Figure 1, section III). Like the graphite, the titanium oxide did not dissolve readily in HNO_3. It was polished by 600-A grit SiC paper followed by 0.5 μm alumina powder (Buehler Ltd.) and was cleaned in the same way as graphite.

Either substrate was mounted onto a copper substrate holder which was mounted onto an electrical feedthrough (U, Figure 4) which was welded to the tip of the insertion probe (T, Figure 4). The voltage was applied to the substrate through an electrical feedthrough within the hollow probe.

Experimental Procedures

Ions selected by the mass spectrometer were first detected by a Channeltron electron multiplier. A 1 ppm solution of the element to be deposited was used to maximize the ion beam intensity by adjusting ion lens voltages, aerosol gas flow rate, and sampling position. The procedures of handling the substrate target with the both old and new devices were similar to each other, therefore only the methods and figures for operating the interlock chamber with the new device was described.

Following optimization, the voltages on the detector, detector housing aperture, and ion repeller were turned off. The substrate was moved from the interlock chamber (see Figure 4A) to a position 10 mm behind the ion exit tube (differential pumping tube) (see Figure 4B). The substrate was cleaned by sputtering with $^{40}Ar^{+}$ at 2.5 keV for 10 min. Conveniently, these Ar ions were always present in the plasma. The desired voltage was then applied to the target for ion deposition or ion implantation. Highly concentrated solutions (500 ppm for the old device, 1000 ppm for the new device) were nebulized.

Deposition times varied depending on the ion dose desired. For these exploratory experiments, the deposition time was usually 2.5 - 3.0 hours. After deposition, the target was removed through the interlock. The deposited thin film was then dissolved into 1 - 5 ml 5% HNO_3 solution for 1 hour. This solution was diluted to 10 -100 ml with distilled deionized water, depending on the ion dose. The concentration of deposited material in the solution was determined by a different ICP-MS (SCIEX Elan 250, Perkin-Elmer) with a flow injection method. The data were converted into ion deposition rate (ions s^{-1}). The above target was dissolved again. A blank substrate was also dissolved with the same method

described above. Both solutions were also analyzed by the ICP-MS. There was no detectable Ho in these two solutions, which meant that all Ho atoms deposited on the substrate were dissolved and any Ho atoms in the original substrate were insignificant compared to the deposited Ho.

Standards and Solutions

A Ho^+ solution at 500 ppm was prepared by diluting 1000 ppm Ho (Atomic Absorption Standard, Fisher Scientific Company). Standard solutions at 1 ppm were prepared by diluting aliquots of commercial stock solutions (Fisher) with distilled deionized water (18 MΩ, Barnstead). The 5% HNO_3 was prepared by diluting ultra pure acid (Ultrex II ultrapure reagent grade, J. T. Baker) in distilled deionized water.

RESULTS AND DISCUSSION

Ion Deposition with Old ICP-MS Instrument

The measured Ho ion deposition rate (ions s^{-1}) on titanium oxide as a function of ion kinetic energy is depicted in Figure 5. The deposition rate was highest at 350 eV. The ion beam intensity at this ion energy was 3.5×10^9 ions s^{-1}, which represented a total of about 4×10^{13} atoms deposited on the substrate. At this intensity value, 19 hours would be required to deposit one layer of Ho atoms on the titanium oxide substrate. Definitely, this intensity is too low for practical ion beam deposition.

When a high potential (above 4.5 kV) was applied to the target, a strong discharge occurred. Ion implantation experiments could not be done in this ICP-MS instrument.

Improve Merits in Ion Beam Intensity with Old Instrument

The old apparatus (Figure 1, section III) was used to evaluate the following ways to increase ion beam intensity. First, ion beam intensity increased about 6 - 8 fold by enlarging the sampler orifice from 0.79 mm to 1.31 mm (44) and another two fold by drilling the skimmer orifice from 1.09 mm to 1.31 mm. Second, ion beam intensity increased about 3 - 5 fold when the entrance of the first ion lens electrode (1, figure 1) was moved closer to the skimmer tip (44). Third, ion beam intensity increased about 3 - 5 fold by removing the photon stop, and by using a cone for the second ion lens electrode and a tapered cylinder for the fourth ion lens electrode. In total, the ion intensity increased about 100 -400 fold by these simple changes to the interface and ion optics.

Ion Deposition with New ICP-MS Ion Deposition Device

Based on the results of the above experiments, a new device was built especially for ion deposition, which featured entrance and exit RF only quadrupoles and a ion exit focusing tube. Also the substrate was placed right after the ion exit tube. The reasons for using RF only quadrupoles were to inject the ion beam efficiently into the mass analyzer and to focus the ions to a fine beam for better ion beam transmission through the small diameter exit lens. The substrate right after the exit lens should collect all ions more efficiently than when the substrate was perpendicular to the ion path.

The measured Ho ion deposition rate on the graphite substrate as a function of ion kinetic energy is shown in Figure 6. At low ion energy, the deposition efficiency increased as the ion energy increased. Optimal ion energies were between 50 eV and 2000 eV. For ion kinetic energies in the range of 2 - 3 keV, both the substrate and previously deposited Ho atoms were sputtered, consequently, the amount of Ho that remained on the substrate was reduced. With a further increase in the ion kinetic energy, above 2.5 kV in Figure 6, ions were driven deeply enough into the target that they were not sputtered back out by subsequent Ho ions. Therefore, the deposition rate increased again. The highest ion deposition rate was about $5x10^{12}$ ions s^{-1} (see Figure 6). The highest total amount of Ho on the graphite substrate for 2.5 hours deposition was about $4.0x10^{16}$ ions. The time of deposition of one layer film on the graphite substrate (area = 0.36 cm^2) would be about 1.1 minutes.

These values for ion dose and deposition time represented improvements of a factor of more than 1000 than those obtained with the old device. Furthermore, specious electrical

discharges in the target chamber were not observed at any of the target voltages used. The 5 kV limit in Figure 6 represented the maximum rating for the feedthrough on the insertion probe that held the target. In other experiments with much lower ion counts, up to 18 kV was applied to the target of a Daly detector in this chamber without electrical discharge (44). It is likely that ions could be implanted deeper still by biasing the substrate to a high voltage.

Purity of Ion Deposition

One source of impurity in ion deposition comes from reaction with the residual gas in the deposition chamber. The impurity from residual gas in the deposited thin film can be expressed as:

$$X = (Sn\Gamma n)/(Si\Gamma i) \qquad (1)$$

where Γn is the residual gas atom flux that hits the target surface and Γi is the depositing ion beam flux on the target surface. Here Sn and Si denote the sticking probabilities of residual gas atoms and of deposited ions, which are assumed to be 0.01 and 1, respectively. The quantities Γn and Γi are expressed as (45):

$$\Gamma n = 5.30 \times 10^{20} \text{ P } (\text{cm}^{-2}\ \text{s}^{-1}) \qquad (2)$$

$$\Gamma i = 6.25 \times 10^{12} \text{ Ji } (\text{cm}^{-2}\ \text{s}^{-1}) \qquad (3)$$

where P (torr) is the residual gas pressure in the deposition chamber (45) and Ji (μA/cm^2) is the ion beam current density impinging the target (45). The ion beam intensity in our modified ICP-MS ion beam deposition system is 5×10^{12} ions s^{-1}, e.g., 8×10^{-7} A or 0.8 μA. The target surface area is 0.36 cm^2 and the residual pressure in the deposition chamber is 1.5×10^{-7} torr. So, the calculated amount of impurity in the deposited thin film on 0.36 cm^2

target surface is about 5.7%. Even though this purity is good enough for many ion deposition applications, further reductions in residual pressure or increase in ion beam intensity are still desirable.

Detection Efficiency of Channeltron Detector

Suppose all the ions that left the ion exit lens stuck on the graphite substrate. the detection efficiency (Y) of the Channeltron detector can be calculated as:

$$Y = G/H$$

where G is the ion count rate (ions s^{-1}) detected by the Channeltron detector and H is the ion beam intensity (ions s^{-1}) deposited on the substrate. The highest ion count rate detected by Channeltron detector is $5x10^5$ ions s^{-1} per ppb when low mass resolution and a low threshold for the amplifier-discriminator are utilized. The best ion beam intensity is $5x10^6$ ions s^{-1} per ppb by presuming the dynamic range to be linear up to 1000 ppm. Therefore, the detection efficiency of the Channetron detector, Y, is about 10%, i.e., if 10 ions pass through the ion exit lens, only one ion is detected. Presumably, this 10% efficiency represents a juxtaposition of a) incomplete collection of ions (i.e., some ions that leave the exit lens do not strike the mouth of the detector, and b) incomplete conversion of ions to electrons. This estimate represents the most favorable case for the Channeltron detector. If the probability of deposition is not 1 and the upper end of the linear dynamic range is less than 1000 ppm, the detection efficiency of the Channeltron detector is even less than 10%. Thus, if the ion dose is to be estimated with a Channeltron detector, a correction must be made for this low detection efficiency.

CONCLUSION

An ICP ion source can be combined with a mass spectrometer for direct ion beam deposition or ion implantation. The basic requirements (high ion intensity, low pressure in target chamber, controllable ion energy, and clean ion source) of ion beam deposition are all met by an ICP-MS ion beam deposition system.

This initial research suggests the following follow-up studies with this new ion deposition and ion implantation system: a) modification of the electrochemical properties of metal oxide electrodes by doping them with impurity metal ions; b) deposition of thin films of interest such as pure refractory metals (W or Nb), diamond, or superconductors on appropriate substrates; c) deposition of mixtures of atoms; d) use of a secondary ion mass spectrometer for in-situ analysis of the deposited materials; and e) deliberate leaking of a reactive gas into the target chamber so that controlled chemical reactions between the deposited ions and added gas will yield the desired coating on the target. This objective should be achievable without changing composition or properties of plasma ion source.

The observed ion intensity of 5×10^{12} ions s^{-1} for 1000 ppm only represents 0.005% of the metal ions sampled from the ICP or ~0.5% of the ions through the skimmer; substantial room for improvement remains in the efficiency of ion collection and transport. The deposition chamber should allow application of higher voltages to accelerate ions for implantation. Accelerating ions to very high ion kinetic energy by applying a high voltage, for example 5 kV, on the interface would improve ion beam intensity and implant ions even more deeply into the substrate.

LITERATURE CITED

1. Chopra, K. L. Thin Film Phenomena; McGraw-Hill: New York, 1969.
2. Maissel, L. I.; Glang, R. Handbook of Thin Film Technology; McGraw-Hill: New York, 1970.
3. Chapman, B. In Glow Discharge Processes; Wiley: New York, 1980; Chapter 3 and 5.
4. Itoh, T. Ion Beam Assisted Film Growth; Elsevier: New York, 1989.
5. Mayer, D. E. J. Vac. Sci. Technol. 1974, 11, 168-173.
6. Coburn, J. W.; Eckstei, E. W.; Kay, E. J. Vac. Sci. Technol. 1975, 12, 151-154.
7. Tokuyama, T.; Yagi, K.; Miyake, K.; Tamura, N.; Natsuaki, N.; Tachi, S. Nucl. Instrum. and Methods, 1981, 182/183, Part I, 241-250.
8. Harper, J. M. E. In Thin Film Processes; Vossen, J. L.; Kern, W., Eds.; Academic Press: New York, 1978, 175-206.
9. Aisenberg, A.; Chabot, R. J. Vac. Sci. Technol. 1973, 10, 104-107.
10. Amano, J; Lawson, R. P. W. J. Vac. Sci. Technol. 1977, 14, 690-694; 695-698.
11. Senda, N. Mat. Res. Soc. Symp. Proc. 1991, 223, 335-346.
12. Amano, J; Lawson, R. P. W. J. Vac. Sci. Technol. 1978, 15, 118-119.
13. Miyake, K.; Yagi, K.; Tokuyama, T. Inst. Phys. Conf. Ser., 1978, 38, 78-83.
14. Yagi, K; Miyake, K. Tokuyama, T. Inst. Phys. Conf. Ser., 1978, 38, 136-141.
15. Shimizu, S.; Sasaki, N.; Ogata, S.; Tsukakoshi, O.; Seki, S.; Yamakawa, H. Mat. Res. Soc. Symp. Proc. 1991, 223, 347-352.

16. Appleton, B. R.; Pennycook, S. J.; Zuhr, R. A.; Herbots, N.; Noggle, T. S. Nucl. Instrum. and Methods, 1987, B19/20, 975-982.

17. Herbots, N.; Appleton, B. R.; Noggle, T. S.; Zuhr, R. A.; Pennycook, S. J. Nucl. Instrum. and Methods, 1987, B13, 250-258.

18. Zuhr, R. A.; Alton. G. D.; Appleton, B. R.; Herbots, N.; Noggle. T. S.; Pennycook, S. J. presented at the 1987 Spring MRS Symposium, Anaheim, CA, 1987.

19. Zuhr, R. A.; Appleton, B. R.; Herbots, N.; Larson, B. C.; Noggle. T. S.; Pennycook, S. J. J. Vac. Sci. Technol. 1987, A5, 2135-2139.

20. Shimizu, S.; Tsukakoshi, O.; Komiya, S.; Makita, Y. Jap. Appl. Phys., 1985, B3, 1130-1140.

21. Maruno, S.; Morishita, Y.; Isu, T.; Nomura, Y.; Ogata, H. J. of Crystal Growth, 1987, 81, 338-343.

22. Shimizu, S.; Tsukakoshi, O.; Komiya, S.; Makita, Y. J. Vac. Sci. Technol. 1985, B3, 1134-1140.

23. Ishikawa, J.; Ogawa, K.; Miyata, K.; Tsuji, H.; Takagi, T. Nucl. Instrum. and Methods in Phys. Res. 1987, B21, 205-208.

24. Withrow, S. P.; More, K. L.; ZUhr, R. A.; Haynes, T. E. Vacuum, 1989, 39, 1065-1068.

25. Haynes, T. E.; Zuhn, R. A.; Pennycook, S. J.; Appleton, B. A. Appl. Phys. Lett. 1989, 54, 1439-1441.

26. Gordon, J. S.; Armour, D. G.; Donnely, S. E.; Van den Berg, J. A.; Marton, D.; Rabalais, J. W. Proc. 7th Inter. Conf. on IBMM'90, Knoxville, 1990, 146.

27. Ishikawa, J.; Takeiri, Y.; Ogawa, K.; Takagi, T. J. Appl. Phys. 1987, 61, 2509-2515.

28. Haynes, T. E.; Zuhn, R. A.; Pennycook, S. J.; Larsen, B. C. Proc. 12th Symp. on ISIAT'89, Tokyo, 1989, 363.

29. Ziegler, J. F. Ion Implantation Science and Technology; 2nd Ed. Academic Press: New Yourk, 1988.

30. Rissel, H.; Ruge, I. Ion Implantation, John & Sons Ltd.: New York, 1986.

31. Laursen, T.; Clapham, L.; Whitton, J. L. Nucl. Instrum. and Methods in Phys. Res. 1991, B59/60, 768-771.

32. White, A. E.; Short, K. T.; Berger, S. D.; Huggins, H. A.; Loretto, D. Mat. Res. Soc. Symp. Proc. 1989, 147, 223-228.

33. Follstaedt, D. M.; Knapp, J. A.; Pope, L. E. Mat. Res. Soc. Symp. Proc. 1989, 128, 389-402.

34. Reed, T. B. J. Appl. Phy. 1961, 32, 821-824, 2534-2535.

35. Reed, T. B. J. Appl. Phy. 1963, 34, 2266-2269.

36. Merkle, B. D.; Kniseley, R. N.; Schmidt, F. A. J. Appl. Phys. 1987, 62, 1017-1021.

37. Houk, R. S.; Fassel, V. A.; Flesch, G. D.; Svec, H. J.; Gray, A. L. and Taylor, C. E. Anal. Chem. 1980, 52, 2283-2289.

38. Olivares, J. A.; Houk, R. S. Anal. Chem. 1985, 57, 2674-2679.

39. Huang, Le-Qun; Jiang, Shiuh-Jen; Houk, R. S. Anal. Chem. 1987, 59, 2316-2320.

40. Crain, J. S.; Houk, R. S.; Eckels, D. E. Anal. Chem. 1989, 61, 606-612.

41. Scott, R. H.; Fassel, V. A.; Kniseley, R. N.; Nixon, D. E. Anal. Chem. 1974, 46, 75-80.

42. Olson, K. W.; Haas, W. J., Jr.; Fassel, V. A. Anal. Chem. 1977, 49, 632-637.

43. Bear, B. R.; Fassel, V. A. Spectrochim. Acta, Part B 1986, 41B, 1089-1113.

44. Hu, Ke; Clemons, S.; Houk, R. S. J. Amer. Soc. Mass Spectrom. 1992, Submitted.

45. Miyake, K.; Tokuyama, T. In Ion Beam Assisted Film Growth; Iton, T. Ed.; Elsevier: New York, 1989, Chapter 8.

Table I. Operating conditions for new ICP-MS apparatus (Figure 1)

Component	Operation conditions
Plasma forward power	1.30 kW
Plasma reflected power	< 5 W
Plasma argon gas flow	17 L min^{-1}
Auxiliary argon gas flow	0
Aerosol argon gas flow	1.30 L min^{-1}
Sampling position	13 mm from load coil, on center
Sampler - skimmer separation	11 mm
Expansion chamber pressure	2.30 torr
Second stage pressure	$5x10^{-4}$ torr
Third stage pressure	$5x10^{-6}$ torr
Fourth stage pressure	$1.5x10^{-7}$ torr
Ion lens setting	
first cylindrical lens	-260 V
second copper cone lens	-60 V
third cylindrical lens	-250 V
fourth cylindrical lens	-180 V
differential pumping orifice	-200 V
ELFS lens	-200 V

Table I. continued

Ion exit tube	-50 V
Ion deflecting plate	+700 V
Detector housing aperture	-250 V
Channeltron electron multiplier	
pulse counting	-3000 V
ion current	-2500 V
Mean DC voltage on mass analyzer	-5.0 V
Mean DC voltage on RF-only quad rods	-65 V

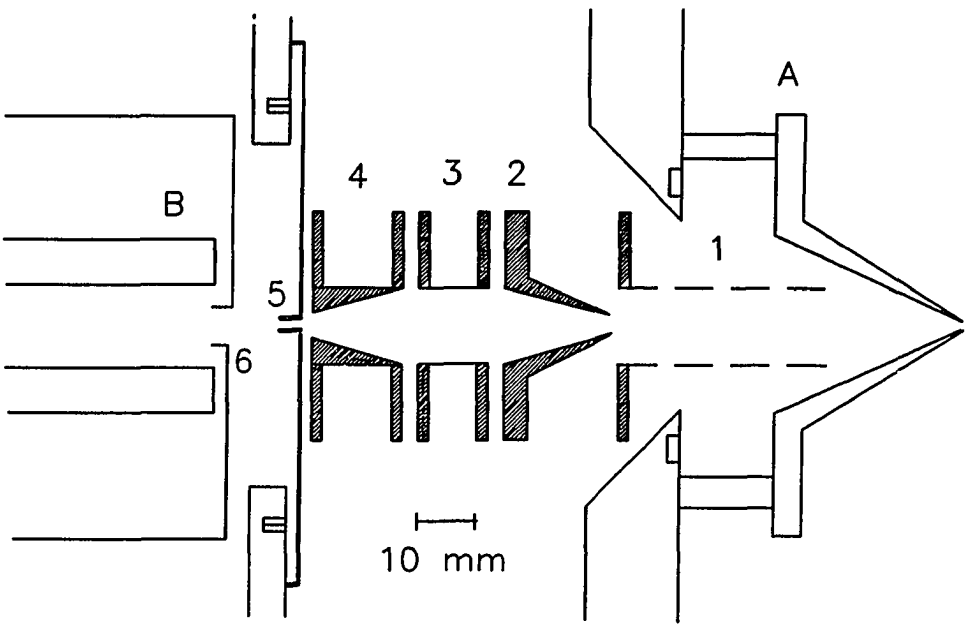

Figure 1. Schematic diagram of ion lens system: (A) skimmer; (B) RF-only quadrupole; (1) perforated stainless cylinder, first electrode of ion lens; (2) copper cone, second electrode of ion lens; (3) stainless steel cylinder, third electrode of ion lens; (4) stainless steel taper cylinder, fourth electrode of ion lens; (5) differential pump orifice (DPP); (6) quadrupole ELFS lens.

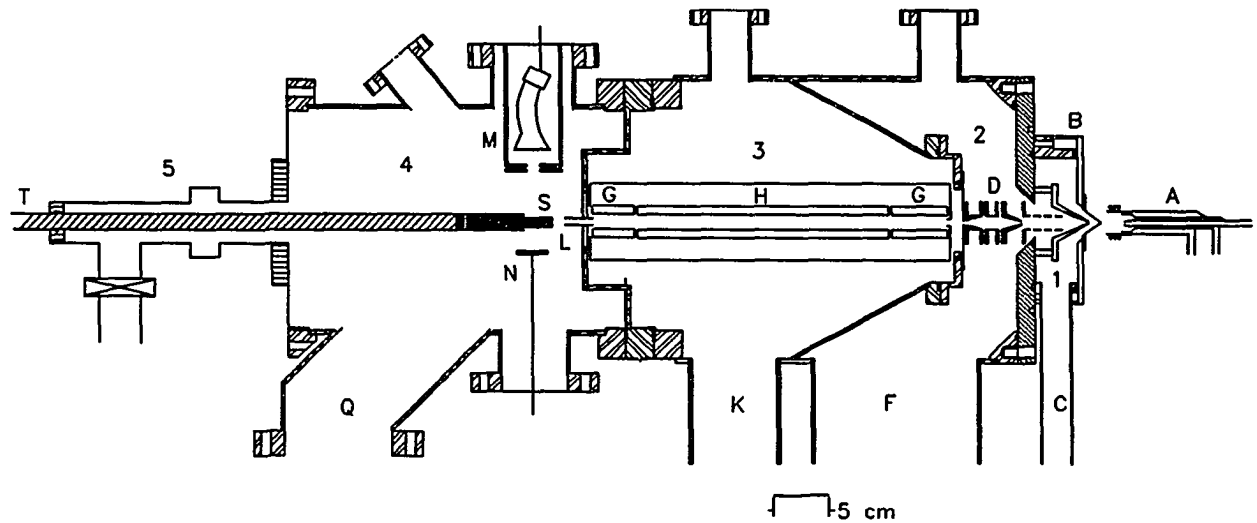

Figure 2. New ICP-MS ion deposition system: (1) first stage chamber; (2) second stage chamber; (3) quadrupole chamber; (4) deposition chamber; (5) interlock chamber; (A) ICP; (B) ion extraction interface; (C) port to rotary pump; (D) ion lens (see Figure 2); (F) port to diffusion pump (1600 L s^{-1}); (G) RF-only quadrupoles; (H) quadrupole mass analyzer; (K) (Q) ports to turbomolecular pumps (400 L s^{-1}); (L) ion exit lens; (M) Channeltron electron multiplier; (N) deflection plate; (S) substrate or target; (T) target probe.

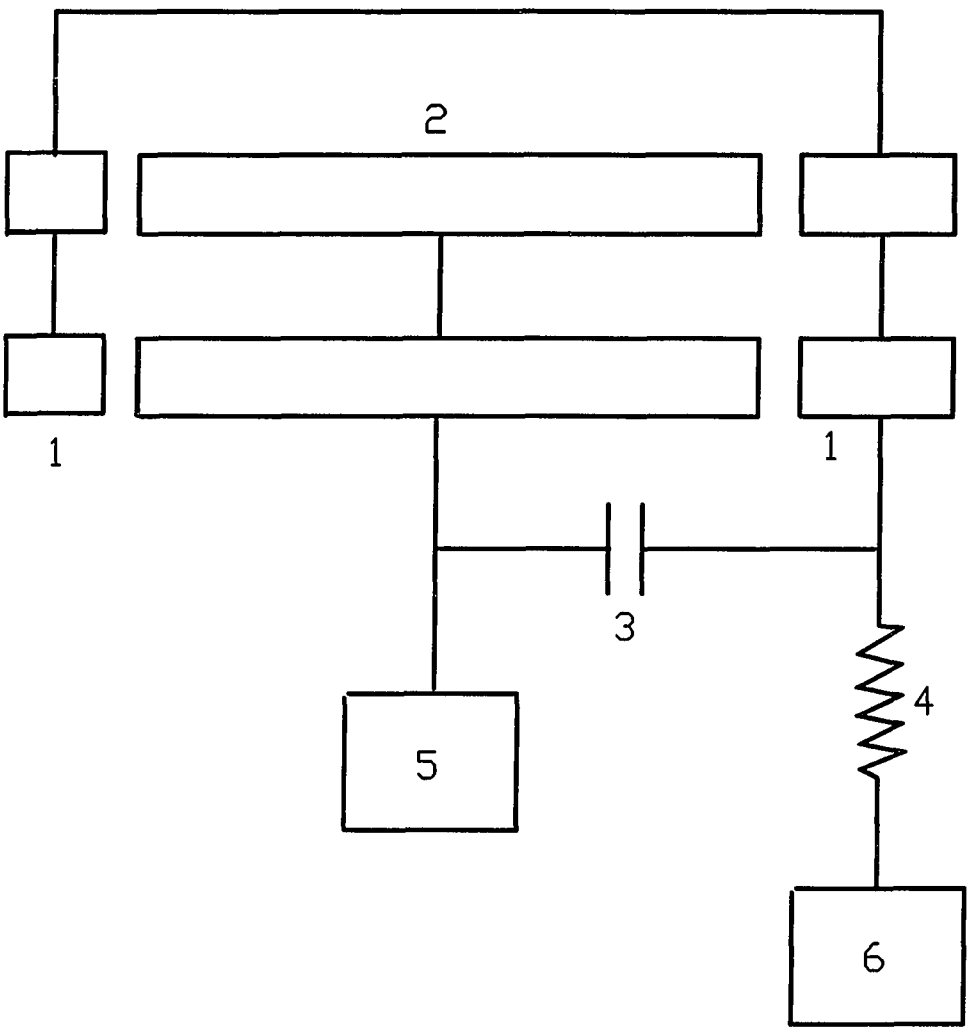

Figure 3. Electrical coupling between RF-only quad rods and mass filter. (1) RF-only quadrupole; (2) mass analyzer; (3) 50 pF capacity; (4) 1 MΩ resistance; (5) mass filter power supply: RF plus DC; (6) DC power supply.

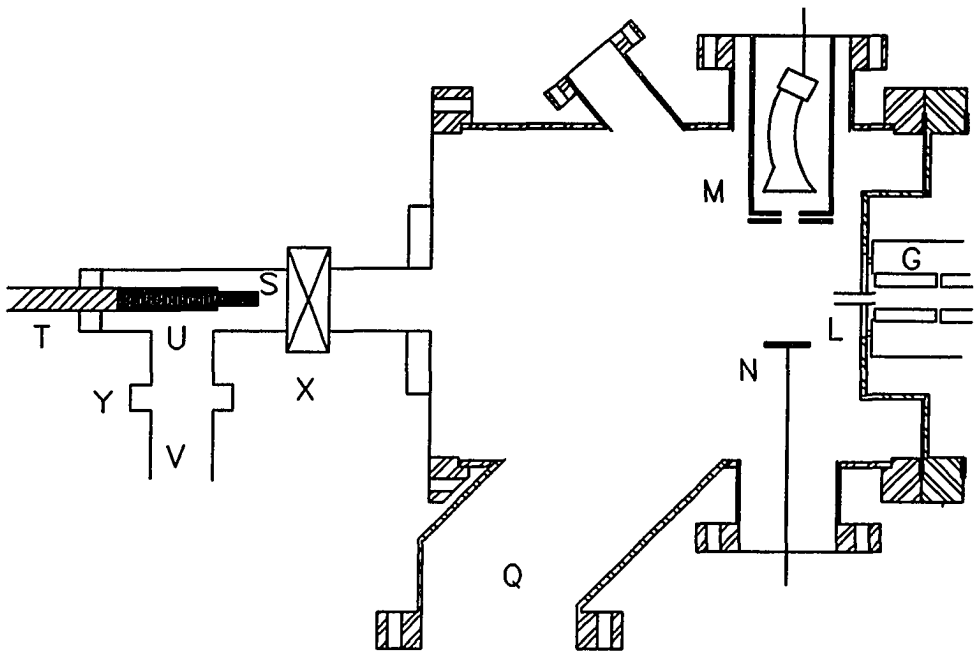

A

Figure 4. Interlock system at pre-evacuation stage (A) and deposition stage (B): (G) RF-only quadrupole; (L) ion exit lens; (M) Channeltron electron multiplier; (N) deflection plate; (Q) port to turbomolecular pump; (S) substrate or target; (T) target probe; (U) substrate holder and electrical feedthrough; (V) port to mechanical pump; (X) valve to deposition chamber; (Y) valve to mechanical pump.

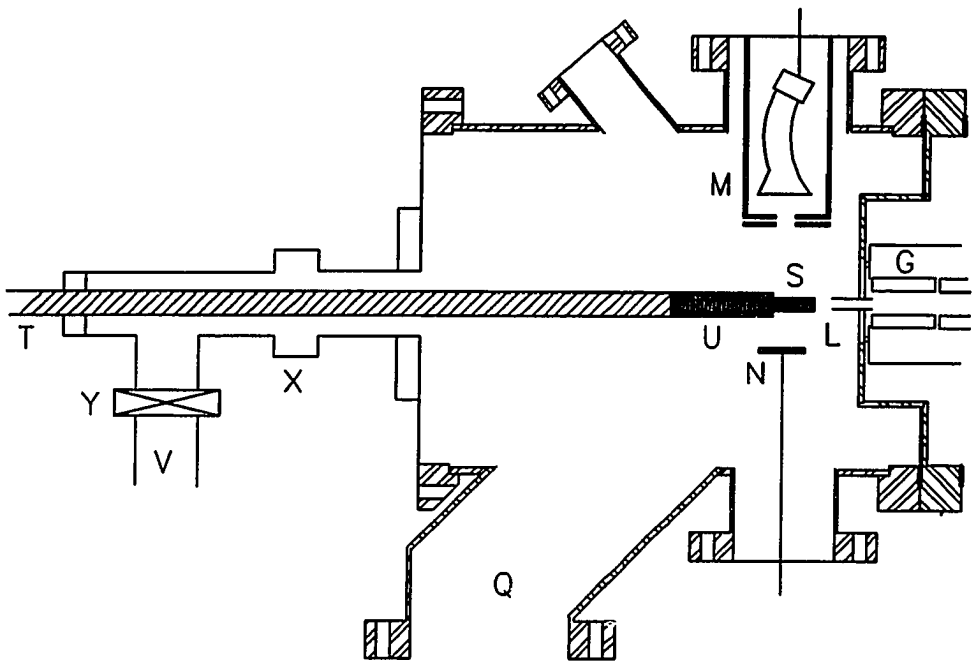

B

Figure 4. (continued).

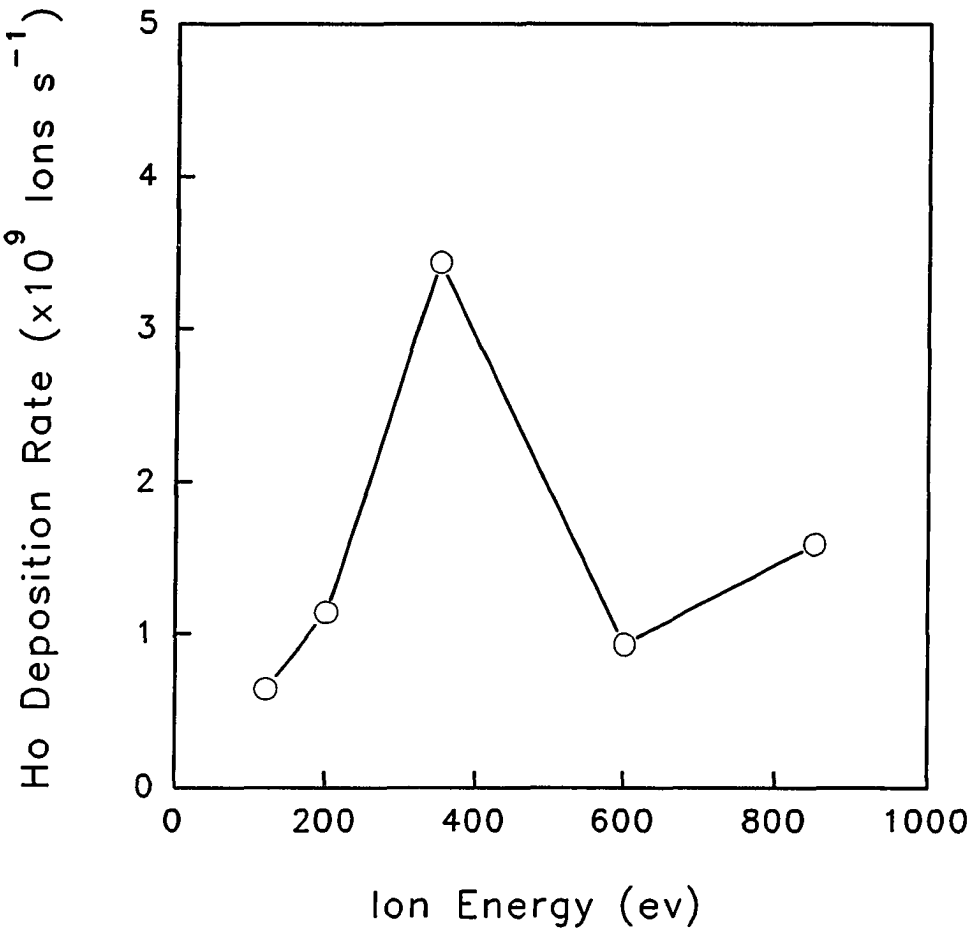

Figure 5. Measured Ho ion deposition rate (ions s^{-1}) as a function of ion kinetic energy for old ICP-MS device. Each point represents a deposition run of 3.0 hrs, following by dissolution of the Ho from the titanium oxide and measurement of the Ho concentration by ICP-MS.

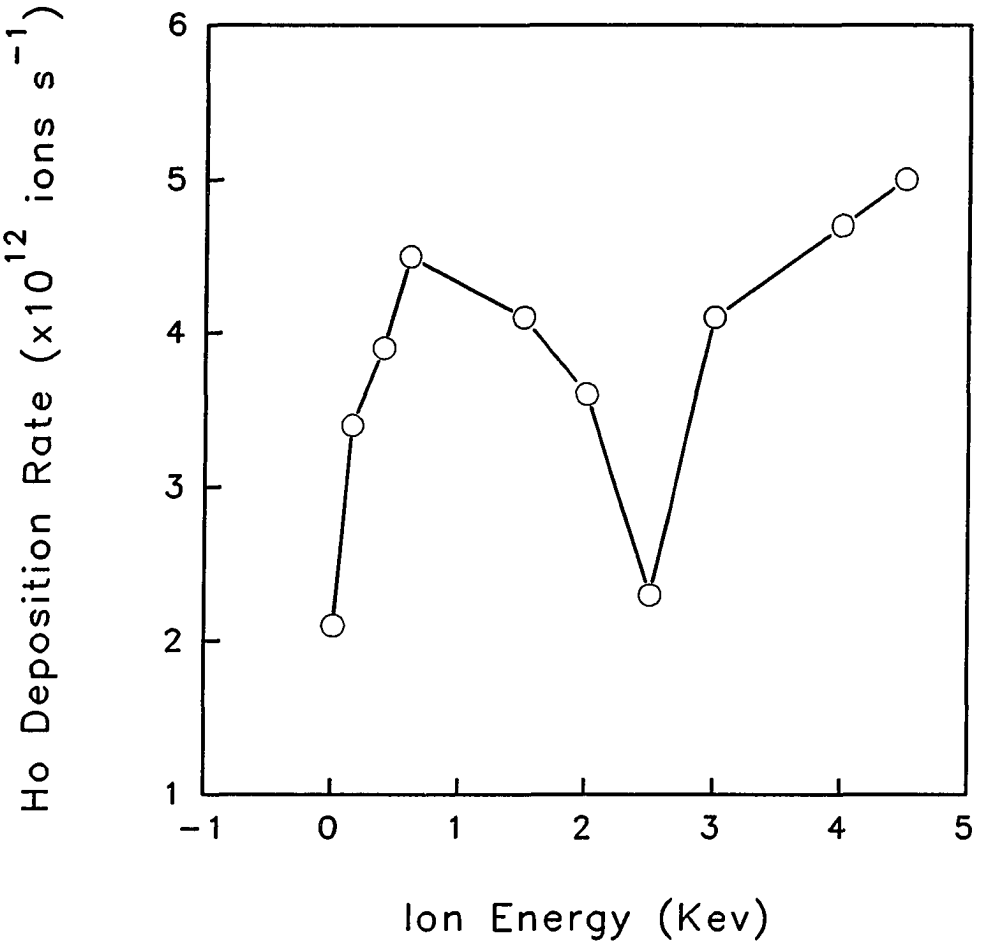

Figure 6. Measured Ho ion deposition rate (ions s^{-1}) as a function of ion kinetic energy for new ICP-MS device. Each point represents a deposition run of 2.5 hrs, following by dissolution of the Ho from the graphite and measurement of the Ho concentration by ICP-MS. The leftmost point corresponds to an ion energy of 10 eV.

SUMMARY

The primary goal of this work has been the enhancement of ion transmission and reduction of background and interferences in ICP-MS. A new ICP-MS instrument has been constructed. Some improvements in instrumentation have been made. Enlarging sampler and skimmer orifices increased ion signals and minimized solid condensation. Almost all photons and neutrals were blocked by the offset ion lens. Background was reduced to nearly the dark current. Because the offset ion lens only transmitted on-axis ions to the mass analyzer, polyatomic ion signals were much lower than on any other ICP-MS device. Matrix effects can be reduced without sacrificing much sensitivity by either grounding the first ion lens or re-adjusting the voltage applied to the first lens with the matrix present. Electrically floating the sampler and/or skimmer greatly improves ion transmission, detection limits, calibration linear range, and mass discrimination. An extra pumping stage and a small diameter long tube between third and fourth stages reduced the pressure in the fourth stage chamber to at least 10 times lower than that in usual ICP-MS. The Daly detector has been successfully used and a relatively pure thin film from ion deposition or ion implantation has obtained with this low pressure. Ion sensitivity or ion beam intensity has been increased about 1000 times, therefore, a thin film can be deposited in a reasonable time.

The analytical characteristics of this new ICP-MS instrument suggest several possible areas for future research. Analytical instruments are never of much significance unless they are useful for analysis of real samples. Each different real sample contains a different matrix and causes different matrix effects, hence, causes errors. Analysis of real samples

containing complicated matrices with this ICP-MS should yield good results, especially by grounding the first electrode of the ion lens. For example, determination of trace vanadium and arsenic in seawater should be straightforward because of low polyatomic ion interferences from ClO^+ and $^{40}Ar^{35}Cl^+$. With other ICP-MS devices, this measurement requires either high spectral resolution or chemical removal of the chloride matrix.

The direct injection nebulizer (DIN) exhibits a lot of advantages for ICP-MS (104). The amount of water introduced by the DIN is much more than with other nebulizers; polyatomic ions containing oxygen and metal oxide ions are substantial. Combining the DIN with this ICP-MS may confine the advantages of efficient sample introduction and low polyatomic ion interferences.

Ion sensitivity with this ICP-MS is somewhat lower than that measured by commercial instruments. The possible source of ion loss is from the offset ion lens used. A number of future projects employing the ion lens are envisioned. The first involves further refinement and modification of the offset ion lens. The ion transmission might be improved by changing the diameter of aperture of each electrode of ion lens, changing the separation of two nearby electrodes of the ion lens, and using more offset plates instead of only four. Second, we have shown that ion transmission is improved by electrically floating the sampling interface with a straight conventional ion lens. Ion transmission might also be improved when the sampling interface is floated with the offset ion lens.

Several application studies also can be investigated with the ICP-MS ion deposition or ion implantation technique. One such project involves continuously modifying the electrochemical properties of metal oxide electrodes by doping them with small amounts of

impurities metal ions, such as Bi or Sb. It was reported that electrocatalysis could be studied by ion implantation (105). Some interesting studies in electrocatalysis can be done with the ICP-MS ion implantation system because mixtures of different elements can be deposited easily in any desired stoichiometry by introducing a multielement sample into the plasma. Another project involves depositing thin films of refractory metals, diamond, or superconductors on appropriate substrates.

An ion trap mass spectrometer could be interfaced more easily to an ICP by using an offset ion lens. One major difficulty in using an ion trap is how to block the total particle beam while the ions are trapped. Nearly all photons and neutrals are blocked by our offset ion lens. All ions would be blocked by applying a high positive potential on one electrode of the ion lens. When appropriate negative voltages are pulsed onto the ion lens, ions will pass through to ion trap for storage and mass separation. Conceivably, high spectral resolution, i.e., separation of polyatomic ions from analyte ions, is possible in a relatively compact instrument with an ion trap (106,107).

ADDITIONAL LITERATURE CITED

1. Houk, R. S.; Fassel, V. A.; Flesch, G. D.; Svec, H. J.; Gray, A. L. and Taylor, C. E. Anal. Chem. 1980, 52, 2283-2289.
2. Jarvis, K. E.; Gray, A. L.; Houk, R. S. Handbook of Inductively Coupled Plasma Mass Spectrometry; Blackie: Glasgow, 1991.
3. Doherty, W. Spectrochim. Acta, 1989, 44B, 263-280.
4. Date, A. R.; Hutchison, D. J. Anal. At. Spectrom. 1987, 2, 269-276.
5. Jarvis, K. E. J. Anal. At. Spectrom. 1989, 4, 563-570.
6. Shabani, M. B.; Masuda, A. Anal. Chem. 1991, 63, 2099-2105.
7. Gregoire, D. C. J. Anal. At. Spectrom. 1988, 3, 309-314.
8. Date, A. R.; Gray, A. L. Spectrochim. Acta, 1985, 40B, 115-122.
9. Date, A. R.; Hutchison, D. Spectrochim. Acta, 1986, 41B, 175-181.
10. Park, C. J.; Hall, G. E. M. J. Anal. At. Spectrom. 1987, 2, 473-480.
11. Park, C. J.; Hall, G. E. M. J. Anal. At. Spectrom. 1988, 3, 355-361.
12. Date, A. R.; Stuart, M. E. J. Anal. At. Spectrom. 1988, 3, 659-665.
13. Jarvis, K. E.; Williams, J. G. Chem. Geol. 1989, 77, 53-63.
14. Jarvis, K. E. Chem. Geol. 1990, 83, 89-103.
15. Imai, N. Anal. Chim. Acta, 1990, 235, 381-391.
16. Garbarino, J. R.; Taylor, H. E. Anal. Chem. 1987, 59, 1568-1575.
17. Gregoire, D. C. J. Anal. At. Spectrom. 1990, 5, 623-626.
18. Ketterer, M. E. Anal. Chem. 1990, 62, 2522-2526.

19. Date, A. R.; Cheung, Y. Y. Analyst 1987, 112, 1531-1540.

20. Hirata, T.; Masuda, A. J. Anal. At. Spectrom. 1990, 5, 627-630.

21. Ward, D. B.; Bell, M. Anal. Chim. Acta, 1990, 229, 157-162.

22. Beauchemin, D.; Berman, S. S. Anal. Chem. 1989, 61, 1857-1862.

23. Falkner, K. K.; Edmond, J. M. Anal. Chem. 1990, 62, 1477-1481.

24. Klinkhammer, G. P.; Chan, L. H. Anal. Chim. Acta, 1990, 232, 323-329.

25. Beauchemin. D.; McLaren, J. W.; Willie, S. N.; Berman, S. S. Anal. Chem. 1988, 60, 687-691.

26. Boomer, D. W.; Powell, M. J. Anal. Chem. 1987, 59, 2810-2813.

27. Ting, B. T. G.; Janghorbani, M. Anal. Chem. 1986, 58, 1334-1340.

28. Igarashi, Y.; Kawamura, H.; Shiraishi, K. J. Anal. Atom. Spectrom. 1989, 4, 571-576.

29. Viczián, M.; Lásztity, A. Barnes, R. J. Anal. Atom. Spectrom. 1990, 5, 293-300.

30. Branch, S.; Ebdon, L.; Ford, M.; Foulkes, M.; O'Neill, P. J. Anal. Atom. Apectrom. 1991, 6, 151-154.

31. Thompson, J.; Ward, N. I. J. Micronutr. Anal. 1989, 6, 85-96.

32. Delves, H. T.; Campbell, M. J. J. Anal. Atom. Spectrom. 1988, 3, 343-348.

33. Gercken, B.; Barnes, R. M. Anal. Chem. 1991, 63, 283-287.

34. Luo, S. K.; Chang, F. C. Spectrochim. Acta, 1990, 45B, 527-535.

35. Osborne, S. P. Appl. Spectrosc. 1990, 44, 1044-1046.

36. Lord III, C. J. Anal. Chem. 1991, 63, 1594-1599.

37. Beck, G. L.; Farmer, O. T. J. Anal. Atom. Spectrom. 1988, 3, 771-773.

38. Peng, Z.; Klinkenberg, H.; Beeren, T.; Van Borm, W. Spectrochim. Acta, 1991, 46B, 1051-1061.

39. Zurhaar, A.; Mullings, L. J. Anal. Atom. Spectrom. 1990, 5, 611-617.

40. Gregoire, D. C. Anal. Chem. 1990, 62, 141-146.

41. Ward, D. B.; Bell, M. Anal. Chim. Acta, 1990, 229, 157-162.

42. Shabani, M. B.; Akagi, T.; Masuda, A. Anal. Chem. 1993, 64, 737-743.

43. LaFreniere, B. R.; Houk, R. S.; Fassel, V. A. Anal. Chem. 1987, 59, 2276-2282.

44. Kawaguchi, H.; Tanaka, T.; Mizuike, A. Spectrochim. Acta Part B 1988, 43B, 955-962.

45. Houk, R. S.; Fassel, V. A.; Flesch, G. D.; Svec, H. J.; Gray, A. L. Taylor, C. E. Anal. Chem. 1980,. 52, 2283-2289.

46. Gray, A. L.; Date, A. R. Analyst 1983, 108, 1033-1050.

47. Ross, B. S.; Hieftje, G. M. Spectrochim. Acta Part B 1991, 46B, 955-962.

48. Bradshaw, N.; Hall, E. F. H.; Sanderson, N. E. J. Anal. Atomic Spectrom. 1989, 4, 801-803.

49. Morita, M.; Ito, H.; Uehiro, T.; Otsuka, K. Anal. Sci. (Japan) 1989, 5, 609-610.

50. Sakata, K. 18th FACSS Conf., Anaheim, CA October 1991, Paper No. 528.2

51. Vaughan, M. A.; Horlick, G. Spectrochim. Acta, 1990, 45B, 1289-1299.

52. Douglas, D. J.; Kerr, L. A. J. Anal. Atom. Spectrom. 1988, 3, 749-752.

53. Houk, R. S.; Fassel, V. A.; Svec, H. J. Dynamic Mass Spectrom. 1981, 6, 234-251.

54. Gray, A. L. Spectrochim. Acta, 1985, 40B, 1525-1537.

55. Gray, A.; Spectrochim. Acta, 1986, 41B, 151-167.

56. Vaughan, M. A.; Horlick, G. Appl. Spectrosc., 1986, 40, 434-445.

57. Tan, S. H.; Horlick, G. Appl. Spectrosc., 1986, 40, 445-460.

58. Date, A. A.; Gray, A. L. Application of Inductively Coupled Plasma Mass Spectrometry; Blackie: Glasgow, 1989.

59. Gray, A. L.; Williams, J. G. J. Anal. Atom. Spectrom. 1987, 2, 599-606.

60. Horlick, G.; Tan, S. H.; Vaughan, M. A.; Rose, C. A. Spectrochim. Acta, 1985, 40B, 1555-1572.

61. Zhu, G.; Browner, R. F. J. Anal. Atom. Spectrom. 1988, 3, 781-789.

62. Douglas, D. J.; French, J. B. J. Anal. Atom. spectrom. 1988, 3, 743-747.

63. Olivares, J. A.; Houk. R. S. Anal. Chem. 1985, 57, 2674-2679.

64. Gillson, G. R.; Douglas, D. J.; Fulford, J. E.; Halligan, K. W.; Tanner, S. D. Anal. Chem. 1988, 60, 1472-1474.

65. Tan, S. H.; Horlick, G. J. Anal. Atom. Spectrom. 1987, 2, 745-763.

66. Crain, J. S.; Houk, R. S.; Smith, F. G. Spectrochim. Acta, 1988, 43B, 1355-1364.

67. Beauchemin, D.; Mclaren, J. W.; Berman, S. S. Spectrochim. Acta, 1987, 42B, 467-490.

68. Kawaguchi, H.; Tanaka, T.; Mizuike, A. Spectrochim. Acta, 1988, 43B, 955-962.

69. Pierce, J. R. Theory and Design of Electron Beam, 2nd Ed. Van Nostrand, New York, 1954.

70. Bradshaw, N.; Hall, E. F. H.; Sanderson, N. E. J. Anal. Atom. Spectrom. 1989, 4, 801-803.

71. Turner, P. J. Fourth Surrey Conf. on Plasma Source Mass Spectrometry, Guildford, UK, July 1991.

72. Turner, P. J. In Applications of Plasma Source Mass Spectrometry, 1991, Holland, G.; Eaton, A. N. Eds.; Thomas Graham House. Science Park. Cambridge.

73. Gregoire, D. C. Appl. Spectrosc. 1987, 41, 897-903.

74. Boorn, A.; Gillson, G.; Fulford, J.; Douglas, D.; Quan, E. Presented at the 1987 Winter Conference on Plasma and Laser Spectrochemistry, Lyon, France, 1987.

75. Wang, J.; Shen, W.-L.; Sheppard, B. S.; Evans; E. H.; Fricke, F. L.; Caruso, J. A. J. Anal. Atom. spectrom. 1990, 5, 445-449.

76. Sheppard, B. S.; Shen, W.-L.; Caruso, J. A. J. Amer. Soc. Mass Spectrom. 1991, 2, 355-361.

77. Ross, B. C.; and Hieftje, G. M. Spectrochim. Acta, 1991, 46B, 1263-1273.

78. Wilson, D. A.; Vickers, G. H.; Hieftje, G. M. Spectrochim. Acta, 1987, 42B, 29-38.

79. Ross, B. S.; Chambers, D. M.; Vickers, G. H.; Yang, P.; Hieftje, G. M. J. Anal. Atom. Spectrom., 1990, 5, 351-358.

80. Russ, G. P. III In Applications of ICP-MS, 1989, Date, A. R.; Gray, A. L. Eds.; Blackie, London, Chapter 4.

81. Daly, N. R. Rev. Sci. Instrum. 1960, 31, 264-267.

82. Gibbs, H. M; Commins, E. D. Rev. Sci. Instrum. 1966, 37, 1385-1390.

83. Ridley, B. W. Nucl. Instrum. Methods, 1961, 14, 231-236.

84. Huang, L. Q.; Jiang, S.-J; Houk, R. S. Anal. Chem. 1987, 59, 2316-2320.

85. Ishikawa, J.; Takeiri, Y.; Ogawa, K.; Takagi, T. J. Appl. Phys. 1987, 61, 2509-2515.

86. Bhattacharya, R. S.; Wu, R. L. C.; Yust, C. S. Nucl. Instrum. and Methods in Phys. Res. 1991, B59/60, 1383-1386.

87. Appleton, B. R.; Pennycook, S. J.; Zuhr, R. A.; Herbots, N.; Noggle, T. S. Nucl. Instrum. and Methods, 1987, B19/20, 975-982.

88. Herbots, N.; Appleton, B. R.; Noggle, T. S.; Zuhr, R. A.; Pennycook, S. J. Nucl. Instrum. and Methods, 1987, B13, 250-258.

89. Zuhr, R. A.; Alton. G. D.; Appleton, B. R.; Herbots, N.; Noggle. T. S.; Pennycook, S. J. presented at the 1987 Spring MRS Symposium, Anaheim, CA, 1987.

90. Zuhr, R. A.; Appleton, B. R.; Herbots, N.; Larson, B. C.; Noggle. T. S.; Pennycook, S. J. J. Vac. Sci. Technol. 1987, A5, 2135-2139.

91. Shimizu, S.; Tsukakoshi, O.; Komiya, S.; Makita, Y. Jap. Appl. Phys., 1985, B3, 1130-1140.

92. Maruno, S.; Morishita, Y.; Isu, T.; Nomura, Y.; Ogata, H. J. of Crystal Growth, 1987, 81, 338-343.

93. Gordon, J. S.; Armour, D. G.; Donnely, S. E.; Van den Berg, J. A.; Marton, D.; Rabalais, J. W. Proc. 7th Inter. Conf. on IBMM'90, Knoxville, 1990, 146.

94. Ishikawa, J.; Ogawa, K.; Miyata, K.; Tsuji, H.; Takagi, T. Nucl. Instrum. and Methods in Phys. Res. 1987, B21, 205-208.

95. Withrow, S. P.; More, K. L.; ZUhr, R. A.; Haynes, T. E. Vacuum, 1989, 39, 1065-1068.

96. Haynes, T. E.; Zuhn, R. A.; Pennycook, S. J.; Appleton, B. A. Appl. Phys. Lett. 1989, 54, 1439-1441.

97. Shimizu, S.; Tsukakoshi, O.; Komiya, S.; Makita, Y. J. Vac. Sci. Technol. 1985, B3, 554-559.

98. Haynes, T. E.; Zuhn, R. A.; Pennycook, S. J.; Larsen, B. C. Proc. 12th Symp. on ISIAT'89, Tokyo, 1989.

99. Ziegler, J. F. Ion Implantation Science and Technology; 2nd Ed. Academic Press: New York, 1988.

100. Rissel, H.; Ruge, I. Ion Implantation, John & Sons Ltd.: New York, 1986.

101. Laursen, T.; Clapham, L.; Whitton, J. L. Nucl. Instrum. and Methods in Phys. Res. 1991, B59/60, 768-771.

102. White, A. E.; Short, K. T.; Berger, S. D.; Huggins, H. A.; Loretto, D. Mat. Res. Soc. Symp. Proc. 1989, 147, 223-228.

103. Follstaedt, D. M.; Knapp, J. A.; Pope, L. E. Mat. Res. Soc. Symp. Proc. 1989, 128, 389-402.

104. Wiederin, D. R.; Smith F. G.; Houk, R. S. Anal. Chem. 1991, 63, 219-225.

105. Kelly, E. J.; Heatherly, D. E.; Vallet, C. E.; White C. W. J. Electrochem. Soc. 1987, 134, 1667-1675.

106. Schwartz, J. C.; Syka, J. E. P.; Jardine, I. J. Amer. Soc. Mass Spectrom. 1991, 2, 198-204.

107. Kaiser, R. E., Jr.; Cooks, R. G.; Moss, J.; Hemberger, P. H. Rapid Commun. Mass Spec. 1989, 3, 50-53.

108. Kaiser, R. E., Jr.; Louris, J. N.; Amy, J. W.; Cooks, R. G. Rapid Commun. Mass Spec. 1989, 3, 225-229.

ACKNOWLEDGMENTS

First, I would like to greatly acknowledge my major professor, Dr. R. S. Houk. He always took the time to talk to me about my research and about technical writing. None of this work could be done without his support, understanding, tolerance, and guidance. I will never forget the moment we played volleyball together and caught up the "gold shoe" trophy of the department championship.

I would like to thank Mr. T. W. Modelland, machinist of Ames Laboratory machine shop, for constructing my vacuum chamber and a lot of parts, and his friendship. I wish to express my appreciation to other members of the machine shop (J. L. Hand, C. Burg, and S. E. Lee) for their help, assistance, and kindness.

I would like to thank the members of Dr. Houk's group for their assistance and friendship: Fred Smith, Dan Wiederin, Sam Shum, Luis Alves, Shen Luan, Rocky Warren, Jeff Crain, and Steve Gilles (our adopted group member). The vacuum chamber could not be put together without their help. I would particularly like to thank Scott Clemons for his assistance in construction of offset ion lens and Daly detector, Xiaoshan Chen and Dr. Ho-Ming Pang for their help in the use of some computer programs, and Hongsen Niu for making the stainless steel injector tube. My thanks are also given to three new students in the Houk's group (Tonya Bricker, Lloyd Allen, and Steve Johnson) for their help for passing tiger team inspection and for the kindness they have shown to me. I owe deep appreciation to many friends for the friendship they have show me during the time I have spent at Ames. I will miss all of you.

This work was performed at the Ames Laboratory under contract no. W-7405-ENG-

82 with the U. S. Department of Energy. The United States government has assigned DOE report no. IS-T-1600 to this dissertation.

Financial support from the U. S. Department of Commerce through the Center for Advanced Technology Development for construction of the ICP-MS ion deposition device is gratefully acknowledged. I also thank CETAC Technologies Inc. for providing an ultrasonic nebulizer.

I am very grateful to my parents, Zhihua Chang and Yuzhong Hu, for their love and support throughout my education, and my older brother, Weijia Hu, for his support and encouragement. I thank Xuemei Li and Hongde Su the kindness and generosity they have shown to me since I married their daughter and for taking care of my son for three years before he joined my wife and me here.

Above all, I wish to acknowledge my wife, Dongling Su, for her love, patience, understanding, support, and encouragement. I thank my son, Jing, for giving me many happy times.